Microfluidic Western Blotting with Increased Sample Loadability and Fast Immunoassay

by

Natalie E. Arvin

A dissertation submitted in partial fulfillment
of the requirements for the degree of
Doctor of Philosophy
(Chemistry)
in the University of Michigan
2020

Doctoral Committee:

Professor Robert Kennedy, Chair
Professor Mark Burns
Professor Zhan Chen
Professor Mark Meyerhoff

Natalie E. Arvin

necleave@umich.edu

ORCID iD: 0000-0002-5765-6380

Acknowledgements

Thank you to my research advisor, Professor Robert Kennedy for the opportunity to work on these projects. I would like to thank my committee members Professor Mark Burns, Professor Zhan Chen, and Professor Mark Meyerhoff for their input, suggestions, and time throughout my research. Thank you to Dr. Mohamed Dawod for his mentorship, ideas, and contributions to these projects, I am grateful we had the opportunity to work together. I would like to thank Dr. Shi Jin for the training and input he provided. I would like to thank Cara D'Amico for her collaborations and discussions and to acknowledge her contributions in exploring deep etching of D263 glass. I would like to thank all other Kennedy lab members who have contributed ideas and support in project development.

I would like to thank all my undergraduate professors at the University of North Florida who helped me get to where I am today. Thank you very much to Professor Stuart Chalk, Professor Rahda Pyati, Mrs. Melissa Bush, Professor Thomas Mullen, and Dr. Frederick Troendle. Thank you to Professor Stuart Chalk for getting me started analytical chemistry research and mentoring me along the way. Thank you very much to Professor Jeff Michelman for his mentorship and the leadership opportunities I had through working with him and Rotaract on campus.

Thank you very much to my partner and family. I would not be where I am today without your endless love and support. I would particularly like to thank my parents for all the times they listened and encouraged me. They are always supportive of me and here for me, even in the midst of chaos. Thank you especially to Joey for the support and encouragement you provided me. Thank you very much to my grandparents for their love and encouragement.

Table of Contents

List of Tables

List of Figures

Abstract

Western blotting is a widely used protein assay method that combines a size-based separation with specific antigen detection. The technique, in its conventional form, involves the separation of proteins by sodium dodecyl sulfate-polyacrylamide gel electrophoresis (SDS-PAGE), transfer of separated proteins from the gel to a binding membrane, and immunoassay for detection of target proteins. The technique has been widely used for decades, yet it requires long analysis times and multiple manual steps. Microchip gel electrophoresis (MGE) and microfluidic approaches to Western blotting have been developed to reduce analysis times, reduce sample and reagent consumption, and increase automation for Western blots. Microchip electrophoresis separations for Western blotting can be directly captured on protein-binding membranes by dragging a diced microchip outlet across the membrane. In this work, we examine 3 aspects of this approach to Western blotting: 1) microfabrication, 2) sample loading, and 3) immunoassay.

For microchips to perform good, reproducible electrophoretic separations, glass microchip fabrication methods must reproducibly etch smooth channels into the glass substrate. Photolithography and wet chemical etching have produced inconsistent etching results in borosilicate glasses. Poor etching has hampered the development of microchip Western techniques. Rough etching of the glass substrate was hypothesized to be originating from stress induced in the glass substrate during the manufacturing of the glass. A new fabrication method using D263 borosilicate glass allowed for consistent microchip fabrication with smoothly etched channels.

A critical feature for electrophoresis of proteins is the sample injection method into the separation channel. Electrokinetic injection (EKI) modes, such as a gated injection, have limited injection time before band broadening will occur and diminish the electrophoretic separation. Improved sample loadability can be achieved by on-line preconcentration or sample stacking. Field amplified sample injection (FASI) allows for preferential injection of analytes over the low conductivity sample matrix. Transient isotachophoresis (tITP) is a powerful stacking method that allows for concentration of a sample plug by sandwiching the sample between a leading electrolyte (LE) and a terminating electrolyte (TE). The combination of FASI with tITP, termed electrokinetic supercharging (EKS) preconcentration, has served as a preconcentration method in capillary and microchip gel electrophoresis for protein analysis for decades. The development of a fixed length sample plug with on-line EKS precontraction was explored in this work for overcoming limitations of EKI. This new injection method was applied to microchip Western blotting and provided a 30-fold improvement in detection sensitivity compared to a timed, gated injection for microchip Western blotting.

Immunoassay analysis steps require 4-20 h to complete overall limiting the analysis speed of microfluidic Western blotting methods. The speed of conventional immunoassay methods suffers from diffusion limited mass transport; the development of a microscale immunoassay with direct deposition of immunoassay reagents overcomes these challenges. By applying immunoassay reagents directly to the microchip Western blot protein trace, using low μL/min flow rates, the entire immunoassay can be completed in 1 h. The detection sensitivity was comparable to incubation steps requiring 20 h. Additionally, antibody consumption was reduced 30-fold with the flow immunoassay method. Developments in microfluidic Western blotting including new etching methods for glass microchips, implementation of on-line preconcentration with increased

sample loadability, and a microscale deposition method for a fast immunoassay are described. These methods are applied to protein detection in cell lysate.

Chapter 1 Introduction

Protein Separation by Electrophoresis

Proteins are biological macromolecules constructed for specific functions in cells; thus, the determination of proteins is critical for investigation of normal and diseased cell function.[1,2] For such measurements, fast, high resolution electrophoretic separations are useful. Protein electrophoresis originated from the discovery of the migration of charged molecules relative to a fluid under a spatially uniform electric field.[3,4] The electrophoretic mobility of a molecule depends upon the strength of the applied electric field and the size, shape, and net charge of the molecule which is derived from the following equation:

$$\mu = q/6\pi\eta r$$

The electrophoretic mobility is a ratio of the charge on the molecule (q) over the size of the molecule where the viscosity of the solution (η) and the Stokes' radius of the particle (r) are considered. However, with increasing molecular weight, the electrophoretic mobility of two molecules barely differ. The separation of macromolecules is thus achieved through a purely-size-based electrophoretic separation.

During its introduction in the late 1940s, electrophoretic separations of proteins were limited to low electric fields because Joule heating resulted in convective mixing of separated zones. The use of anticonvective media such as paper, starch, and agarose improved the separation of DNA, RNA, proteins, and peptides by preventing mixing. Such anticonvective media for electrophoresis also serves as a sieving medium, thus altering the selectivity of electrophoresis and

enabling sized based separations. During sieving electrophoresis, shorter molecules migrate faster than longer molecules because shorter ones migrate more easily through the media/gel pore. By the 1960s, the establishment of cross-linked gels led to the use of polyacrylamide gel separations for native and denatured proteins.

For denatured proteins, sodium dodecyl sulfate-polyacrylamide gel electrophoresis (SDS-PAGE)[5–8] results in a size-based separation.[9,10] SDS is an anionic detergent that associates with proteins imparting approximately two negative charges to every two amino acids so that all proteins have similar electrophoretic mobility.[11–13] In combination with heat, SDS promotes unfolding by interactions with both polar and nonpolar portions of protein structure.[14,15] Once this occurs, SDS monomers bind to proteins through hydrophobic interactions (**Figure 1-1**). To form a saturated SDS-protein complex, 1.4 g of SDS/g of protein results in a uniform negative charge.[12,17] Reducing agents, typically beta-mercaptoethanol or dithiothreitol, disrupt disulfide bridges formed from any cysteine amino acid groups to aid in linear unfolding of protein structures.

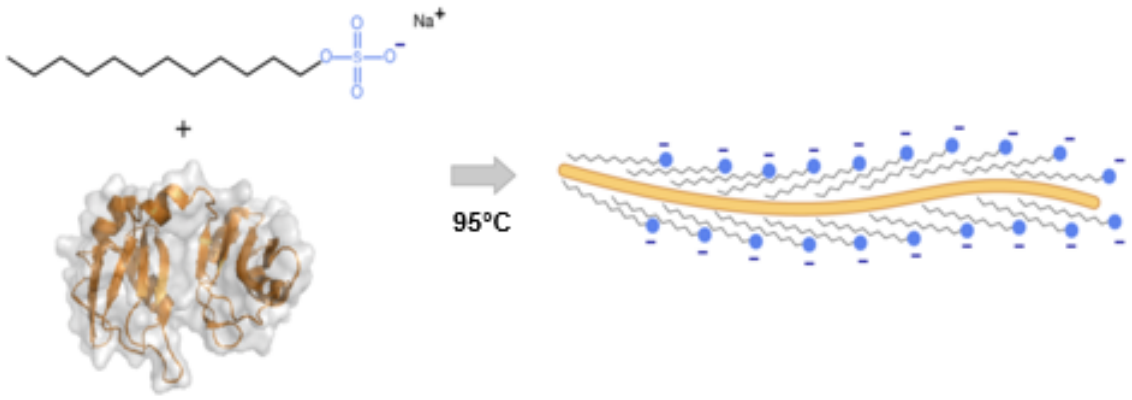

Figure 1-1. Denaturation of a protein (bottom-left) by sodium dodecyl sulphate (top-left). Detergent molecules coat the unfolded protein chain (right), which adopts a rod-like shape as a consequence of electrostatic repulsion. Negative charges contributed by SDS dominate the total charge of the aggregate and are used at the driving force in SDS gel electrophoresis. Reprinted.[16]

Denatured, SDS-complexed proteins undergo a sieving separation through gel pores wherein smaller molecular weight proteins migrate faster than larger molecular weight proteins.[18–20] Polyacrylamide gels include stacking and resolving buffer systems for high-resolution separations of macromolecules.

Western Blotting Overview

The adsorption and binding of macromolecule complexes to blotting membranes (such as cellulose-based membranes) allowed for protein blotting method development.[21–24] Binding to cellulose membranes largely occurs through hydrophobic interactions strengthened by denaturation of the protein, dehydration of the protein-membrane complex, and an increase in salt concentration.[25–28] The combination of SDS-PAGE with blotting preserves the separation on the binding membrane. This technique was coined Western blotting; in its entirety, the Western blot combines a molecular weight-based electrophoresis separation and membrane blotting with specific antigen detection using an immunoassay (**Figure 1-2**).[23,29]

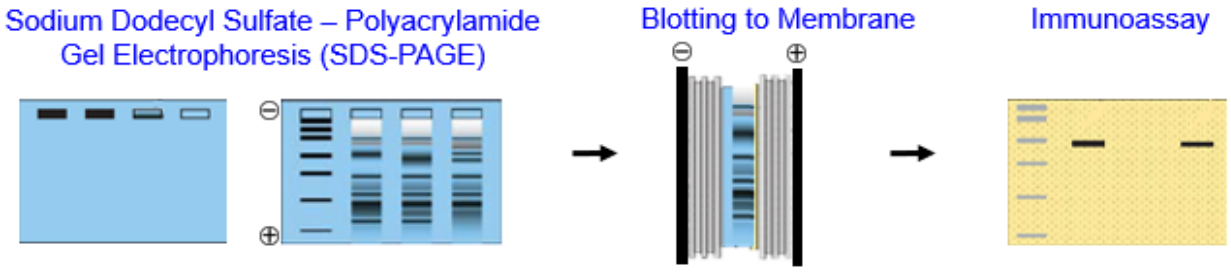

Figure 1-2. A schematic representation of Western blotting procedure. Samples are loaded into the wells of SDS-PAGE. When the electric field is applied, protein separations occur. The bands shown are hypothetical. A replica of the SDS–PAGE obtained by transfer of the proteins to a binding membrane. The immunoassay uses a primary antibody for target binding. A secondary antibody binds to the primary antibody for detection. Adapted with permission.[30] Copyright 2007 Springer-Verlag London Limited.

In total, the research and development that led to Western blotting has been founded in or influenced by research receiving several Nobel prizes. In 1948, Arne Tiselius received the Nobel

Prize in Chemistry for his research on electrophoresis, particularly on the complex nature of serum proteins. Rosalyn Yalow was part of a team that received the Nobel Prize in Physiology of Medicine 1977 for the development of radioimmunoassay, while the production of monoclonal antibodies received the 1984 Nobel Prize in Medicine.

There are many advantages for Western blotting in comparison to purely immunological methods of detection. The technique provides confirmation of the target by providing both a molecular weight analysis and antibody binding. If Western blotting results and target binding data varies from an expected outcome, Western blotting data aids in investigating the cause. Data including protein band size, multiple bands, and unexpected molecular weight targets could indicate protein cleavage or multimer formation. Western blotting is applied broadly in life science research fields for assessing protein expression in cells or various tissues, protein responses to diseases or drugs, protein molecular weight determination, protein/antibody purity, and medical diagnostics. Such diagnostic applications include the detection of HIV infection, hepatitis B (HBV) hepatitis C (HCV), Lyme disease, syphilis, and some autoimmune disorders.

Despite their impact, Western blotting methods have several limitations and can be time consuming.[31] Procedures are manually intensive and consume large sample mass (10-50 μg) and reagent volumes. The transfer step between slab gels and binding membranes can result in inadequate protein transfer as well as challenges in efficiently transferring broad ranges of molecular weight proteins simultaneously. Blotting membranes have limited ability for re-probing the separation for multiple targets. This requires stripping of antibodies which may also result in stripping of sample protein bands. In this dissertation, work designed to markedly improve all aspects of the Western blot is described.

Capillary Gel Electrophoresis for Protein Detection

The introduction of narrow-bore silica capillary for capillary zone electrophoresis (CZE)[32,33] paved the way for improvements in SDS-PAGE separations. The small inner diameter (i.d.) of capillaries exhibit larger surface-to-volume ratios which improves heat dissipation in comparison to slab gels (**Figure 1-3**). Therefore, higher electric fields are applied leading to increased separation efficiency, improved separation resolution, and shorter analysis time.[35–39] For capillary

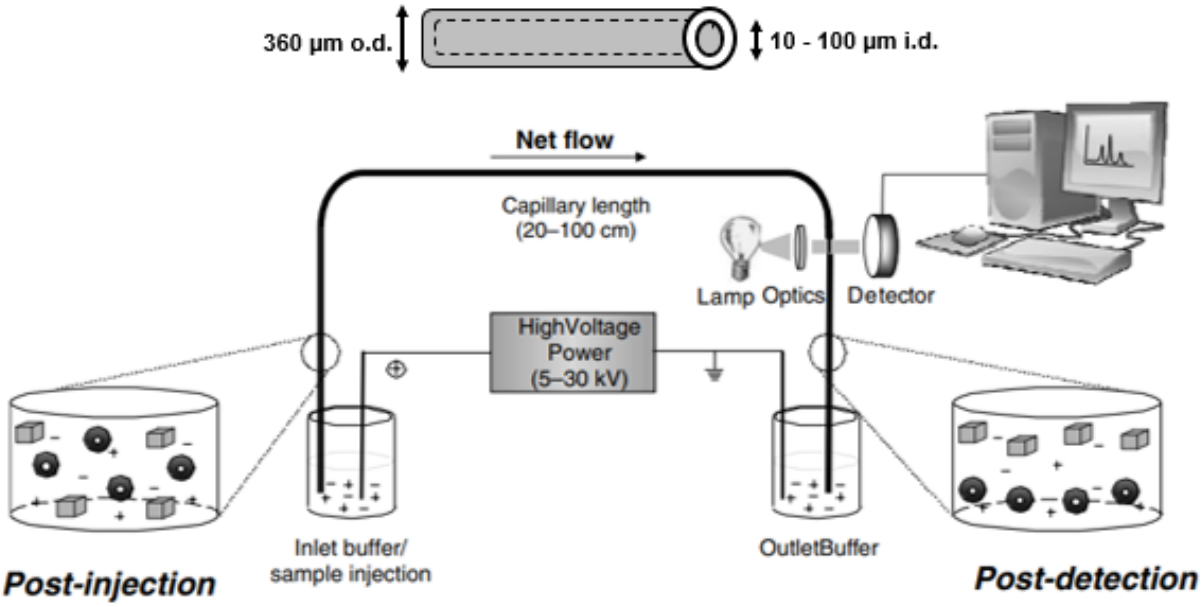

Figure 1-3. General schematic of a CE instrument. Adapted with permission.[34] Copyright 2008 Taylor & Francis Group, LLC.

electrophoresis (CE), the development of non-cross linked polymer gels, which are generated from entangled polymer mixtures, allows for the regeneration and reuse of capillaries.[40–43] Capillary gel electrophoresis (CGE) combined with SDS-protein complexes has allowed for fast separations of complex biological samples.[43–46] Several instruments and commercialized methods allow for SDS-CGE of proteins on a capillary, including the 2100 bioanalyzer instrument.[47] These methods

provide protein sizing and purity analysis information. Capillaries have been employed for Western blotting with two main approaches developed.

A capillary for SDS-CGE protein separations was interfaced with sheath capillary through which the proteins are captured exiting the outlet of the capillary onto a mobile blotting membrane.[31] The sheath capillary aids in the transfer from the proteins to the membrane; the membrane is placed on an X-Y translation stage. Electrophoresis was performed by applying a negative voltage at the inlet of the capillary with a ground connection through the translation stage supporting the membrane. This membrane was soaked in a 50:50 (v:v) methanol and buffer mixture to maintain electrical contact. This capillary Western blotting membrane was combined with immunoassay methods for the detection of standard proteins.

A capillary based method for employing *in-situ* immunoprobing with SDS-CGE for Western blotting has also been developed offering advantages of parallel analysis and automation.[47–51] The Simple Western technique uses small sample volumes and can perform analysis of up to 96 capillaries at one time. One drawback of this commercialized system is that it requires specialized separation compartments, sieving medium, reagents and antibodies. These methods require some added optimization for the immunoassay since traditional membranes are not used for protein capture and immunoprobing. Both methods/technologies were both introduced in the early 2010s. The advantages that CGE provides over slab gel separation are further developed with microchannel separations.[10,43,52–54]

Glass Microchip Electrophoresis for Western Blotting

The introduction of microchannels in insulating glass substrates has allowed for electrophoretic separations to occur on a microchip.[55] With further reduction in channel dimensions, higher electric fields can increase separation speed, separation efficiency, and resolution. Microchip

electrophoresis allows for low sample consumption and the potential for parallelized analysis easily on one microchip.[56–59] On a microchip device, the LabChip® GX performs rapid protein sizing on-chip.[60] The analyzer can interface with 94- and 364-well plates for higher throughput run capability. The advantages of microchip separations have also been employed for microfluidic Western blotting.

With dicing the separation outlet of the microchip, the deposition of separated proteins directly onto blotting membranes occurs (**Figure 1-4**).[61,62] The X-Y translational stage allows the membrane to move and capture separated proteins instantaneously. Not only does this microfluidic device speed up the separation and reduce the sample consumption compared to conventional Western blotting, the gel-to-membrane transfer step is greatly simplified. This work has allowed for the miniaturization of Western blotting while interfacing with conventional blotting materials.

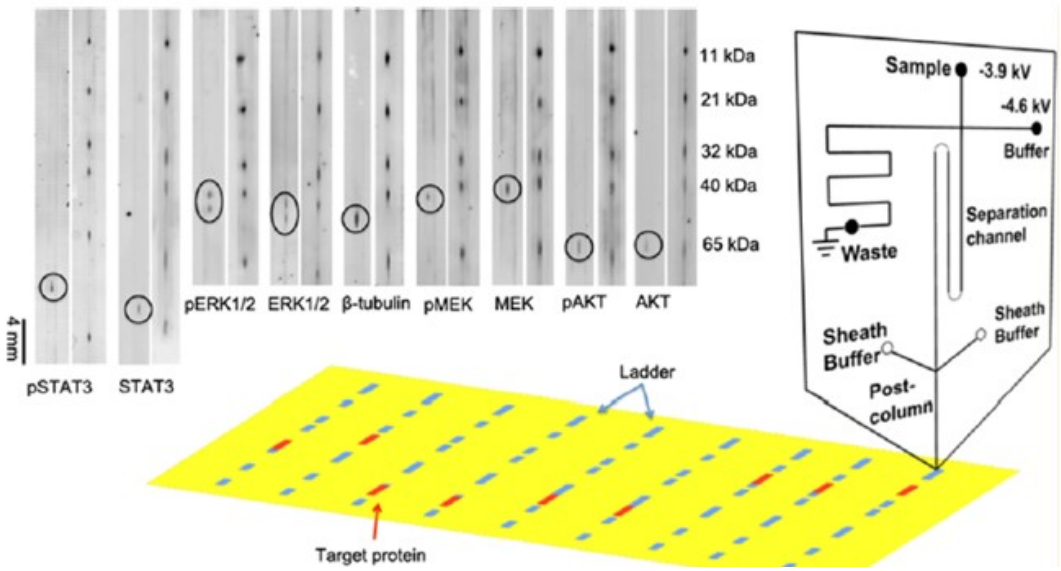

Figure 1-4. Microchip overview. Sample was injected using a gated injection method. SDS−protein complexes separated by size were captured in discrete zones on the PVDF membrane moving beneath the chip outlet to preserve separation information. Sieving media was pumped through the sheath channels to ensure a stable current. Separation channel was between the injection cross and the end of the channel, and length was 86 mm. Drawing is not to scale. The 300 μm post channel was drawn long for clarity. Multiple separation tracks can be laid down in discrete lanes on a binding membrane as illustrated. Eleven proteins are shown being detected from cell lysate via microchip Western blotting. Reprinted with permission.[62] Copyright 2016 American Chemical Society.

Multiplexed target detection with low sample consumption was demonstrated where multiple injections from a small sample volume resulted in detecting multiple protein from one sample. Immunoprobing with the protein separation cross-linked in the gel has been further developed for single-cell Western blotting technology called Milo.™ On one device, about a thousand single cells can be analyzed simultaneously. Cell lysing occurs on chip and a minute-long separation is applied. Conventional Western blotting antibodies can be used for probing.

Glass serves as a good substrate for these microfluidic devices due to its high thermal resistance, high chemical durability, excellent mechanical strength, and good transparency. Glass microchip fabrication is the combination of photolithography and chemical wet etching to create channels in the micron range.[63–66] The amorphous structure of glass materials allows for microchannels to be etched in all directions of the glass exhibiting isotropic etching behavior. Photolithographic patterning of a metal (Cr/Au) mask layer(s) using a photosensitive film layer to pattern the metal layer. Development of the UV exposed film with subsequent etching of the metal layer prepared the glass substrate for microchannel etching. Chemical wet etching, mainly performed in HF-based or KOH-based solutions, typically allows for the smooth etching of glass with complex microchannel designs at various depths (**Figure 1-5**). During the isotropic etch, the metal mask is undercut by HF resulting in curved side walls and a flat bottom.[66,67] In an aqueous HF solution, the chemical reaction for the dissolution of heterogeneous SiO_2 is described by the following, overall reaction:[68]

$$SiO_2 + 6HF \rightarrow H_2SiF_6 + 2H_2O$$

However, microfabrication methods can also result in rough etching of the glass substrate.

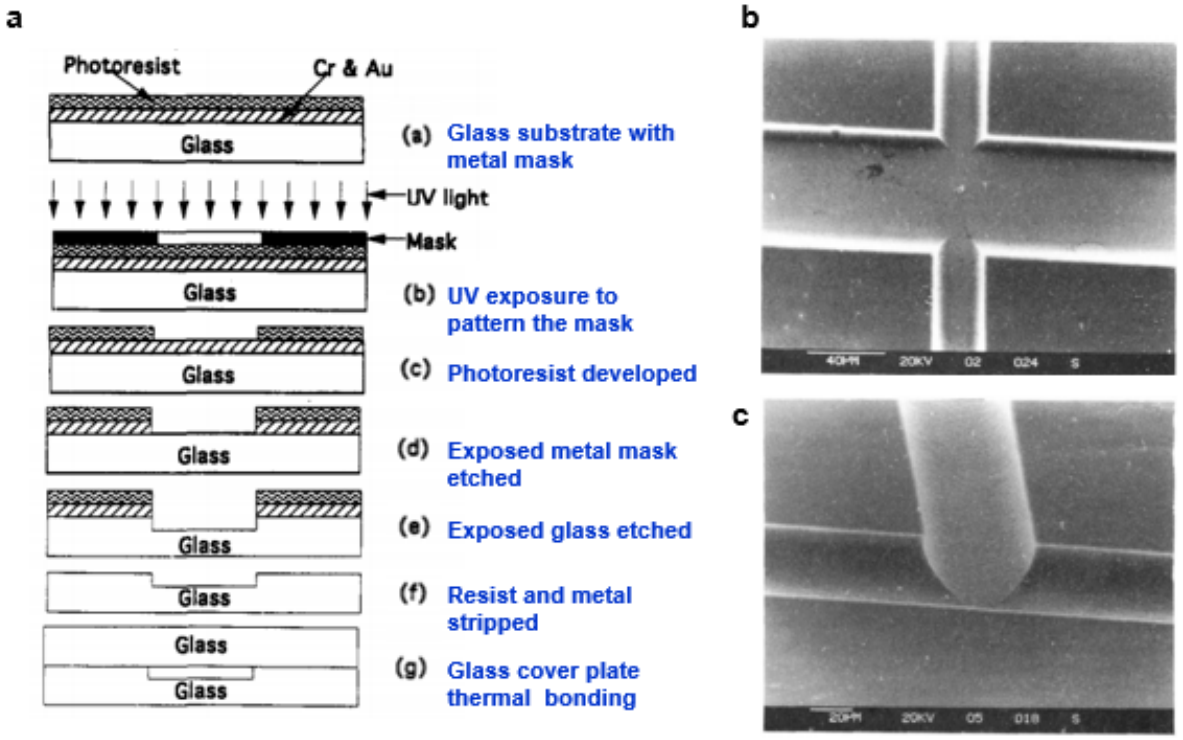

Figure 1-5. Sequence of photolithographic fabrication steps to etch and for microchannels in glass substrates (a). Electron micrographs of isotropic, smooth etching in different conditions of the borosilicate glass starting material where (b) displays the top down view of type I Pyrex and (c) displays the electron micrograph of the intersection of channels etched in type III Pyrex. Adapted with permission.[66] Copyright 1994 American Chemical Society.

The main forms of identified rough etching include resulting rough microchannel surfaces, spikes across microchannels on the glass surface, and dendritic crystals/bumps along the edge of the microchannel (**Figure 1-6**).[67] Rough etching may have various sources or be a combination of sources that are difficult to detect during the fabrication process. Masking materials used in wet etching, such as Cr and Au, are inert to HF. However, cracks or stress in the masking layer can lead to several problems for etching along the channel edges.[69,70] Mixtures of oxides in glass can lead to insoluble products such as CaO, MgO, and Al_2O_3. If these impurities are on the surface of the glass they act as masking layers causing the surface to become rough.[70] Even when the glass

substrate appears to be defect free, localized stressed and microscratches in the glass will cause rough etching. Stress in the glass can be a result of the manufacturing process as well.[71]

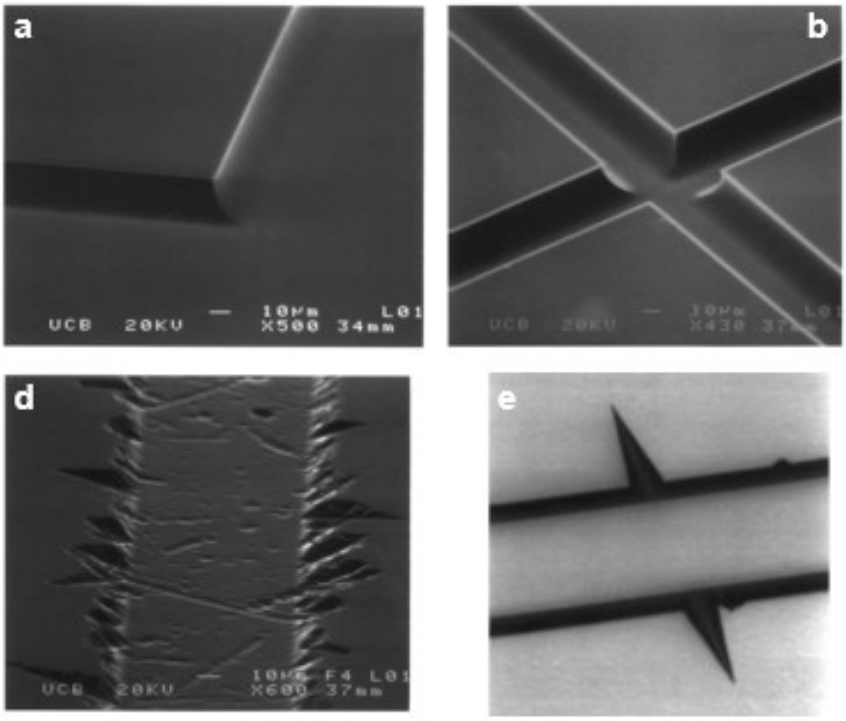

Figure 1-6. Examples of smooth and rough etching in Borofloat glass. Scanning electron micrograph showing a corner of two crossed channels etched 25 µm in Borofloat using a 1500 Å sacrificial mask layer of amorphous silicon (a). Scanning electron micrograph of the intersection of two 25 µm deep channels etched in Borofloat where striations on the side walls of the microchannel are evident near the intersection using a 1700 Å sacrificial mask layer of amorphous silicon (b). Scanning electron micrograph of polished Borofloat etched 7 µm using an Au/Cr etch mask. The patterns in the etched channel and defects in the side wall are due to polishing induced stresses and microscratches on the surface of the glass (c). Optical image of a defect in Borofloat glass etched to a depth of 25 µm using 49% HF and Cr/Au (150 Å /1500 Å) as the etch mask (d). Adapted with permission.[67] Copyright 1993 Chapman & Hall.

Some of these defects can be eliminated by improving or altering the etching mask; more difficult defects to solve are those that occur due to the type and manufacturing of glass and/or the surface condition of the glass. When rough etching occurs in a microchip, the electrophoretic separation suffers or is nearly impossible to perform. In my thesis work, sources of glass rough etching are investigated. New fabrication methods are implemented to overcome poor microchip fabrication.

With smoothly etched glass microchips, new injection designs were investigated to overcome limitations of typical electrokinetic injection (EKI) modes. Common microchip injections include gated, floated and pinched injections.[72,73] In previous work, a gated, timed injection mode was employed; however, limitations existed on the amount of sample that could be injected before band broadening occurs. Another disadvantage of gated injection is the bias against larger proteins that occurs.[74] Electrophoretic mass transport allows for pre-concentrating analytes proper to the separation. With gated injection, some preconcentration could be achieved but was still limited by the sample buffer components. If longer sample plugs are interfaced with on-line preconcentration, then the sample loadability of MGE and microchip Western botting could be increased.

On-Line Preconcentration for Gel Electrophoresis

Preconcentration methods were introduced in CE in order to inject larger samples plugs without compromising the separation efficiency.[35,74–77] Efficient preconcentration strategies are particularly required for the detection of lower abundant proteins in biological samples.[39] A stacking mechanism commonly employed with EKI, is field amplified sample injection (FASI).[78] In the case of a microchip injection, the sample is diluted in a lower conductivity matrix in comparison (water). Stacking occurs upon injection allowing for preferential injection of ionic analytes from a low conductivity sample solution. With larger amounts of analytes injected and longer injection times band broadening will still result.

Transient isotachophoresis (tITP) is an on-line preconcentration method that allows for stacking of sample plugs. This method combines a leading electrolyte (LE) plug, that has a higher electrophoretic mobility then the sample analytes, before the sample injection (**Figure 1-7**).[39] A

low mobility terminating electrolyte (TE) is loaded after the sample plug. Upon application of the electric field, the sample stacks between the LE and TE.

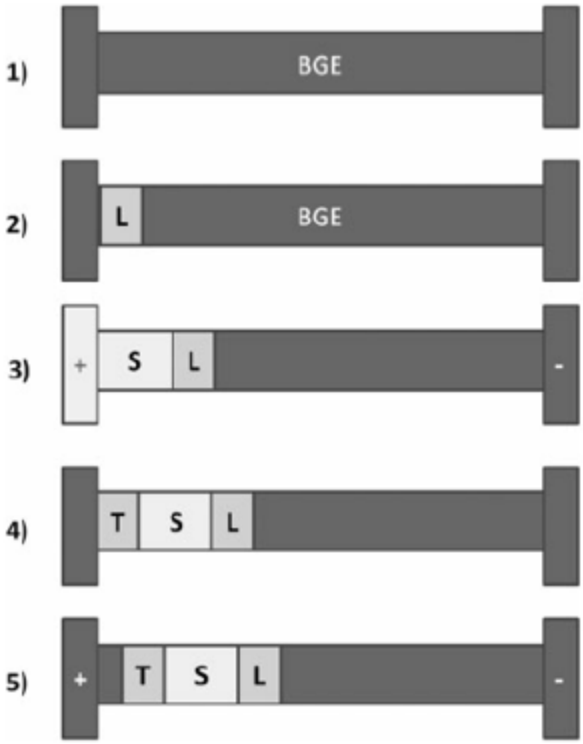

Figure 1-7. Schematic representation of the steps used in EKS. (1) Filling the capillary with the BGE. (2) Hydrodynamic injection of the leader (L). (3) Electrokinetic injection of the sample (S). (4) Hydrodynamic injection of the terminator (T). (5) Starting tITP-CZE. Reprinted with permission.[39] Copyright 2011 WILEY-VCH Verlag GmbH & Co. KGaA, Weinheim.

By implementing tITP, larger sample plugs are preconcentrated and band broadening effects are reduced. Combining FASI with tITP together allows for restacking of the analytes and is a powerful preconcentration method termed electrokinetic supercharging (EKS) preconcentration.[78]

Immunoassays for Western Blotting

Invented in the late 1950s, immunoassays provided a means to detect antigens through binding of an antibody to specific binding sites called epitopes.[79,80] At first, polyclonal antibodies were purified from human and animal sources; however the production of monoclonal antibodies from mouse cells greatly improved the production availability of antibodies.[81] The development

of non-competitive sandwich immunoassay methods, which utilize two antibodies for antigen detection, increased the specificity for detection of proteins even in complex biological matrices.[82,83] This was an important development for Western blotting techniques. The use of two antibodies, first a primary antibody and then a labeled-secondary antibody for detection, increases the specificity and ease of detection for the immunoassay in Western blotting. In current antibody production, antibodies are designed against denatured proteins and optimized for Western blotting methods.

The immunoassay is one of the most time-consuming components of Western blot requiring 4-20 h to complete (**Figure 1-8**). The laborious and lengthy process involves blocking nonspecific binding sites on the membrane (1 h), primary antibody incubation for the target protein (1 h – overnight), washing of unbound primary antibody (~20 min), secondary antibody probing (1 h), and washing of unbound secondary antibody (~20 min).[84,85] Conventional methods also consume large antibody volumes (i.e. 5-10 µL). To address the limitations of the immunoassay

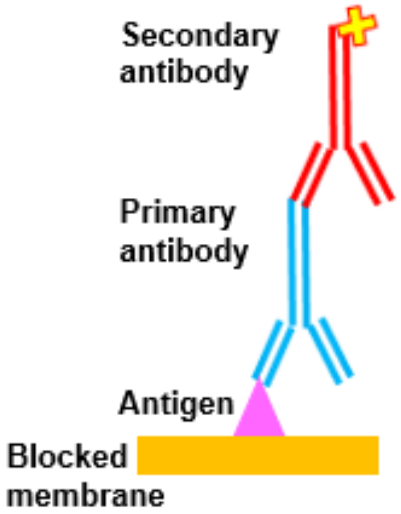

Figure 1-8. Representation of the immunoassay procedure used for protein detection in Western blotting. The membrane is first blocked to prevent non-specific binding, the primary antibody detects the antigen of interest. A host species specific secondary antibody binds to the primary antibody. In this case, the secondary antibody is labeled with a NIR fluorescent dye for detection.

portion of the Western blot, some commercialized systems have been developed to automate[86] and speed up[87,88] the process but often do not reduce antibody consumption. Commercially available technologies have also improved the automation and ease for parallelized Western blot immunoassays.[89,90] For microchip Western blotting, advances in decreasing the sample consumption and analysis time were achieved. The immunoassay portion was still a lengthy process overall lacking a microfluidic solution to the immunoassay (**Table 1-1**).

Table 1-1. Comparison between conventional and microfluidic Western botting steps.

Analysis Component	Conventional Western Blot	Microfluidic Western Blot
Sample Mass	10-50 µg	400 ng
Separation Time	~ 1 h	2 - 8 min
Blotting Time	1-2 h	N/A
Immunoassay Time	4-20 h	X

Western blotting binding membranes have porous structures that enable access of probe antibodies to proteins bound to the membrane surface layers. In surface-based immunoassay methods, the antigen and antibody binding are dependent on the transport of the antibody solute to the membrane-solution interface. A boundary layer exists adjacent to the interface; this layer is an undisturbed layer of solution through which mass transport occurs only through diffusion. Proteins are known to have low diffusion coefficients of ~2 x 10^{-7} cm^2/s^1. The antigen-antibody reaction is limited by mass transport of the antibody to the surface for replenishment of consumed antibody near the binding surface.[91–96] As a result, long antibody incubation times are used to achieve maximum detection sensitivity.

The thickness of the surface-interface boundary layer is dependent upon temperature and stirring. Convective (flow) mass transport allows for coupled convective-diffusion transport that can overcome diffusion-limited kinetics. The antigen-antibody binding reaction will occur more

rapidly by decreasing the time limitations of diffusion allowing for faster replenishment of antibody/solute in the surface binding immunoassay. This thesis explores an alternative microscale immunoassay method that use syringe-driven pumping of immunoassay reagents directly on the membrane in order to reduce the analysis time and consumption of antibody reagents.

Dissertation Overview

This research aims to improve microchip Western blotting methods for faster, more sensitive detection of proteins. Rough glass etching issues are addressed where a new microfabrication method is used to improve the reliability of wet etching. From this development, reliable fabrication of a new microchip electrophoresis injection mode with on-line precontraction is presented. Lastly, limitations of the immunoassay portion of microchip Western blotting are overcome by application of a microscale, fast immunoassay method.

In Chapter 2, the investigation of rough etching in borosilicate glasses is described. Stress induced from the substrate manufacturing was hypothesized as the main cause for rough etching; the etching methods of a new source of borosilicate glass was investigated. The improvement in glass fabrication success is critical to reliable microchip gel electrophoresis used in subsequent chapters.

In Chapter 3, a new injection scheme was designed for a fixed length, constant volume sample plug that is simultaneously injected with a leading electrolyte. In this method, the development of on-line electrokinetic supercharging preconcentration was implemented. The sample loadability of microchip Western blotting is increased while maintaining good separation efficiency.

Chapter 4 presents the development of a microscale immunoassay that uses direct deposition of immunoassay solutions to overcome diffusion limitations of the antigen-antibody

reaction. Methods were developed that provided a reduction in assay time from 20 h to 1 h while also reducing antibody consumption for microchip Western blotting membranes.

Chapter 5 discusses future directions for the continued improvement and implementation of microchip Western blotting techniques. Challenges with world-to-chip pressure connections and robust microchip deposition are discussed. Immunoassay parallelization strategies are presented, and small-scale sample preparation is discussed for the application of microchip Western blotting of signaling protein networks in Islets.

Chapter 2 Improved Etching for Glass Microfluidic Device Fabrication

Introduction

The introduction of microfabrication in glass allowed for the adaption of capillary electrophoresis to microchips.[63,64] Photolithographic fabrication in glass substrates allows for the etching of almost any shape channel, including branched channel systems, for integration of multiple analyses steps including sample preparation, sample injection, separations, detection and more.[97,98] Wet etching, which is mainly performed in HF-based or KOH-based solutions, typically will produce smooth etching in glass which can be etched to various depths.[70] Although wet etching is commonly used for microfabrication of glass devices, there are many issues that can arise and parameters that must be optimized. Problems in achieving good, repeatable separations occur when roughly etched microchips are used.

Components that influence glass fabrication include the following factors: substrate composition, glass manufacturing methods, and the influence of stress in the masking layer. Ultimately, these factors will influence the quality of the surface generated from wet etching.[70,71] Most literature available on fabricating borosilicate glasses, where recent publications date back to early 2000s, used either Corning's Pyrex® 7740 or Schott's Borofloat® 33 glass substrates. These two materials have similar properties to one another. For decades, Borofloat was a reliable glass etching substrate; however, etching current batches of Borofloat glass has yielded a high failure rate due to various forms of rough etching including spikes across channels and dendritic

crystals. The composition and manufacturing of the starting glass material is critical to the etching outcome of microchannels.

We investigate causes of rough etching including the effect of glass substrate annealing on improving rough etching and etching of a different form of borosilicate glass (D263®). Limited publications have discussed HF etching and microfabrication of D263 glass. One of the first reports indicated it yielded in poor/rough etching outcomes; while the second report briefly presented methods for D263 microfluidic device fabrication.[71,99] The advantages of D263 over Borofloat were not particularly highlighted. In this work, we found significant advantages to switching to D263 glass.

Materials and Method

Chemicals and Materials

AZ 726MIF developer and CR-1A chrome etchant were from Microchrome Technologies, Inc. (San Jose, CA). All water used was deionized (DI) water. All other chemicals were from MilliporeSigma (St Louis, MO).

Glass Etching

D263 glass slides (1 in. × 3 in.) that were 500 μm thick were coated with a layer of chrome and a layer of 5300Å AZ1500 photoresist (Telic Company, Valencia, CA). A photomask (Fineline-imaging, Colorado Springs, CO) was used to pattern the resist by exposing it to UV light for 9 s (Optical Associates, Inc., Milpitas, CA). The exposed glass slide was developed with MIF 726 developer for 40 s and rinsed in water. The glass was then placed in CR-1A chrome etchant for 2 min and rinsed with water after. The backs of the glass slides were covered with HF resistant tape (Semiconductor Equipment Corporation, Moorpark, CA). An etching solution of 1:1:2 (v/v/v) HF/HCl/H_2O was used to etch the glass at a rate of 4 μm/min.

Device Fabrication

After etching, access holes were drilled with a 400 μm drill bit (Kyocera, Costa Mesa, CA). One drill bit can be used for hundreds of access holes with D263 due to the softer properties compared to Borofloat. Both etched and drilled glass and blank pieces of glass were placed in a 3:1 (v/v) H_2SO_4/H_2O_2 piranha solution for 20 min. Piranha solution should never be mixed with solvents as it can be aggressive and explosive. The slides were rinsed in water and placed in an "RCA" solution 5:1:1 (v/v/v) $H_2O/NH_4OH/H_2O_2$ at 140°C for 40 min. The slides were rinsed with water, aligned/contacted together, and dried with N_2. The contacted D263 slides were dried in a 70°C oven for 6 h or overnight. The devices were then placed between two Macor ceramic plates (Ceramic Products, Inc, Palisades Park, NJ) with a 400-g stainless steel weight placed on top of the ceramic plates. Using a programmable kiln (Model number 810, Evenheat Kiln, Inc., Caseville, MI), the devices were thermally bonded by ramping the temperature of the kiln at 300°C/h to a temperature of 560°C. This temperature was held for 8 h, and the kiln ramped down to room temperature at 10°C/min.

Results and Discussion

With Borofloat glass substrates, a large increase in cases of rough etching have occurred. Rough etching of glass microchannels for microchip gel electrophoresis render the separation nearly impossible. When attempting to run a separation of a seven protein, FITC-labeled molecular weight ladder mixture no peaks were resolved (**Figure 2-1).** Previously, glass rough etching would

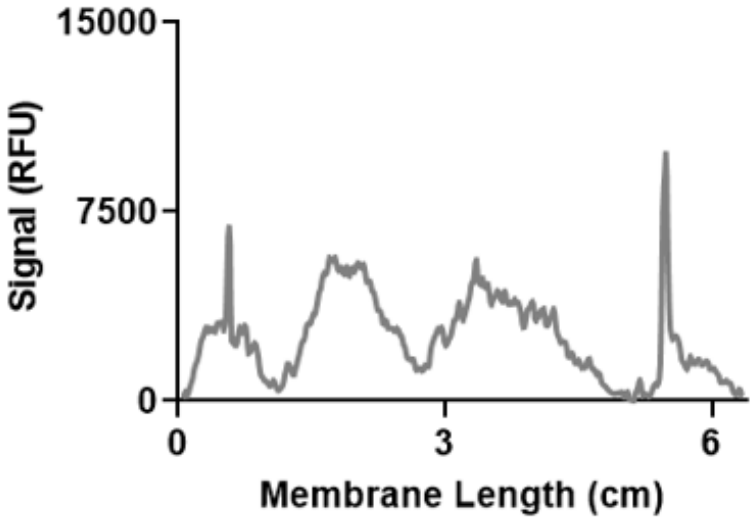

Figure 2-1. Poor microchip gel electrophoresis separation in a roughly etched microchip.

occur when etching deeper channels (>75 μm). This outcome was hypothesized to be caused from stress in the sacrificial Cr layer. Annealing glass substrates has been shown to alleviate some of the surface issues of borosilicate glass to reduce rough etching. With glass substrates that were coated with the Cr mask layer, annealing in a kiln at 310°C for 3 h was done to alleviate surface stress. After annealing and photoresist spin-coating, HF etching then resulted in devices with improved etching.

In recent years of glass batches and etching, however, many different forms of rough etching appeared and increased in occurrence. Rough etching no longer only affected deep etching/deep etching rates; it also affected slower etching rates to depths of 15 μm. **Figure 2-2** displays various forms of rough etching in Borofloat glass that have been observed. It was

estimated that rough etching would occur in at least 90% of glass devices for a batch of 12 devices. This outcome was consistent between various glass batches, fabrication days, etching solution mixtures, and with use of fresh reagents.

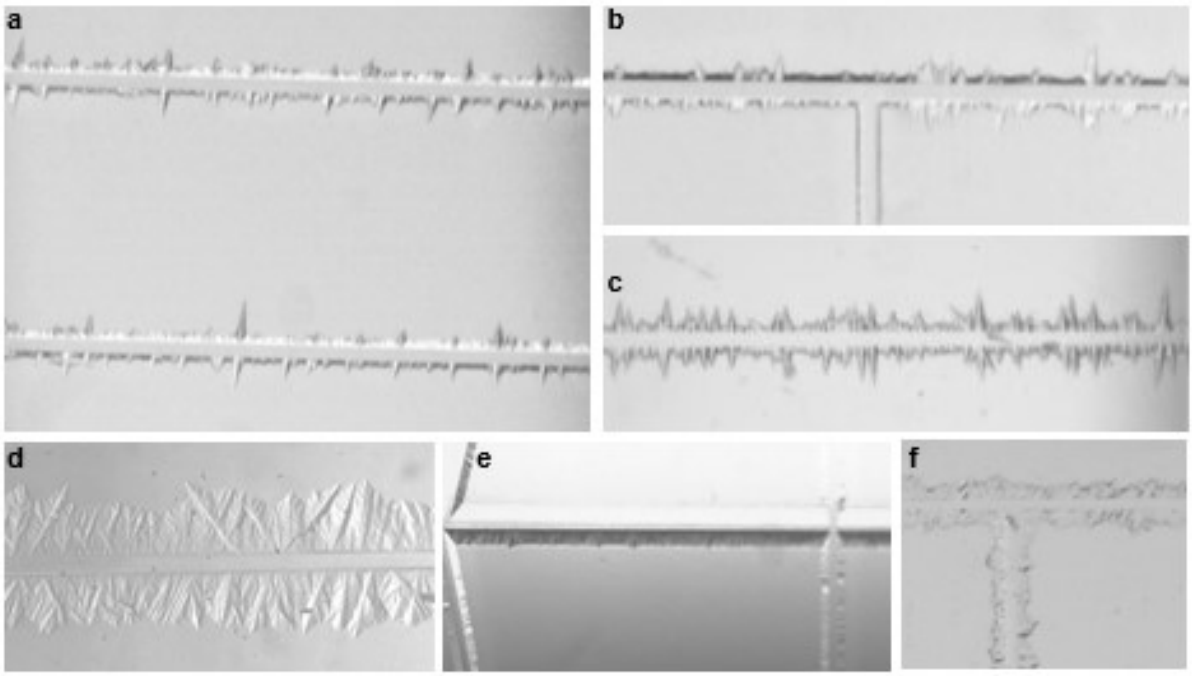

Figure 2-2. Various forms of rough etching observed in Borofloat glass. A heavy occurrence of channel spikes occurred most often (a-c). Other forms of rough etching were also observed (d-f).

Re-investigation of annealing Borofloat substrates was done to further asses the sources of rough etching. Annealing of Borofloat glass substates bare can be performed at 560°C for 1 h. When the glass has a Cr layer deposited, a method of 310°C for 3 h was previously employed. We compared the two annealing procedures of blank glass slides. Utilizing low pressure chemical vapor deposition (LPCVD) to deposit the Cr layer after each annealing procedure was performed with blank Borofloat glass. This only improved device fabrication to a success rate between ~ 45% for n=3 of each procedure tested (**Figure 2-3**). Even with improved etching some small notches or defects were observed. There was not a clear indication for the batches tested if one annealing method was better than another for the blank glass substrate.

With investigation of the effect of annealing on improving rough etching in current batches of Borofloat glass, some improvement was seen. However, this fabrication process required more steps while not resulting in a repeatable fabrication procedure. These results confirmed a second hypothesis for what could be causing the latest forms of rough etching that the main sources rough etching was due to the manufacturing of the glass substrate. It was suspected that the process used to float borosilicate glass could be inducing stress in the material. This hypothesis was further supported by the randomness of rough etching and varying results that repeatedly occurred.

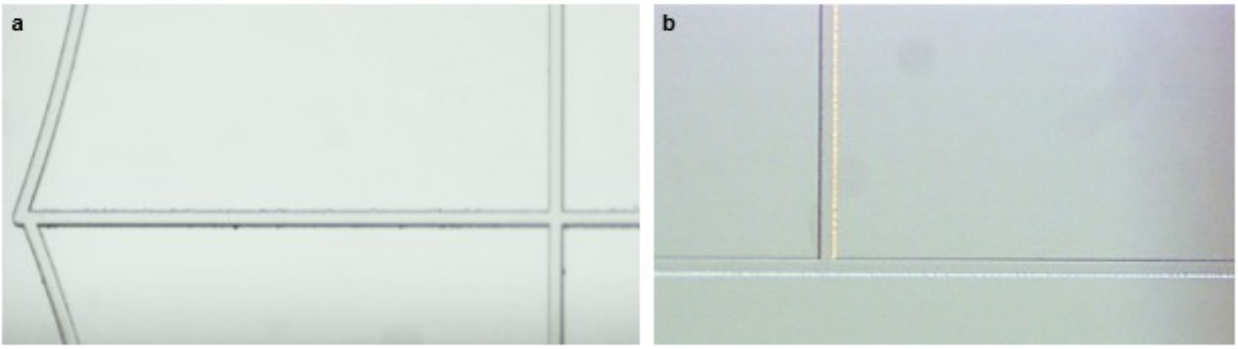

Figure 2-3. Etching of an annealed Borofloat substrate (a) with previous batches of Borofloat glass (b).

The type and final form of glass that is manufactured will be result of the quality of raw materials, composition of raw materials, the way in which heat was applied, and the melting process that was used. The composition of a low-expansion borosilicate glass is approximately 81% SiO_2, 13% B_2O_3, 4% Na_2O/K_2O, and 3% Al_2O_3.[100] Manufacturing of borofloat is achieved through a floated glass production method. The molten glass spreads out across a liquid tin float bath to form a flat surface where it cools. The glass is drawn to form glass ribbon where the drawing speed determines the glass thickness. The resulting flat, parallel glass undergoes rollers across the top of the glass sheet over a long annealing furnace lehr. The glass is pulled and/or stretched to a thinner finished substrate. D263 is a low-alkali borosilicate glass. Although the exact composition was not listed but these slight differences in composition results in slightly lower

thermal properties in comparison to borofloat. This glass is also manufactured in a newer process called a down draw method which is used for producing thin, ultra-clear flat glass substrates. Molten glass is pulled down to form the ribbon and immediately rolled down through an annealing furnace. The glass ribbon is pulled again through rollers and allowed to cool. This method improves manufacturing thin glass substrates (hundreds of micrometers thin) with a flawless surface with roughness <0.5 nm.

When implementing HF etching methods for D263, we observed nearly 100% smooth etching of the material routinely (**Figure 2-4**). This result was consistent between different glass batches, fabrication days, and etching solution mixtures. Switching to etching of D263 glass confirmed that the difference in manufacturing methods between Borofloat and D263 borosilicate glasses influence the outcome of HF wet etching. The development of D263 etching methods proved to be a successful change of glass substrate. New wet etching rates and thermal fusion binding conditions were investigated to implement a microfabrication method with a high, nearly perfect success rate while following the same photolithography and other fabrication steps

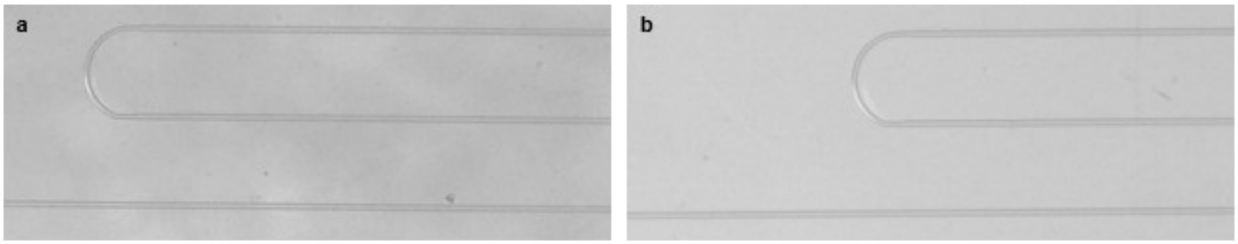

Figure 2-4. Images of D263 (a) and Borofloat (b) with smooth etching.

previously used with Borofloat glass. With D263 glass coated with CR and AZ1500 photoresist, photolithography was performed as previously described.[98] Utilizing a 1:1:2 HF:HCl:H_2O etching solution produced an etch rate of 4 μm/min for 0.5 mm thick D263 glass. This procedure was used to etch channels resulting in a depth of 15 μm and a width of 50 μm. Deep etching is also easy to achieve in D263 glass. **Figure 2-5** compares the deep etching of the two substrates. For Borofloat,

an etch rate of 4.4 µm/min was used to etch to ~78 µm with very poor results. The new protocol with D263 and an etch rate of 4 µm/min produces smooth channels to a depth of ~80 um.

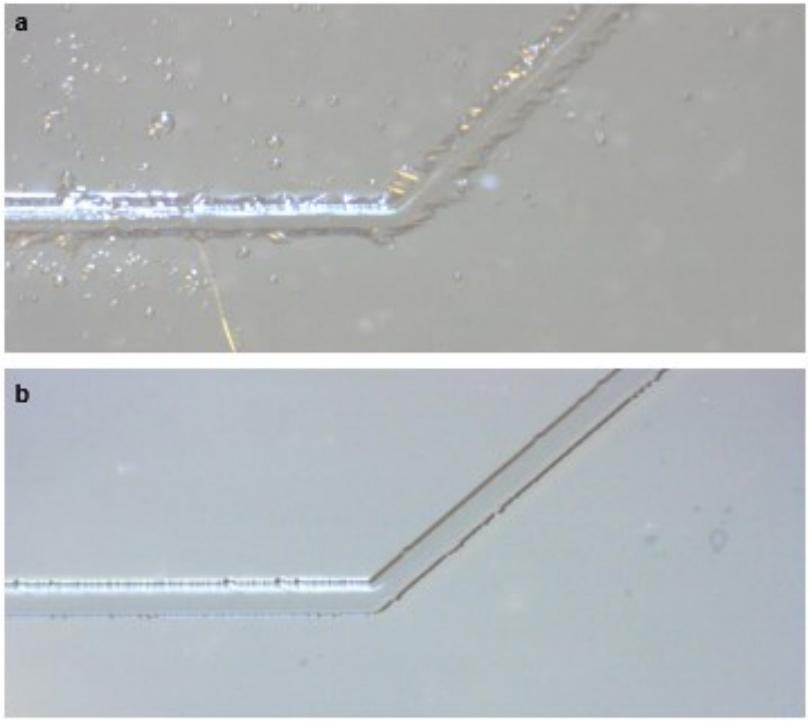

Figure 2-5. A comparison between Borofloat and D263 with deep etching. The Borofloat substrate was etched with 96 mL HF, 17 mL nitric acid, and 7 mL water providing an etch rate of 4.4 µm/min and the channel was etched to approximately 78 µm (a). The D263 substrate was etched with 25 mL HF, 25 mL hydrochloric acid, and 50 mL of water providing an etch rate of 4 µm/min and the channel was etched to approximately 80 µm (b).

When comparing the thermal properties of the two borosilicate compositions, they vary in their glass transition temperatures and temperature sensitivities (**Figure 2-6).** Both materials thermal bonding procedures can be sensitive to any water remaining in the etched channels prior to bonding in kiln. In good practice, Borofloat slides are dried in a 70°C oven for two hours. With D263, the devices must be allowed to dry in a 70°C oven for at least 6 h or overnight; otherwise, the devices shattered in the kiln. **Figure 2-6** compares the T_g of Borofloat versus D263 which values are 525°C and 557°C, respectively. Plotted with that value are the differing kiln program methods followed to thermally bond microchips for the different glass compositions. Thermal

bonding methods for Borofloat commonly were ramped up to 610-650°C. For D263 thermal

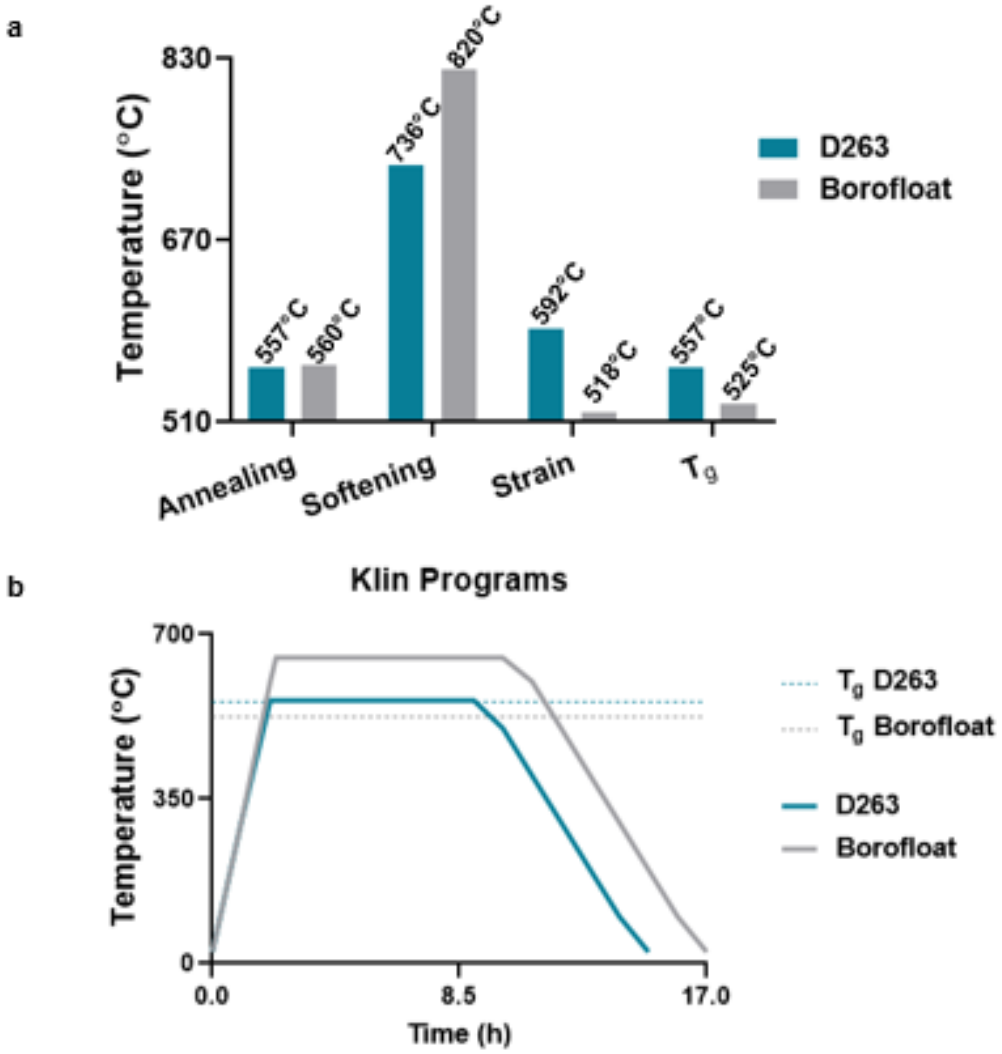

Figure 2-6. Thermal properties of both glass materials (a). Thermal bonding method for Borofloat utilized the following temperature program: ramping of kiln at 300°C to 650°C, holding 650°C for 8 h, heat dissipation to room temperature. Thermal bonding method for D263 utilized the following temperature program: ramping of kiln at 300°C to 560°C, holding 560°C for 8 h, heat dissipation to room temperature (b).

bonding, if the temperature exceeds **5**60°C the glass melts. After successful fabrication methods for D263 were developed, these microchips were implemented for microchip electrophoresis.

Conclusions

An increase in rough etching in Borofloat glass led to failed microchip electrophoresis separations. Annealing methods that can reduce surface stress layer only partially aided in improving to

smoothly etched microchips. The hypothesis that the Borofloat manufacturing and/or processing process was introducing glass in the substrate that could not be easily corrected. By switching to another form of borosilicate glass, which utilized a down drawn process versus floated to form thin glass substrates, the etching of glass was completely improved. Rough etching has not occurred with D263 glass produced by the down draw manufacturing process. Development of these new fabrication methods has solved all previous microfabrication issues. Etching deeper channels in glass can be challenging, but the new glass source also mitigated this challenge. This microfabrication method has allowed for once again performing microchip electrophoresis separations.

Chapter 3 Constant Volume Injection with On-Line Electrokinetic Supercharging Preconcentration for Increased Sample Loadability in Microchip Western Blotting

Introduction

Electrophoretic stacking methods are used with capillary zone electrophoresis (CZE) to preconcentrate samples and enable better sensitivity.[75–77] One of the most effective on-line preconcentration methods for protein separations is electrokinetic supercharging (EKS). EKS combines field amplified sample stacking (FASI) and transient isotachophoresis (tITP). FASI provides substantial stacking in samples with low conductivity; but injection times are limited to avoid band broadening.[39] In EKS, tITP is used to refocus bands after FASI allowing more extensive preconcentration without deleterious band broadening. In tITP, a leading electrolyte (LE) plug is positioned in front of the sample plug and a terminating electrolyte (TE) is introduced behind the sample plug. The LE has a higher effective electrophoretic mobility than the sample components, while the TE has lower electrophoretic mobility then the sample components.[39,101] The sample plug forms focused/concentrated zones in order of electrophoretic mobility in between the LE and TE. The self-sharpening effect between the boundaries of adjacent analyte zones counteracts diffusion and makes tITP resistant to band broadening.

EKS has been mostly used with CZE due to the simplicity of coupling CZE with ITP. Many applications including the analysis of trace inorganic cations, weak organic acids, chemical pollutants, non-steroidal anti-inflammatory drugs, and biomolecules (peptides, DNA, and proteins) amongst others have been reviewed.[102] For these applications, signal enhancements of

1000- to 500,000-fold have been reported. However, many of these applications do not demonstrate real sample analysis with one report of plasma samples. EKS could be highly beneficial for protein analysis, especially when coupled to selective detection. Nevertheless, reports applying EKS for the separation of SDS-protein complexes by capillary gel electrophoresis (CGE) and microchip gel electrophoresis (MGE) are sparse.[102]

MGE has been combined with tITP and demonstrated on a mixture of FITC-labeled SDS-proteins ranging from 31-78 kDa.[103] An EKS preconcentration method for MGE applied to a standard mixture of SDS-protein complexes ranging from 14-97 kDa resulted in a 30-fold improvement on the detection limit.[104] The use of a T channel design in this application required manual intervention between loading the sample, LE, and TE. Some of these manual loading limitations were avoided by implementing an autosampler with the microchip electrophoresis device.[104] In comparison to a conventional cross-chip MGE method, a 30-fold enhancement in sensitivity level was obtained. These pioneering papers illustrate the potential of coupling EKS with MGE for protein analysis. Further development and exploration are warranted based on these results. At present, EKS-MGE has yet to be reported with detection in complex biological samples.

Double-T injection designs on microchips allow for larger sample plug formation.[105] This injection style involves pinching[106] the sample into the analyte waste reservoir by applying potentials from the analyte and buffer to the analyte waste. Initially only the fast-moving analytes will be in the cross; however, after sufficient time all analytes will migrate into the cross at representative concentrations. This injection approach has also been referred to as a constant volume injection (CVI).[34] Thus, the inherent bias of EKI can be overcome by introducing such sample plugs for microchip electrophoresis.

In this work, we report the use of a microfluidic network that allows for EKS to be performed without replacement of the reservoir buffers due to dedicated channels for each the sample and LE. The chip also uses a fixed length sample channel for CVI. Combining the CVI with on-line EKS preconcentration allows for restacking of the large sample plug before electrophoretic separation. The development of CVI EKS microchip electrophoresis is further explored for microchip Western blotting. These methods were developed for application to the detection of protein in cell lysates.

Materials and Methods

Chemicals

All buffers were made using 18 MΩ water deionized by a Series 1090 E-pure system (Barnstead Thermolyne, Dubuque, IA). FITC-protein ladder containing 7 proteins with masses from 11 kDa-155 kDa with a total protein concentration of 1 mg/mL was from Invitrogen (LC5928, Grand Island, NY). Anti-β-tubulin antibodies were from Millipore Sigma (St Louis, MO). Anti-MAPK (Erk 1/2) and anti-Stat3 antibodies were from Cell Signaling Technology (Danvers, MA). A431 cell lysate, goat anti-rabbit secondary antibody, goat anti-mouse secondary antibody, and blocking buffers were from LI-COR Bioscience (Lincoln, NE). Radioimmunoprecipitation assay (RIPA) lysis buffer, sodium chloride, tris base, and a protein 660 nm assay were from Fisher Scientific (Hampton, NH). All other chemicals were from MilliporeSigma (St Louis, MO).

Sample and Reagent Preparation

The A431 cells were lysed with RIPA buffer and denatured in 2% sodium dodecyl sulfate (SDS) and 2.5% β-mercaptoethanol with heat at 95°C for 5 minutes. After cooling to room temperate, the cell lysate was further diluted 100-fold in water and filtered several times by centrifuging at 12,100 x g for 10 min using Amicon® Ultra Centrifugal Filters with a 10 kDa cut off from

Millipore Sigma (St Louis, MO). The concentrated filtrate protein was collected from the filter. The final concentration was measured using a protein 660 nm assay. For gated injection microchip Western blotting, the sample was mixed with 1.5 µL FITC-ladder and diluted with water to 50 µL. For constant volume injection (CVI), the sample was mixed with 0.5 µL FITC-ladder and diluted with water to 100 µL. The gel sieving matrix was 800 mM tris-borate, 2 mM EDTA disodium salt, 0.2% (w/v) SDS, 10% (w/v) sorbitol, and 10% (w/v) dextran (1,500-2,800 kDa). The leading electrolyte was 800 mM Tris/HCl pH 7.6. Tris buffered saline with Tween 20 (TBST) was made with 137 mM NaCl, 2.7 mM KCl, 190 mM Tris, and 1% (v/v) Tween 20.

Microchip Electrophoresis and Western Blotting

Glass device fabrication was achieved by etching 0.5 mm thick D263 glass slides and bonding to a blank glass slide (Telic Company, Valencia, CA). Channels were etched to a depth of 15 µm, a width of 50 µm, and the post-separation channel to a width of 90 µm. Gated microchips were fabricated with a 4 cm long separation channel. CVI microchip were fabricated with an 8 cm long separation channel (Figure 1**)**. The microchips were diced using an ADT 7100 series dicing saw (Horsham, PA) to create a point and outlet in the post-separation channel that interfaced with two sets of sheath flow channels. The inner set of sheath channels had sieving gel pumped through at 30 nL/min to deliver eluted proteins to the binding membrane. The outer set of sheath channels provided the ground electrical contact at the end of the separation channel. The microchips were interfaced directly with a strip of nitrocellulose membrane. A USB microscope was used to monitor the contact with the membrane. During the separation an XY-translational stage was moved at 4 mm/min for the separated proteins to deposit on the membrane.

Microchip conditioning solutions were filtered with 0.22 µm syringe filter. The channels of the microchip were conditioned by filling the reservoirs sequentially with 1 M NaOH (20 min),

water (5 min), 1 M HCl (20 min), water (20 min) and gel sieving matrix (minimally 60 min) by applying vacuum to pull from one reservoir at a time. Due to the multiple injection side channels, it was necessary to alternate applying the vacuum between three or more different ports for each step. The gel loading step required the most time, mainly due to limited access to the separation channel from one side channel/reservoir. It was necessary to pull gel from almost every port for the most robust chip preparation.

For gated microchip electrophoresis, -2.0 kV was applied at the gating reservoir; -1.5 kV was applied at the sample reservoir with a separation field of 315 V/cm using a home-built relay system. A gated injection of 30 s was used for A431 cell lysate. For CVI microchip electrophoresis, a high voltage sequencer was employed (LabSmith, Livermore, CA). For the sample and LE injection, -200 V and -400 V were applied producing field strengths of 178 V/cm and 218 V/cm, respectively. The first injection of the microchip run typically required the longest injection equilibrium time (up to 8 min). Otherwise, an injection time of 4-5 min was used. The separation was first applied with -3 kV from the top reservoir producing a field strength of 288 V/cm. The separation can also be performed from a secondary separation location. When applying the voltage from the side separation channel, the field strength was 340 V/cm. An Olympus IX71 (Tokyo, Japan) fluorescence microscope was used for on chip detection of the FITC-labeled protein ladder.

Immunoassays

After separations, the membranes were scanned for detection of the FITC-protein ladder using an Amersham Typhoon NIR Plus (GE Healthcare, Pittsburgh, PA) with 488 nm fluorescence measurement. Immunoassays were completed at room temperature with gentle shaking unless otherwise noted. The membranes were blocked with Odyssey® blocking buffer for 1 h; primary antibody incubation was applied overnight in a 4°C fridge with primary antibodies diluted 1000-

fold in Odyssey® blocking buffer; and TBST was used for washing away excess antibodies four times at 5 min. each; secondary antibodies diluted 10,000-fold in Odyssey® blocking buffer and 0.05% Tween 20; and finally four washes at 5 min each with TBST were done. Secondary antibodies were provided with either 680-nm dye or 800-nm dye conjugation from LI-COR Bioscience. After the immunoassay, an Odyssey® near-IR fluorescence imager at 700 nm and 800 nm was used to scan the membrane and results (LI-COR Bioscience, Lincoln, NE). Line scans were generated using ImageJ (NIH) and imported into Cutter 7.0 software.[107] After a baseline correction, a median filter of 2.0 pixels was applied. The noise was selected from the baseline in between peaks. Peak heights were measured for calculating signal-to-noise (S/N) ratio. Data was plotted in GraphPad Prism 8 where an average and standard deviation were calculated. A relative standard deviation (RSD) was plotted as an error bar.

Results and Discussion

Development of CVI Microchip Gel Electrophoresis with EKS

In microchip electrophoresis, electrokinetic injection (EKI) is the most common injection method; however, EKI suffers from sample bias in comparison to hydrodynamic injections. Pressure injections on microchips are complicated to implement due to having branched channels with open access to the separation channel.[73,108] In this work, a fixed length sample plug was formed through electrokinetic sample injection into two ground, side channels resulting in a constant volume injection sample plug (**Figure 3-1**). The sample plug was introduced under FASI conditions. A designated LE channel was used to allow LE to be loaded simultaneously with the sample plug. The design allowed a fixed length leading electrolyte plug to be inserted upstream the sample plug (**Figure 3-1b**). Voltage was applied to pinch this plug against the waste channel and prevent leakage into the separation channel. After 4-8 min of loading we found that stable current values

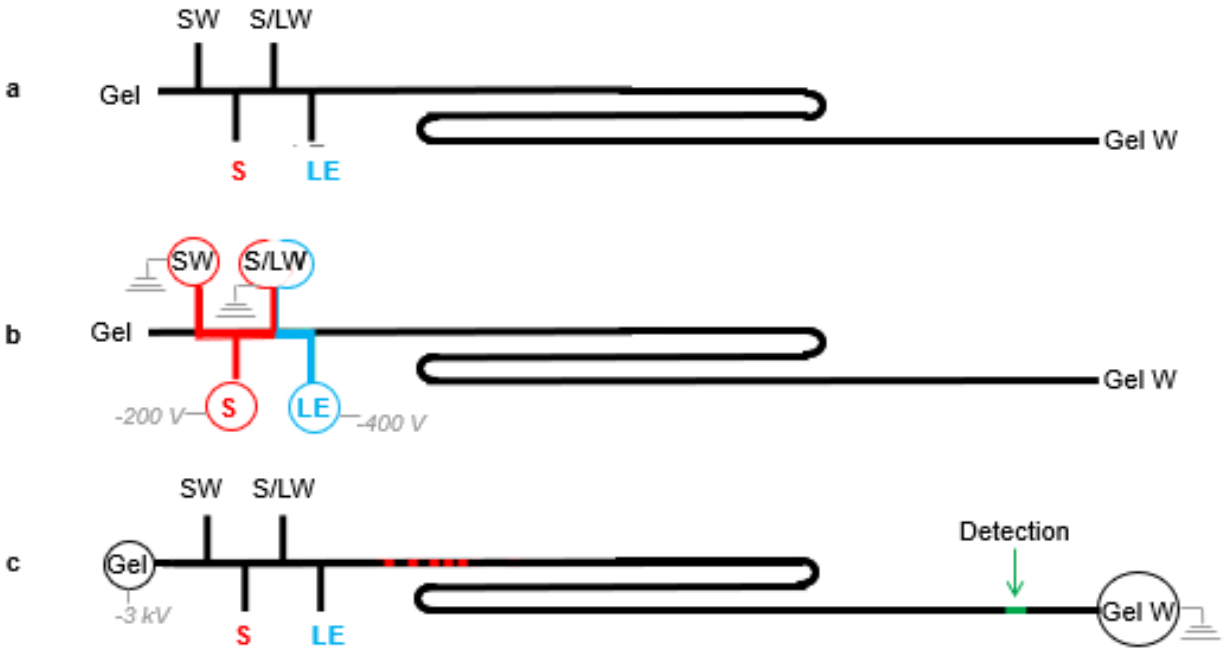

Figure 3-1. Schematic representation of the steps of EKS after filling the microchip channels with gel, sample (S) and leading electrolyte (LE) (a). The S is injected into two waste channels (SW and S/LW), and the LE is injected into the S/LW channel simultaneously (b). The separation is then applied from the top gel channel and separated proteins are detected at the end of the separation channel before the gel waste (Gel W) channel (c).

were reached (**Figure 3-2**). With application of the separation voltage (**Figure 3-1c**), tITP was initiated, completing the EKS injection, and eventually electrophoresis resulted in a size-based separation of SDS-protein mixtures. In MGE with on-chip detection, the fluorescent signal of the analytes was recorded to capture the separation before the end of the separation channel.

Design of this CVI EKS method began with sample injection scheme development. In pilot experiments, the length of the sample plug was extended to 6.8 mm while the separation channel was 8 cm in length. This plug length was found provide high signal without compromising separation efficiency. It was important to extend the sample plug formation from one side ground channel to two (**Figure 3-1b**). This change improved the sample pinching from the two sides of the formed sample plug into the ground side channels (the LE side and the gel side).

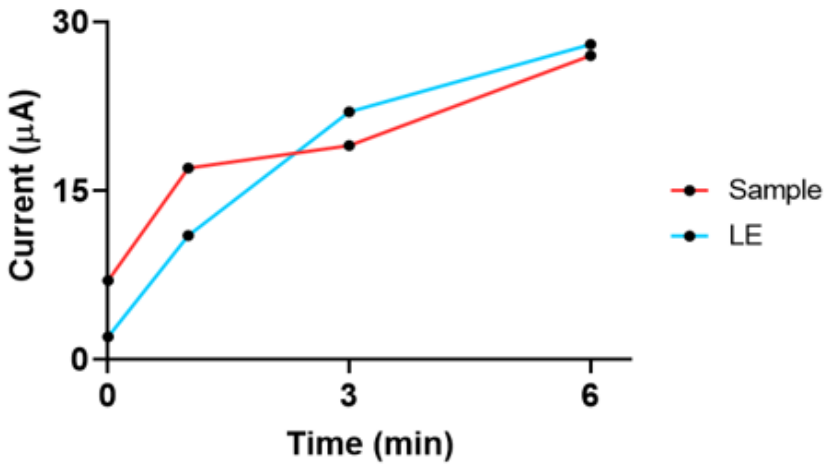

Figure 3-2. Current profile for the injection of sample and leading electrolyte.

The degree of the concentration effect of tITP can be derived from the Kohlrausch equation:

$$\frac{C_L}{C_A} = \frac{\mu_L}{\mu_L + \mu_R} \frac{\mu_A + \mu_R}{\mu_A}$$

where C_L is the molarity of the leading electrolyte, C_A is the analyte's concentration in the stacked sample zone, and μ is the electrophoretic mobility where μ_R refers to the counterion. From this equation, it can be concluded that the final concentration of the analyte is largely proportional to the initial concentration of the leading ion. Tris/HCl, where Cl^- serves as the LE, is commonly used as a leading ion for negatively charged analytes. The concentration of 800 mM Tris/HCl produced the highest enrichment while not causing Joule heating. At this concentration, the LE injection current did not exceed <30 μA; current values above this limit could result in Joule heating. The formation of a sample vacancy zone resulted in a sample/system-induced "OH^-" TE to allow tITP.[109]

With on-chip fluorescence detection, a comparison between signal enhancement from CVI with EKS was compared for a protein ladder mixed with cell lysate and diluted 200-fold in water (**Figure 3-3a**). In comparison to CVI with no stacking, an average 54-fold enhancement for the

ladder protein signal peaks was observed. **Figure 3-3b** displays signal height comparisons between CVI EKS, no stacking, and gated injection. For both no stacking and gated injections, a downward trend resulted when plotting the signal in order of the smallest ladder protein (11 kDa) to the largest protein (155 kDa). For example, the first peak (11 kDa) had a peak height that was 3-fold and 10-fold higher than the slowest migrating peak (155 kDa) for no stacking and gated injections, respectively. This disparity, while possibly due in part in differences between concentration, was

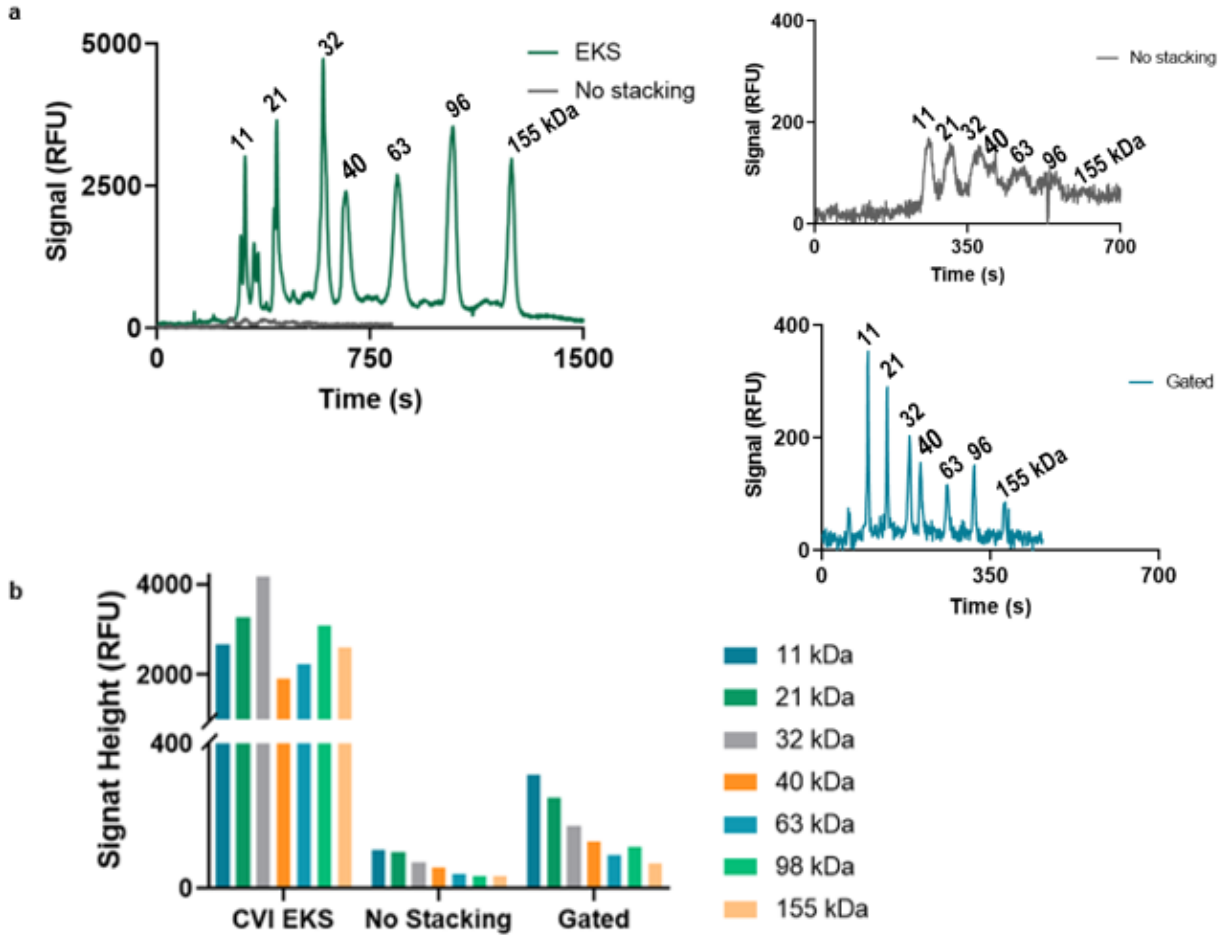

Figure 3-3. Electropherograms showing the enhancement in detection sensitivity of (6.8 mm sample plug, sample: protein ladder mixed with cell lysate and diluted 200-fold in water) vs. conventional injection (no stacking, cross injection 100um plug, sample: protein ladder 1:1 in cell lysate without dilution. Electropherogram with on-chip detection of the protein ladder with a gated injection from a 4 cm separation channel where bias against larger proteins is seen (a). Representation of the non-discriminating nature of the CVI EKS injection scheme is displayed by comparing the signal heights for each injection (b).

driven largely by injection bias. In contrast, with CVI EKS injection the peak heights are relatively uniform (**Figure 3-3**). For example, the first peak and last peak had approximately the same height. These results illustrate the relatively low bias against slow moving analytes in the CVI EKS injection. The CVI EKS method also increased the sample loadability while maintaining good separation resolution. For on-chip microchip electrophoresis repeatability of the CVI method with RSDs < 3.0% (**Table 3-1**). The resolution between the third and fourth peaks of the protein ladder was 1.11 and 1.0 for CVI EKS and gated methods, respectively.

Table 3-1. RSD% for migration time and peak area of the seven proteins of the ladder.

Protein ladder (kDa)	Within-day RSD% (n=5)			Between-day RSD% (n=5)		
	Migration Time	Peak Area	Peak Height	Migration Time	Peak Area	Peak Height
11	0.97	1.27	2.38	1.31	1.99	2.89
22	0.78	1.58	2.39	1.25	1.96	2.39
33	0.81	1.33	2.49	1.23	1.94	2.69
41	0.77	1.71	2.67	1.19	2.09	2.55
65	0.89	1.41	2.75	1.21	2.01	2.18
100	1.07	1.39	2.71	1.20	2.16	2.23
155	1.18	1.69	2.87	1.28	2.22	2.98

Application of CVI EKS to Microchip Western Blotting

This new injection method with on-line sample preconcentration was then combined with microchip Western blotting. **Figure 3-4a** displays the CVI Western microchip. To perform Western blotting, the outlet of the chip is dragged across a membrane so that separated proteins can be captured as previously described (*citation*). Two sheath flow channels are added in comparison to the chips used with on-column fluorescence detection (**Figure 3-1**). Fluid pumped through one sheath helps transport the proteins out of the chip. The second sheath channel provides ground for the chip. The chip is diced to a point to help facilitate protein deposition in a narrow

band. **Figure 3-4b** illustrates the design of the Western blotting chip used for gated injections which provides comparison data.

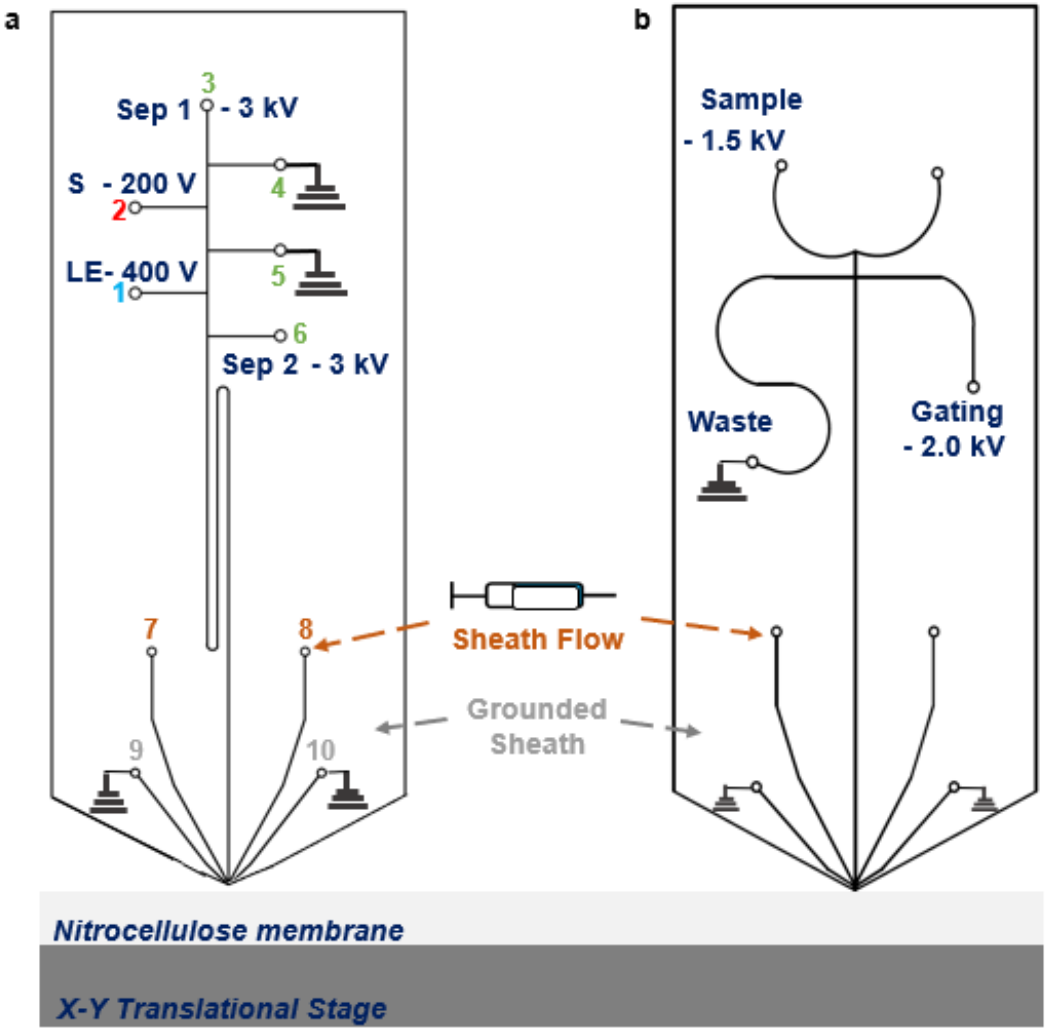

Figure 3-4. Microchip Western blotting microchips with a constant volume injection with on-line preconcentration (a) and gated injection (b). For the constant volume injection, the sample (2) and LE (1) are injected simultaneously. The sample is injected into both ground channels (4-5), and the LE pinches against the sample plug into the ground channel (5). Separation voltage is then applied from the top separation 1 location (3). The voltage can then be applied from the separation 2 location (6) after stacking into the separation channel is complete. Sheath flow at 30 nL/min occurs from (7-8). Grounding sheath are connected to (9-10).

In comparison to the on-column detection chip, the Western blotting chip required more conditioning steps and preparation time. With the un-diced chip in **Figure 3-1**, ease of conditioning and filling the separation channel with gel is achieved more easily due to the direct application of

vacuum at the end of the separation channel. With the diced microchip, the solution may only be pulled from the last side channel of the injection scheme making gel conditioning much more challenging. Pre-conditioning chips uses a vacuum to pull solutions through the channel network for treating the glass (e.g. water, base, buffer) and the separation media. A chip could require 210 min to condition compared to 120 min for that used in **Figure 3-1**. A second separation channel was added (6) to aid in microchip conditioning that also allowed for the separation to be applied post-injection scheme. After applying the separation voltage at the top (3) channel of the injection zone for 5 min, the separation voltage was then applied from the side (6) gel channel. The separated proteins were deposited onto a dry nitrocellulose membrane strip. **Figure 3-5** compares the protein

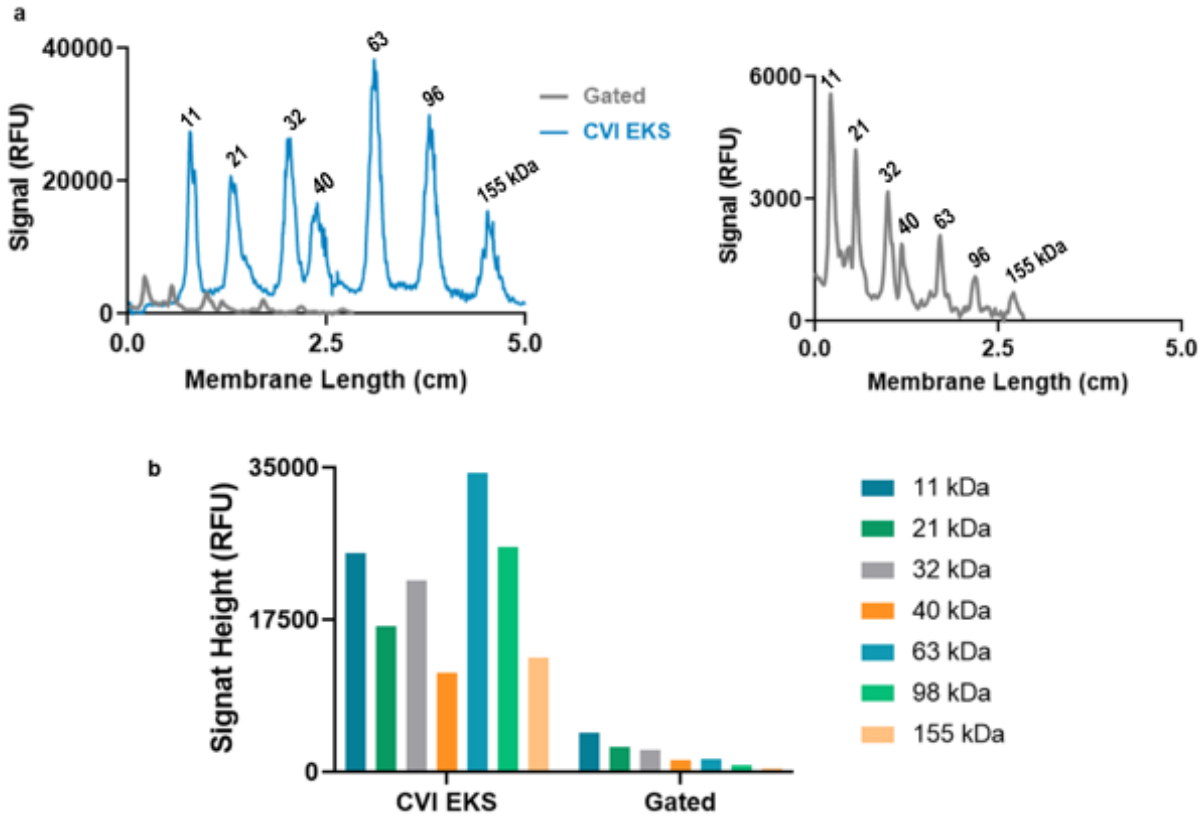

Figure 3-5. Electropherograms showing the enhancement in signal from the CVI EKS Western for the protein ladder versus gated injection Western (a). Representation of the non-discriminating nature of the CVI EKS injection scheme is displayed by comparing the signal heights for each injection mode in microchip Western blotting with the protein ladder (b).

ladder separation between CVI EKS and gated microchip Western blotting. Once again, the results displayed signal height showing a non-discriminating injection mode. Resolution between the third and fourth peaks of the protein ladder was 1.13 and 0.9 comparison between CVI EKS and gated microchip Western blotting, respectively.

This method was applied to the separation and microchip Western blotting of MAPK Erk 1/2 (42/44 kDa) from A431 cell lysate (**Figure 3-6**). The line scans for the detected protein peak were overlaid with the protein molecular weight ladder for both CVI EKS (3 µg/mL) and gated

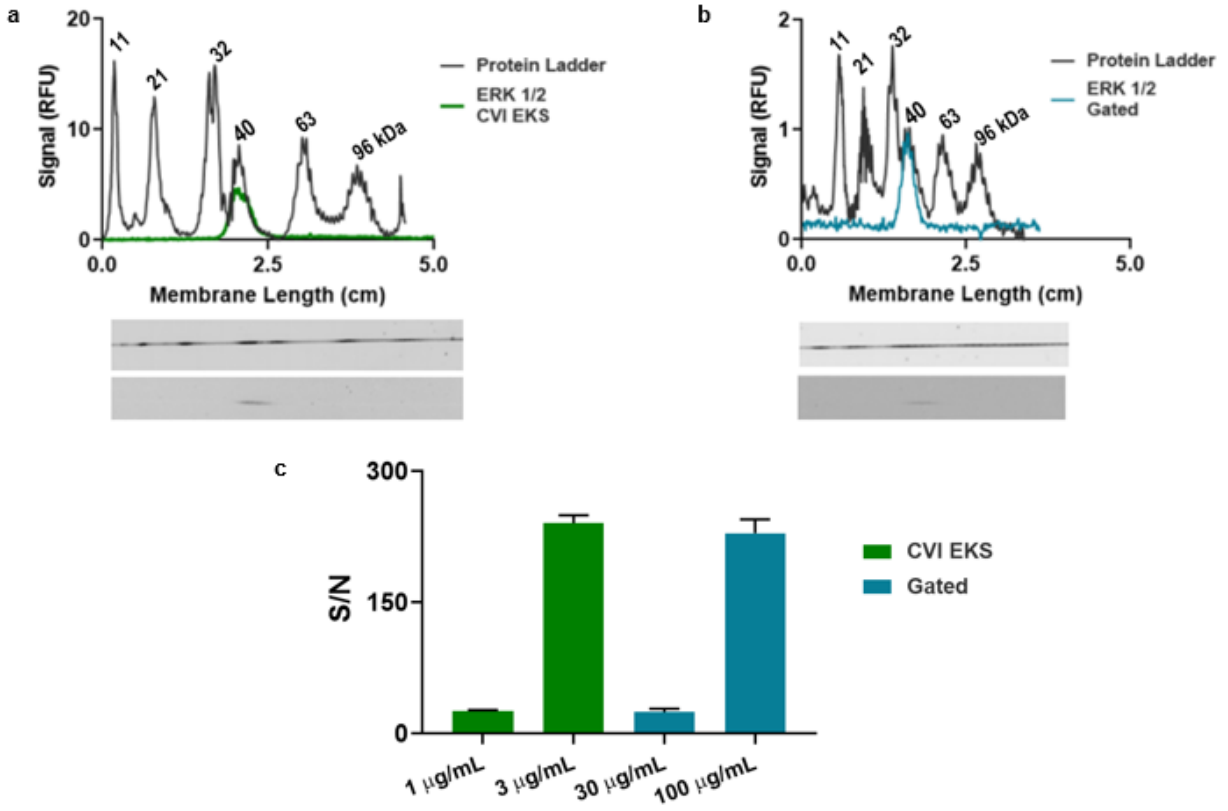

Figure 3-6. Comparison between a CVI EKS Western blotting results with gated Western blotting (a) for the detection of with detection of ERK 1/2 from A431 lysate. In both plots, the line scan for the detected antigen is overlapped with the protein ladder signal line trace. The arbitrary units of the signal intensities of the FITC-protein ladder were divided by 1000 to scale the ladder for the plots above. Membrane images for each ladder scan and detection scan for CVI EKS and gated microchip Western blotting results are displayed below the line traces. The S/N of detection of ERK 1/2 show the enhancement in detection sensitivity for the CVI EKS microchip Western blotting (b). The S/N values calculated and plotted with n=3 injected and detected protein peaks by each method.

injection (30 µg/mL) of A431 lysate (**Figure 3-6a,b**). Below the line scans are membrane images of the protein ladder (scanned at 488 nm) and ERK 1/2 detection (scanned at 800 nm) for the corresponding signal plots. The CVI EKS has a 10-fold better S/N for these injections. The preconcentrating effect of CVI EKS allowed comparable signals to be obtained on ~30-fold less concentrated sample compared to gated (**Figure 3-6c**). For loading the microchip sample for at least n = 3 injections, 15-fold less sample mass is loaded into the CVI microchip.

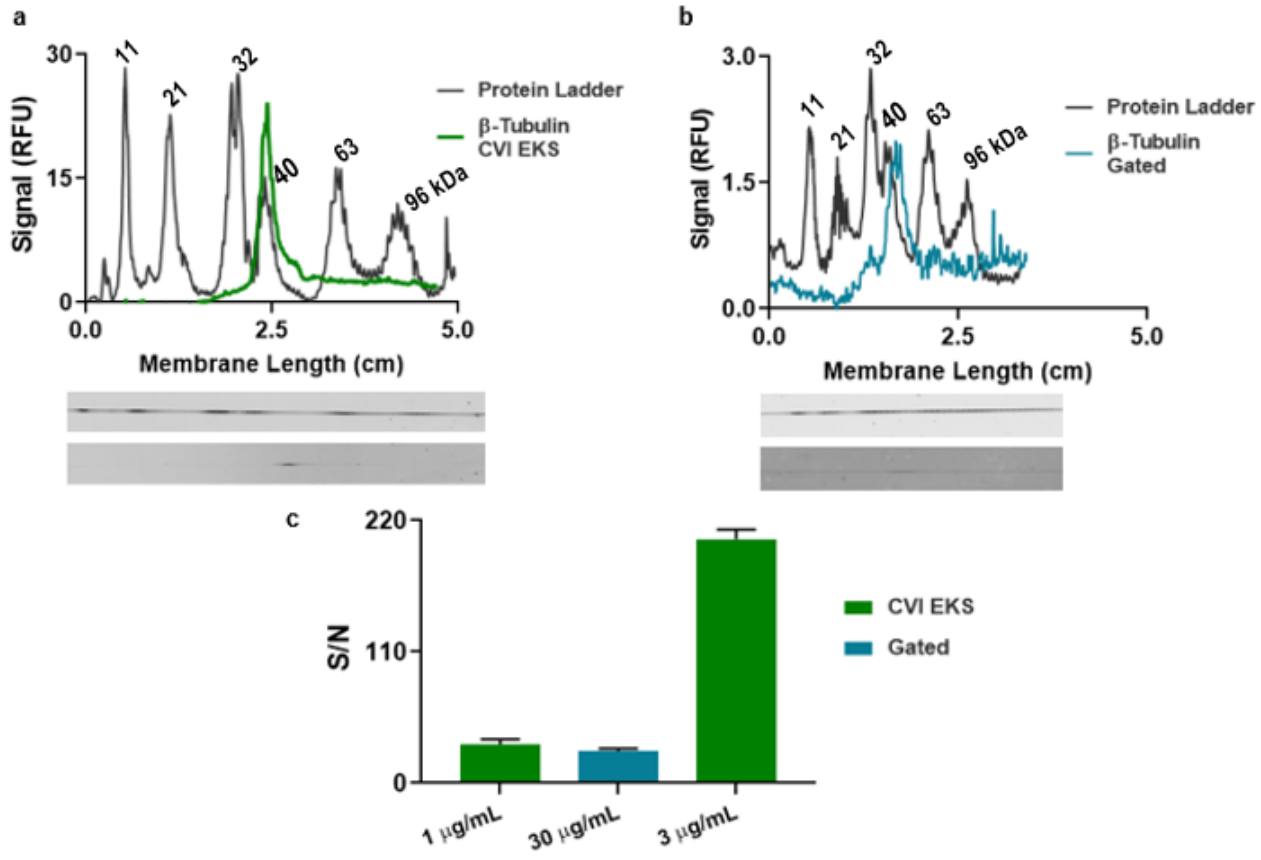

Figure 3-7. Comparison between a CVI EKS Western blotting results (a) with gated Western blotting (b) for the detection of with detection of β-Tubulin from A431 lysate. In both plots, the line scan for the detected antigen is overlapped with the protein ladder signal line trace. The arbitrary units of the signal intensities of the FITC-protein ladder were divided by 1000 to scale the ladder for the plots above. Membrane images for each ladder scan and detection scan for CVI EKS and gated microchip Western blotting results are displayed below the line traces. The S/N of detection of ERK 1/2 show the enhancement in detection sensitivity for the CVI EKS microchip Western blotting (c). The S/N values calculated and plotted with n=3 injected and detected protein peaks by each method.

We achieved similar results for detection of β-tubulin (**Figure 3-7)** and Stat3 (**Figure 3-8**). S/N enhancements were 8-fold and 30-fold, respectively, for these proteins. Sample loadability of microchip Western was increased while the resolution between the third and fourth peaks of the

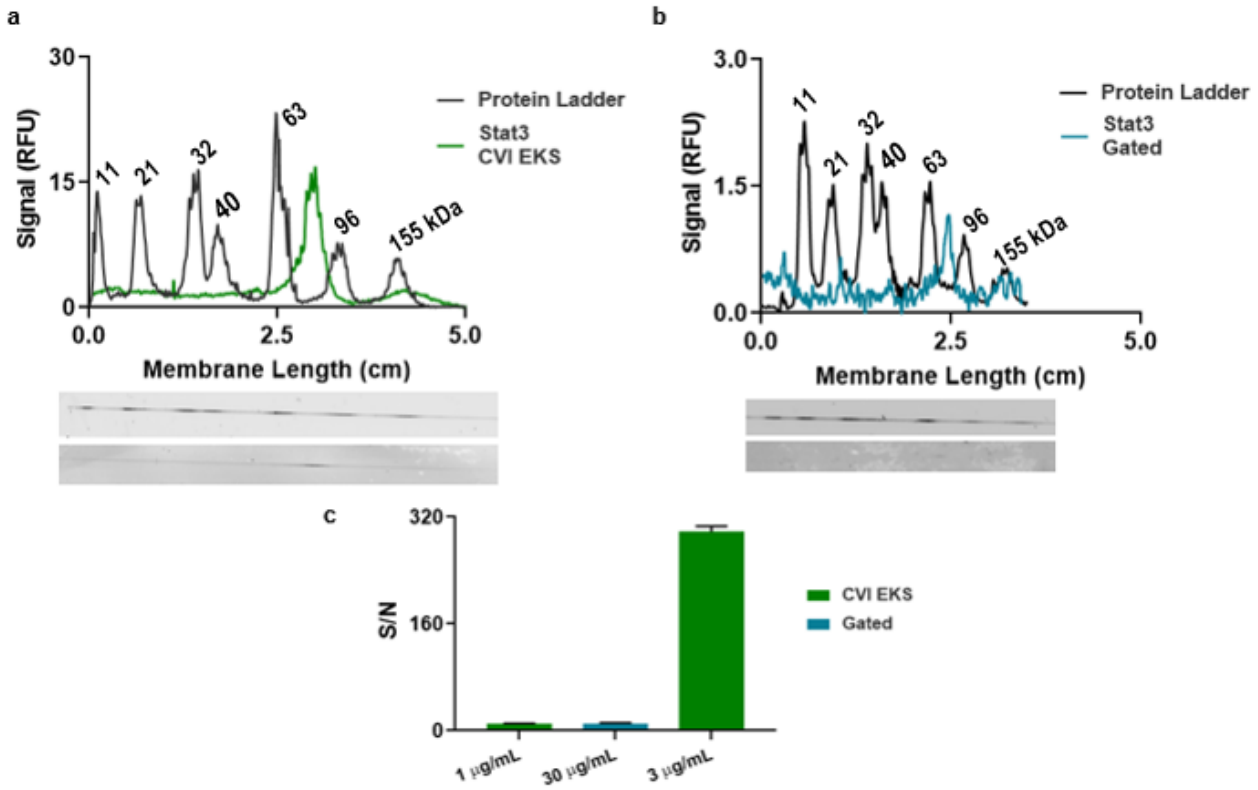

Figure 3-8. Comparison between a CVI EKS Western blotting results (a) with gated Western blotting (b) for the detection of with detection of Stat3 from A431 lysate. In both plots, the line scan for the detected antigen is overlapped with the protein ladder signal line trace The arbitrary units of the signal intensities of the FITC-protein ladder were divided by 1000 to scale the ladder for the plots above. Membrane images for each ladder scan and detection scan for CVI EKS and gated microchip Western blotting results are displayed below the line traces. The S/N of detection of ERK 1/2 show the enhancement in detection sensitivity for the CVI EKS microchip Western blotting (c). The S/N values calculated and plotted with n=3 injected and detected protein peaks by each method.

protein ladder was 0.94 and 0.89. The results indicate the general applicability of this method for determining proteins in complex samples.

Conclusions

This work is the first report of the detection of SDS-proteins from complex biological samples with on-line EKS preconcentration. Particularly, methods for MGE with on-line preconcentration has seen limited application. Compared to previous reports, of using EKS with MGE, this method has increased automation due to inclusion of channels for adding the LE electrokinetically. The use of the fixed sample volume allowed injections with low bias. The method was shown to be compatible with cell lysate samples and microchip Western blotting, thus illustrating the potential for use in complex sample analysis. It also illustrates a new approach to preconcentrating samples for Western blots.

The development of constant volume injection with on-line electrokinetic supercharging preconcentration increased the sample loadability of microchip electrophoresis and microchip Western blotting. By injecting a long sample plug with FASI a LE plug for tITP, on-line EKS preconcentration was achieved. The application of this method to microchip Western blotting resulted in a 30-fold improvement in detection sensitivity through signal enhancement while consuming less sample mass then the gated microchip Western. This work was applied to the detection of ERK 1/2, β-Tubulin, and Stat3 from A431 cell lysate. This new method should continue to be explored with other complex biological samples. With increased sample loadability, as well as increased injection/loadability of larger molecular weight targets, further applications could involve the detection of a broad range of molecular weight targets. As discussed, the increased complexity of the injection scheme with the diced microchip did present preparation

challenges. Future investigation of improved world-to-chip connections that could improve the ease of microchip conditioning.

Chapter 4 Fast Immunoassay for Microfluidic Western Blotting by Direct Deposition of Reagents onto Capture Membrane

Introduction

Western blotting is one of the most widely used analytical techniques for determination of proteins in biological samples. It combines size-based separation with immunoaffinity binding to achieve selective and robust protein assays.[23,110] Despite its popularity, the technique as commonly practiced requires long analysis times (8-24 h), large sample and reagent requirements (10-50 µg total protein and 2-5 µg of antibodies), minimal automation, and limited ability to multiplex.[31,59,85] Over the last decade, improvements in increasing sensitivity and automation have been made to Western blotting as recently reviewed.[110] To address the limitations of the immunoassay portion of the Western, some commercialized systems have been developed to automate[86,89,90] and accelerate[87,88] different aspects of the process, but often do not address the entire Western blot, nor do they reduce antibody consumption.

Interest in employing microfluidics for Western blotting to reduce sample and reagent volumes, decrease analysis time, and increase automation is growing.[47–51,59,61,62,110–117] In some systems, the separation and immunoassay are integrated directly into a microchip or capillary. For example, proteins can be captured on a photoactive gel or wall after separation in a microchannel via photoinduced cross-linking of proteins to allow *in-situ* immunoprobing.[47–51,116] This approach completes assays in just over 1 h with a 10^3-fold reduction in antibody and reagent requirements.

Extensive parallelization to a thousand channels with a 0.5 mm separation channel length on one glass slide has also been demonstrated.[116,117]

For conventional Western blotting membranes, microfluidics has been employed in several ways to speed up the immunoassay and reduce reagent consumption. These methods generally mitigate diffusion-limited kinetics of conventional Western immunoassays to reduce incubation times.[91–96,118,119] A thin-film direct coating approach has been developed yielding a ~1.5 h method with 10^2 to 10^4-fold reduction in antibody consumption depending on the coating width from left to right down the membrane. This method gave a comparable result to a 4 h conventional immunoassay.[120] In another approach, a microfluidic PDMS chip with seven parallel microchannels was clamped onto a conventional Western blot membrane so that reagents could be applied through the microfluidic network. This arrangement enabled parallel immunoassays in 1 h, with a ~7-fold reduction in antibody consumption, and multiplexed detection.[121] Sensitivity comparisons to conventional immunoassay methods were not reported. A PDMS-glass microfluidic device has been developed with three microchannels per blotting lane for a miniaturized immunoassay for conventional Western blotting membranes.[122] The method requires 4 h for the immunoassay; therefore, it does not speed up interactions greatly, but reduces antibody consumption 5380-fold. In another approach, a rotational glass tube incubation chamber was developed with a cyclic draining and replenishing method to better facilitate mixing of the antibody depletion layer.[123] Results showed higher signal in 20 min of primary antibody binding in the chamber compared to 60 min on a conventional shaker allowing for a shorter method with 2-3-fold less antibody consumption.

Our lab developed an approach for separation and transfer steps of a Western blot wherein proteins are separated by microchip gel electrophoresis while the outlet of the microchip is dragged

across a membrane. Proteins are captured as they exit the separation channel so that separation and transfer is completed in 2-8 min.[61,62] The separation media is an entangled polymer solution which can be easily replaced allowing long term operation of the microchip for multiple injections.[43,124] In this method, proteins are deposited on the surface of the binding membrane in a strip that is less than 700-µm wide. The immunoassay step was performed using traditional methods;[62] however, this approach is relatively slow and uses much more reagent than necessary for the small protein tracks made by the method. Here, we report a method of directly applying immunoassay reagents using syringe-driven flow that reduces the area within which the antibodies must diffuse to bind with target proteins. The flow deposition approach has some similarity to vertical flow assay methods that have been used to decrease assay time for sandwich immunoassays.[125,126] In these vertical flow assays, the reagents are applied perpendicular to the membrane by pressure driven flow, decreasing assays to 10-min.

In the work presented here, the flow immunoassay method reduces immunoassay time to 1 h while maintaining the detection sensitivity of an overnight, diffusion-only based immunoassay. Antibody consumption is reduced ~35-fold in comparison to a traditional Western blot immunoassay. In conventional Western blotting, cross-linking has previously been shown to increase protein retention on the binding membrane and improve binding signal for many targets that were poorly detected.[127–134] Such cross-linkers, formaldehyde or glutaraldehyde, have not been reported to interfere with antibody-target binding in Western blotting immunoassays. Cross-linking is used after microchip Western blotting deposition to increase the retention of the proteins that can be lost during the washing steps of the flow-driven assay. Combining the microchip electrophoresis blotting method with this fast immunoassay method, yields a microfluidic Western

blot that detects proteins in less than 1.5 h with reduced sample and reagent consumption and potential for multiplexing.

Materials and Methods

Reagents

All buffers were made using 18 MΩ water deionized by a Series 1090 E-pure system (Barnstead Thermolyne, Dubuque, IA). Actin from rabbit muscle was from Millipore Sigma (St Louis, MO), and A431 cell lysate was from LI-COR Bioscience (Lincoln, NE). FITC-protein ladder containing 7 proteins with masses from 11 kDa-155 kDa with a total protein concentration of 1 mg/mL was from Invitrogen (LC5928, Grand Island, NY). Anti-actin and anti-β-tubulin antibodies were from Millipore Sigma (St Louis, MO). Anti-GAPDH antibody was from Santa Cruz Biotechnology (Dallas, TX). Goat anti-rabbit secondary antibody, goat anti-mouse secondary antibody, nitrocellulose membranes, and blocking buffers were from LI-COR Bioscience (Lincoln, NE). Sodium chloride was from Fisher Scientific (Hampton, NH) and tris was from Bio-Rad Laboratories (Hercules, CA). Radioimmunoprecipitation assay (RIPA) lysis buffer with a composition of 25 mM Tris, 150 mM NaCl, 1% NP-40, 1% sodium deoxycholate, 0.1% SDS, and adjusted to pH 7.6 with HCl was from Thermo Scientific (Waltham, MA). All other reagents were from Millipore Sigma (St Louis, MO). Tris buffered saline with Tween 20 (TBST) was made with 137 mM NaCl, 2.7 mM KCl, 190 mM Tris, and 1% (v/v) Tween 20.

Sample Preparation

Samples were denatured and prepared as previously described[62] with the following exceptions. A final concentration of 1 mg/mL was prepared with actin. A431 cell lysate was lysed with RIPA buffer. After denaturation, the cell lysate was further diluted 100-fold in water and then filtered by centrifuging at 12,100 x g for 10 min using an Amicon® Ultra Centrifugal Filters with

a 10 kDa cut off from Millipore Sigma (St Louis, MO). The concentrated filtrate protein was then collected from the filter and the final concentration was measured using a Bradford assay (Fischer Scientific).

Dot Blotting

For dot blotting, after sample preparation as described above, denatured actin was diluted 300-fold in water for a concentration of 3.3 μg/mL. Dot blots of actin were prepared by spotting 0.2 μL of protein sample directly onto a nitrocellulose membrane strip. The membrane was dry before starting an immunoassay.

Microchip Western Blotting

For microchip Western blotting, denatured actin was diluted 10-fold in water. Then, 1 μL of the diluted actin was mixed with 1 μL of FITC-protein ladder and 28 μL of water for a final concentration of 3.3 μg/mL of actin. For A431 cells, 2 μL of the denatured and filtered lysate was mixed with 1 μL of FITC-protein ladder diluted in 27 μL of water for a final concentration of 100 μg/mL total protein.

Glass microchips were fabricated and conditioned as previously described[62], and microchip conditioning solutions were filtered through a 0.22 μm syringe filter. The electrophoresis gel sieving matrix used was a dextran based entangled polymer solution. Figure 4 displays a schematic and image of the microchip. As shown, flow through sheath channels was used to carry eluted proteins to the membrane. A second set of sheath channels was used to provide electrical contact for grounding the end of the separation channel. This arrangement allowed the microchip to be interfaced directly with a strip of nitrocellulose membrane. Microchips with a 4-cm long separation channel were used where -2.0 kV was applied at the gating reservoir and -1.5 kV was applied at the sample reservoir with a separation field of 315 V/cm. A gated injection[135] of 10 s for actin and

60 s for A431 cell lysate was used. During separation, sieving gel was pumped through the inner sheath flow channels at 30 nL/min and the stage was moved a 4 mm/min across the membrane surface.

Immunoassays

Traditional immunoassays were completed at room temperature unless otherwise described. The following steps were used: 1) block with Odyssey® blocking buffer (TBS) for 1 h, 2) incubate overnight at 4 °C with primary antibody diluted 1000-fold in Odyssey® blocking buffer (TBS) and 0.05% Tween 20, 3) wash with TBST four times at 5 min each, 4) incubate for 1 h with secondary antibody diluted 5000-fold in Odyssey® blocking buffer (TBS) and 0.05% Tween 20, and 5) repeat step 3. During incubation steps the solutions were gently shaken.

Flow immunoassays were completed, unless otherwise stated, as depicted in Figure 2 at room temperature. Membranes were placed on a 3D printed stage (Figure 1**)** that allowed vacuum to be applied to pull the solutions through the membrane. Syringe pumps (IDEX Health & Science, LLC, Oak Harbor, WA), connected to 500 µm i.d. fluorinated ethylene propylene (FEP) tubing, were used to deliver antibody, blocking, and washing solutions. The outlet of the tubing was mounted on an x-y-z positioner to allow the tubing to be swept across the membrane during solution delivery.

Unless otherwise stated, membranes were treated with 40% (v/v) glutaraldehyde for 10 s to cross-link proteins and then rinsed for 1 min and 50 s with water prior to beginning the immunoassay. After cross-linking, the following procedure was used: 1) block with Intercept™ protein-free blocking buffer (TBS) with a 0.6 mL/min deposition flow rate with stage speed for 8 mm/min back and forth for 15 min, 2) deposit primary antibody diluted 1000-fold in Intercept™ protein-free blocking buffer (TBS) 0.05% Tween 20 with a 20 µL/min deposition flow rate and 4

mm/min stage speed for 25 min, 3) wash with TBST with a 6.0 mL/min deposition flow rate and stage at 130 mm/min back and forth for 2.5 min with -0.2 bar vacuum applied to the stage to pull wash solution through the membrane, 4) deposit secondary antibody diluted 1000-fold diluted in Intercept™ protein-free blocking buffer (TBS) 0.05% Tween 20 with a 5 μL/min deposition flow rate while moving the stage at 70 mm/min back and forth for 15 min, and 5) repeat step 3. Tests revealed that blocking with Intercept™ protein-free blocking buffer (TBS) could also be applied with gentle shaking for 15 min. Washing with TBST could also be achieved by using a pipette to spray on.

For some experiments no cross-linking was used. This method follows that of the flow method described above except that washing was done four times at 2.5 min each with TBST and secondary antibody diluted 1000-fold in Intercept™ protein-free blocking buffer (TBS) and 0.05% Tween 20 was incubated for 1 h.

Detection on membrane

After separation and transfer of the sample mixed with FITC-protein ladder, the fluorescent ladder was detected on the membrane using an Amersham Typhoon NIR Plus (GE Healthcare, Pittsburgh, PA) with 488 nm fluorescence measurement. After the immunoassay, the membrane was dried at room temperature and imaged on an Odyssey® near-IR fluorescence imager at 700 nm (LI-COR Bioscience, Lincoln, NE). Line scans were generated using ImageJ (NIH) and imported into Cutter 7.0 software[107] where a median filter at 4.0 pixels was used. After a baseline correction, the noise was selected from the baseline in between peaks. Peak heights were measured for calculating signal-to-noise (S/N) ratio. Data was plotted in GraphPad Prism 7 where an average and standard deviation were calculated. A relative standard deviation (RSD) was plotted as an error bar. For dot blots, the average and RSDs were generated from multiple protein spots on the

same membrane, minimally n = 3 protein spots. For microchip Western blotting, data was averaged from three injections of the same sample. All statistical analyses were performed in GraphPad Prism 7. For statistical analysis between traditional and flow immunoassay data of the same sample, an unpaired Student's t test was applied where differences deemed significant if $P < 0.01$.

Results and Discussion

Microscale immunoassay method

In surface-based immunoassay methods, antibody diffusion is the rate determining step of the assay; as a result, long incubation times are used to achieve maximum detection sensitivity.[25-32] Mechanisms of mass transport for analytes in a solution reacting with surface binding targets include diffusion based on a concentration gradient, diffusion in a temperature gradient (thermal), diffusion in a pressure gradient, and diffusion aided by external forces acting on a chemical species/analytes including free and forced convection.[136–138] We used flow deposition to achieve convective transport and reduced diffusion distance resulting in shorter time scales for antibody binding. **Figure 4-1** shows the 3D printed tubing mount and vacuum stage that was used to perform fast immunoassays. The membrane is placed on the vacuum stage and flow deposition of the immunoassay solutions occurs through a syringe connected to tubing as depicted in **Figure 4-2**.

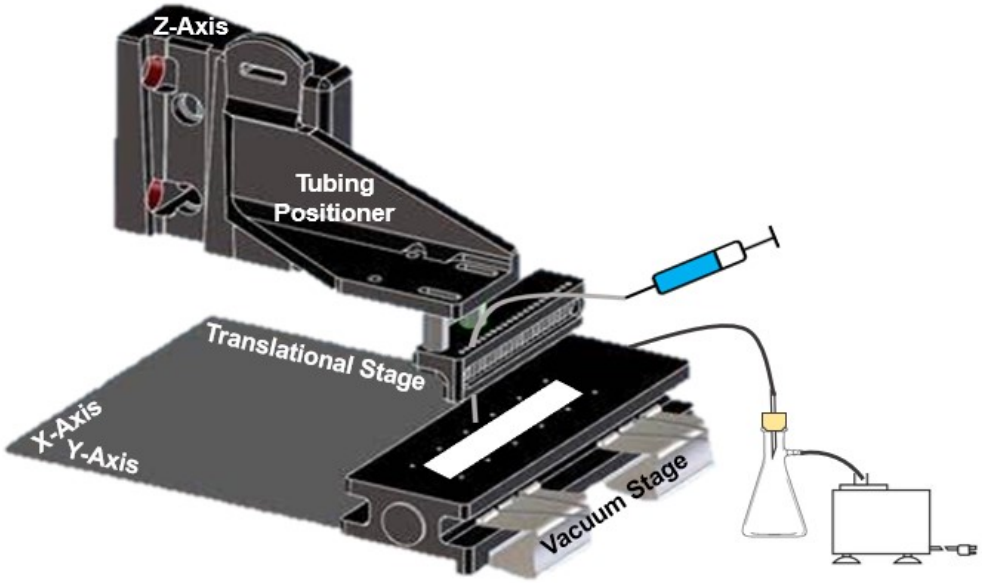

Figure 4-1. Representation of the 3D printed parts that are used for the fast immunoassay. A tubing holder is used for precise positioning of the deposition, and the membrane is placed on the vacuum stage. The immunoassay solutions are flowed directly on and over the protein trace that is deposited on the membrane from microchip Western blotting.

We developed conditions for the assay by performing dot blots of 3.3 µg/mL actin dissolved in water and varying immunoassay solution deposition conditions. We found that

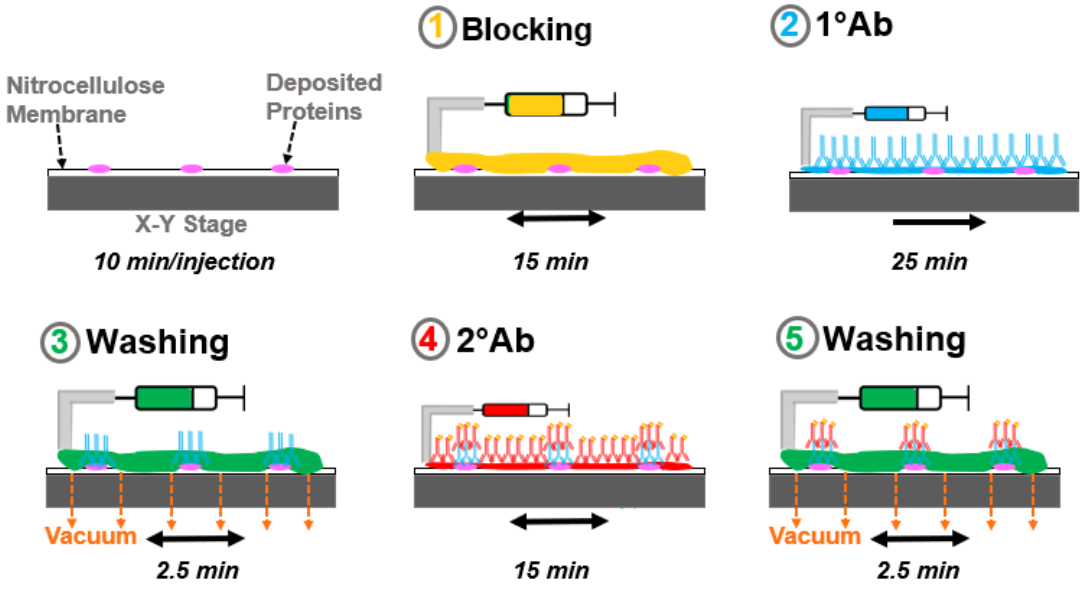

Figure 4-2. Representation of the fast immunoassay method from a side-view perspective where the reagents are applied directly to the mm-wide protein trace on a nitrocellulose membrane. The nitrocellulose membrane strip is placed on a 3D printed vacuum stage, and reagents are applied sequentially as shown. The vacuum is turned on during the washing steps. The entire fast immunoassay is completed in 1 h.

depositing primary antibody at 20 µL/min with a stage speed of 4 mm/min gave comparable signal intensity to a traditional overnight immunoassay method (**Figure 4-3**). The total primary antibody binding time was 25 min and total primary antibody used was 175 ng, a 40-fold and 30-fold reduction respectively over the conventional method.

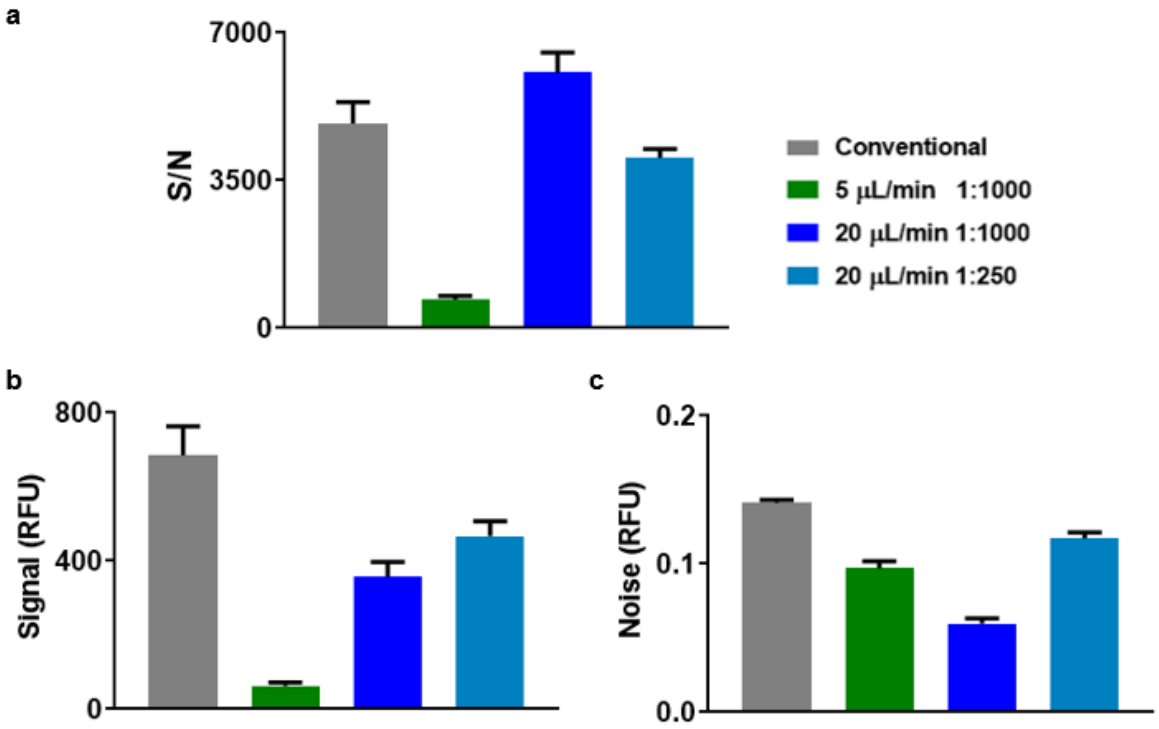

Figure 4-3. Investigation of primary antibody deposition parameters where all steps followed the microscale immunoassay method except for secondary antibody incubation which was applied with a traditional incubation step. Investigation of antibody deposition indicated that flow rates from 5-20 µL/min with stage speeds from 2 8 mm/min were adequate for completely saturating the width of a deposited protein trace. Primary antibody deposition was investigated between parameters of 5 and 20 µL/min, and the results shown here were at the selected stage speed of 4 mm/min for 50 µg/mL actin dot blotted with n=4 protein spots. The S/N (a), signal (b), and noise (c) values calculated and plotted are compared for selection a of deposition parameters that give the most comparable result to the traditional immunoassay. As shown, increasing the concentration of the primary antibody does not improve the S/N ratio within the selected deposition parameters.

We next examined the secondary antibody deposition step. Flow deposition at 20 µL/min with stage speeds from 2-8 mm/min, resulted in poor signal and high background and noise levels. Specifically, under these conditions we observed formation of large fluorescent spots on the binding membrane that could not easily be removed. It was determined that using lower flow rates

(3.5-7.5 µL/min) while the stage moved back and forth at 70 mm/min so that the membrane and protein samples pass through the secondary antibody several times, resulted in much less formation of these background spots and comparable sensitivity to conventional immunoassays (**Figure 4-4**). Using 5 µL/min, the total secondary antibody deposition time was 15 min and total secondary antibody used was 75 ng, a 4-fold and 27-fold reduction respectively over conventional method.

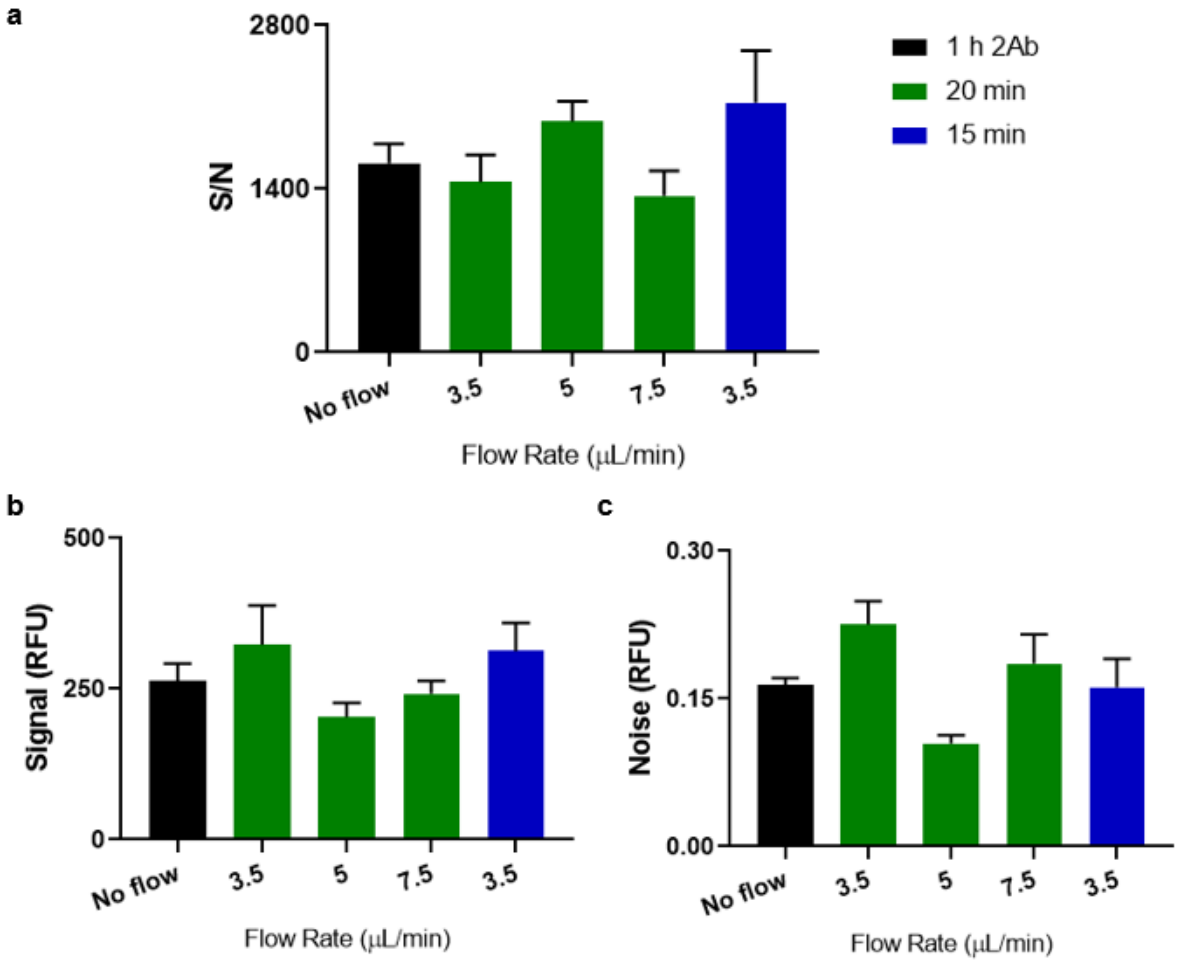

Figure 4-4. Investigation of secondary antibody deposition parameters where all steps are applied via the microscale, fast immunoassay method. Detection of actin 50 µg/mL dot blotted with n=4 protein spots was investigated with flow rates ranging from 3.5-7.5 µL/min with a fast stage speed of 70 mm/min that repeated movement along the x-axis. This deposition approach produced better binding with acceptable background and noise levels. The S/N (a), signal (b), and noise (c) are compared with a modified, microscale 2 h immunoassay that had previously been determined to give comparable results to a traditional immunoassay.

It is unclear why different conditions were required for the primary and secondary antibody deposition; however, differences are also seen in traditional immunoassay method that seem to correlate with our observations. Incubation times for secondary antibodies are typically much shorter (1 h) than primary antibodies (overnight). Fluorescent secondary antibodies are typically used at more dilute concentrations than primary antibody as well. Several factors are likely to contribute to the differences primary and secondary antibody binding. The binding kinetics of secondary to primary antibody may differ from those of primary antibody to surface-bound antigen. The presence of fluorescent tags provides hydrophobic groups on the secondary antibody that may also affect the potential for non-specific binding and aggregation to alter background signals.

Regardless of the reason for the differences, using these deposition methods, and rinsing in between each deposition while with using vacuum to pull solutions through the membrane as shown in **Figure 4-2**, a complete dot blot immunoassay is completed in 1 h (**Table 4-1**). S/N ratios

Table 4-1. Comparison of traditional and fast immunoassay method analysis times and antibody consumption for dot blotting membranes.

	Traditional Immunoassay	**Flow Immunoassay**
Time Per Step		
Blocking	1 h	15 min
Primary Antibody	17 h	25 min
Washing	20 min	2.5 min
Secondary Antibody	1 h	15 min
Washing	20 min	2.5 min
Total Time	20 h	1 h
Antibody Consumption		
Primary Antibody	5 µg	175 ng
Secondary Antibody	2 µg	75 ng

These values are based on a membrane trace that is 7-cm in length.

obtained by this abbreviated procedure are comparable to those obtained using a 20 h analysis time (**Figure 4-5**).

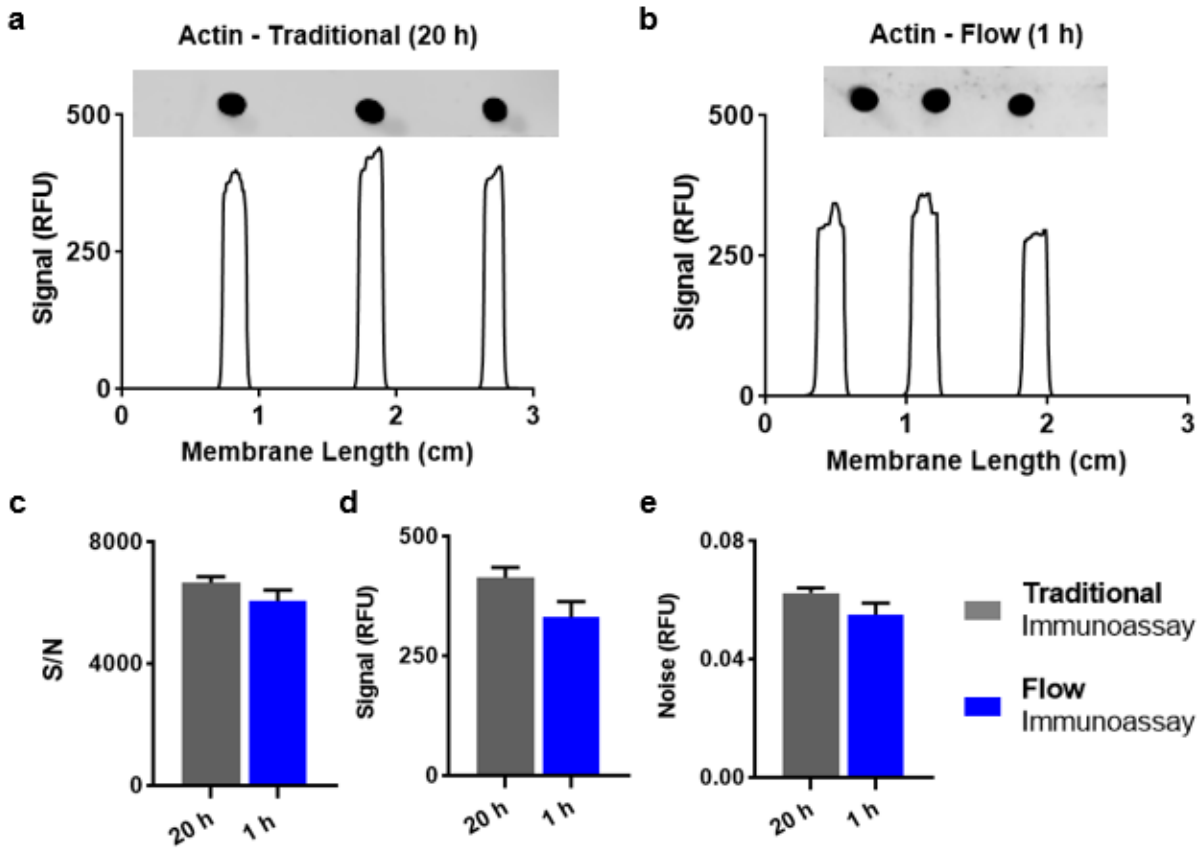

Figure 4-5. Comparison between a 20 h, traditional immunoassay (a) and the developed 1 h, fast immunoassay (b) for dot blots of 3.3 µg/mL actin. The S/N (c), signal (d), and noise (e) values calculated and plotted with n=3 protein spots are displayed showing comparable detection between the two immunoassay methods. Unpaired two-tailed Student's t-test statistics were performed with $p < 0.01$ to compare the S/N (c) of the traditional and flow immunoassay results in which the two data sets are not significantly different.

Microchip Western blotting with direct deposition immunoassay

The flow immunoassay method was then applied to proteins deposited by microchip gel electrophoresis. **Figure 4-6** displays a schematic and image of microchip Western blotting. The sample is introduced using a gated, timed injection after which proteins migrate through the separation channel. In this work, an outer set of sheath flow are used to ground the end of the separation channel while the inner sheath flow channels are used to deposit separated proteins onto

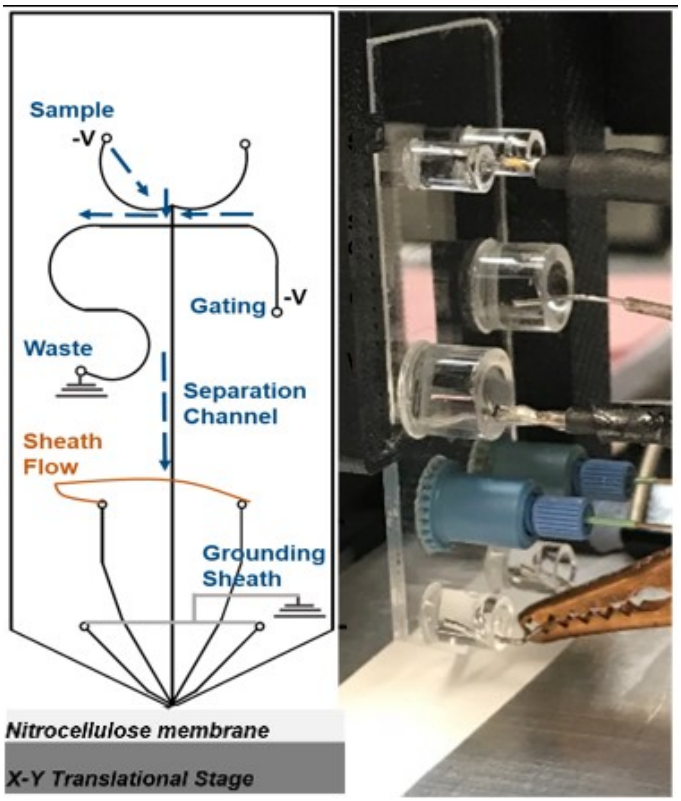

Figure 4-6. Representation of gated microchip Western blotting onto nitrocellulose membranes.

a nitrocellulose membrane strip. Pilot experiments using this system to deposit actin onto a member unexpectedly resulted in low or no signal when using the fast immunoassay described above. To determine cause of this loss in signal, we performed the flow process for all steps except secondary antibody addition, which was performed on a shaker for 1 h. This modified flow method allowed detection of proteins from microchip Western blotting but with a reduced S/N compared to the traditional, 20 h immunoassay (**Figure 4-7**). These results suggested that the protein was not captured effectively with the flow deposition system in the presence of gel and was hypothesized to be due to the effect of gel on the interactions of proteins with the binding membrane. To test this hypothesis, experiments comparing dot blots of protein diluted in water and gel solution were performed. These experiments showed lower signal intensity for the gel dot blots with the fast

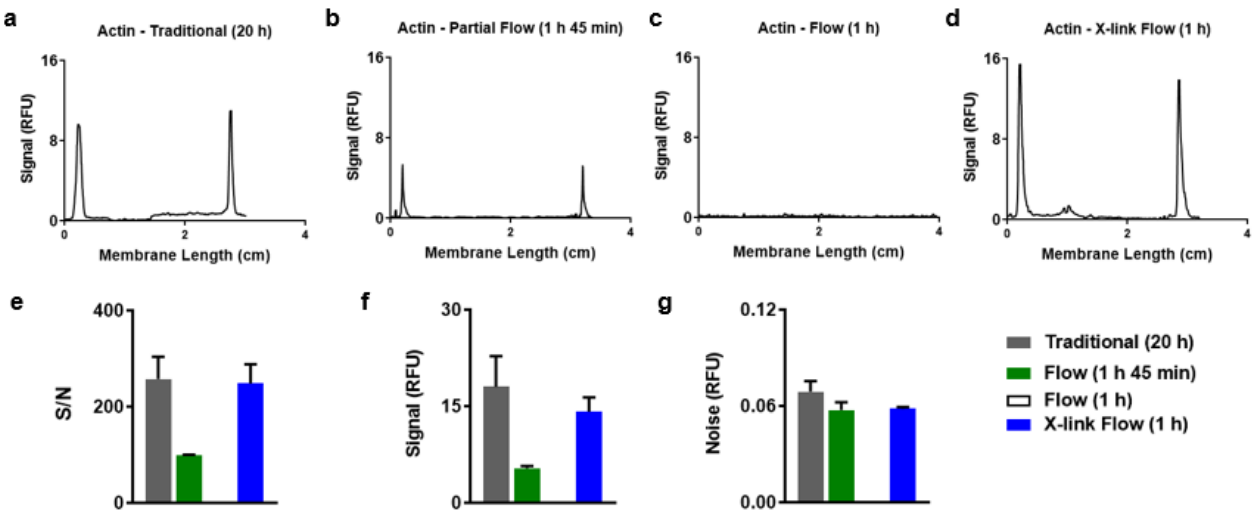

Figure 4-7. Comparison of a traditional immunoassay (a) with initial protein loss from non-crosslinked, partial flow immunoassay method (b), a non-crosslinked flow immunoassay (c), and a cross-linked flow immunoassay (d) for microchip Western blotting of 3.3 µg/mL actin. The S/N (e), signal (f), and noise (g) values calculated and plotted with n=3 injected and separated protein peaks.

immunoassay approach (**Figure 4-8**) supporting the hypothesis that the gel contributed to loss of signal.

To address the loss of proteins co-deposited with gel sieving matrix, glutaraldehyde was used to cross-link proteins for membrane fixation, a method used in some cases with conventional Western blotting.[127,128,131,132] Cross-linking for the improvement of protein retention on binding

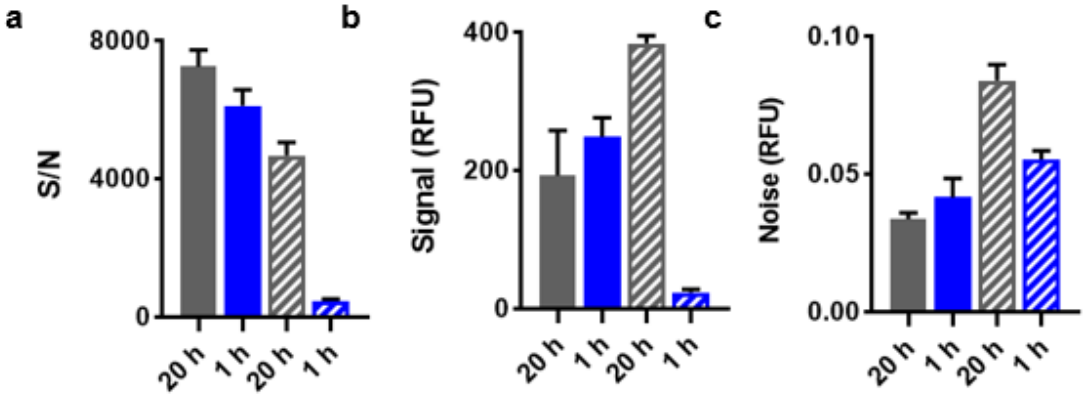

Figure 4-8. Comparison of dot blots of actin diluted in water (solid) versus dot blots of actin diluted in electrophoresis gel (hatched) with 3.3 µg/mL actin. The S/N (a), signal (b), and noise (c) values calculated and plotted demonstrating the effect on protein binding and protein loss seen with the non-crosslinked fast immunoassay.

membranes is attributed to result from multi-point attachments of the cross-linked proteins.[129,132,134] In prior Western blot methods, treatment with 0.5% (v/v)-2.5% (v/v) glutaraldehyde for 15-60 min was used to improve protein retention on blotting membranes.[128,129,131,132] We have recently used 40% (v/v) glutaraldehyde to achieve cross-linking in 10 s for protein-protein interaction (PPI) studies.[139] Inspired by this approach, we found that exposing the blotted proteins and membrane to 40% (v/v) glutaraldehyde for 10 s and rinsing with water for ~ 2 min prior to the microscale immunoassay mitigated protein loss issues so that results for microchip Western blotting membranes were comparable between a traditional and a flow immunoassay (**Figure 4-7**). **Figure 4-7** compares the initial S/N level achieved with a modified (1.75 h) immunoassay, with a non-cross-linked (1 h) method, and a cross-linked (1 h) flow method with a traditional (20 h) immunoassay showing that glutaraldehyde cross-linking is effective at preventing loss of proteins from the gel trace of microchip Western blotting.

A calibration curve of microchip Western blotting for actin by the traditional and cross-linked flow immunoassays yields a linear response (**Figure 4-9**). From these data, concentration limits of detection (LODs) were calculated as 2 nM for the traditional immunoassay and 7 nM for the cross-linked flow immunoassay. Since we estimate 4.5 nL were injected, this concentration corresponds to a mass LOD of 9 amol or 400 fg for the traditional immunoassay and 30 amol or 1 pg for the cross-linked flow immunoassay. Of course, 20 μL were used to fill the reservoir, so more sample was used for the assay. Miniaturized sample preparation and loading methods would be needed to take full advantage of the mass LOD that is possible.

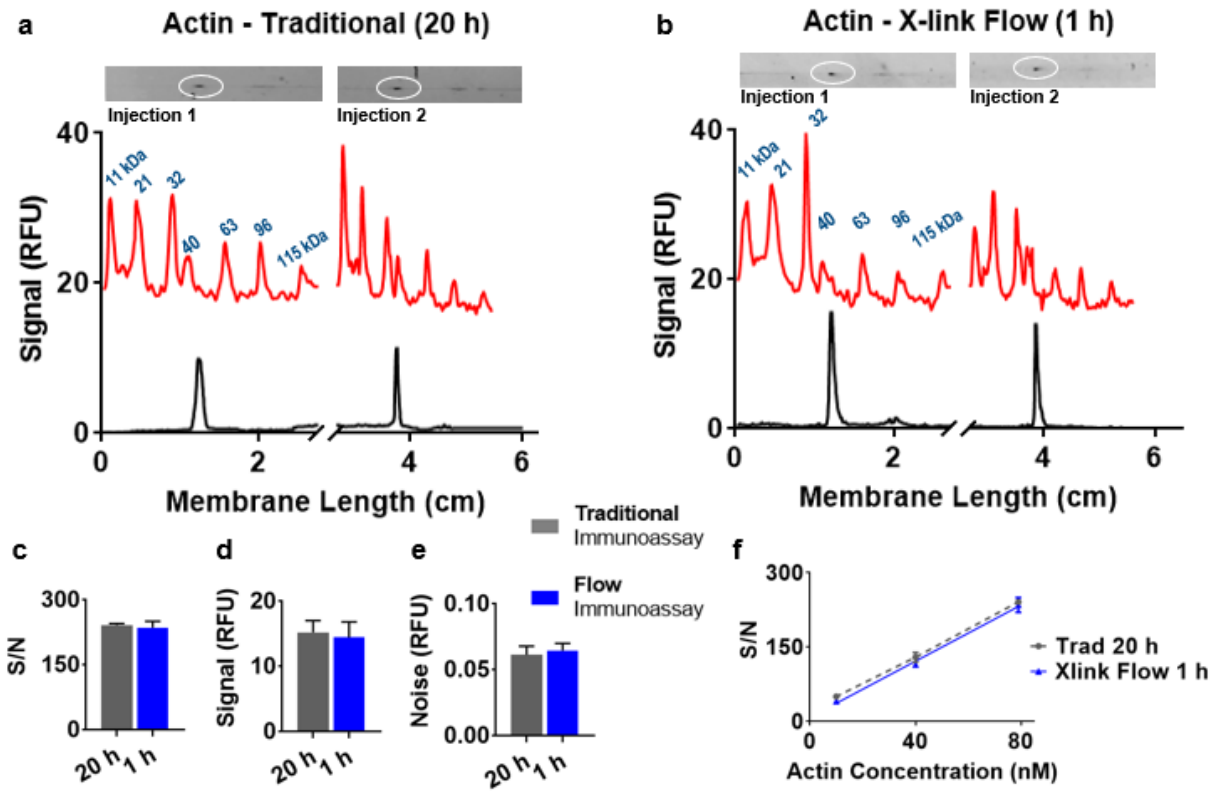

Figure 4-9. Comparison between a traditional immunoassay (a) and the cross-linked (X-link) flow immunoassay (b) for microchip Western blotting of 3.3 µg/mL actin. Membrane images and line scans from ImageJ are shown (black trace), where the line scan of the FITC-protein ladder (red trace) are overlaid. The arbitrary units of the signal intensities of the FITC-protein ladder were divided by 250 to scale the ladder for the plot above. The error bars represent the standard deviation of the protein detected by the various immunoassay methods for repeated injections, separations, and depositions of the protein sample from the microchip. The S/N (c), signal (d), and noise (e) values calculated and plotted with n=3 injected and detected protein peaks are displayed showing comparable detection between the two immunoassay methods. The relationship between S/N and actin concentration for a traditional immunoassay and X-link flow immunoassay gives an R2 equal to 0.9995 and 0.996, respectively (f). Limits of detection were calculated accounting for limit of the blank with an LOD of 2 nM for traditional immunoassay and a LOD of 7 nM for X-link flow immunoassay. Unpaired two-tailed Student's t-test statistics were performed with $p < 0.01$ to compare the S/N (c) of the traditional and flow immunoassay results in which the two data sets are not significantly different.

Table 4-2 summarizes the cross-linked, flow immunoassay method. Further experiments revealed that if some speed could be sacrificed, the processing steps that impact the protein loss from reduced adherence of proteins from the microchip deposition gel trace can be modified so that a 2 h immunoassay method is used for protein detection without cross-linking, as summarized

in Table 2. In this case, the secondary antibody is incubated for 1 h with shaking similar to a traditional immunoassay. These different flow immunoassay methods allow for the flexibility of either using a cross-linking step prior to the immunoassay or not. The non-cross-linked method could be useful if cross-linking inhibits antibody binding, although this has not been seen or previously reported b y other cross-linking Western techniques.[48-55]

Table 4-2. Comparison of traditional, modified microscale, and fast immunoassay methods analysis times and antibody consumption for microchip Western blotting membranes.

	Traditional Immunoassay	**Modified Flow Immunoassay**	**X-link Flow Immunoassay**
Time Per Step			
Cross-Linking	-	-	10 s
Rinsing	-	-	110 s
Blocking	1 h	15 min	15 min
Primary Antibody	17 h	25 min	25 min
Washing	20 min	10 min	2.5 min
Secondary Antibody	1 h	1 h	15 min
Washing	20 min	10 min	2.5 min
Total Time	20 h	2 h	1 h 2 min
Antibody Consumption			
Primary Antibody	5 µg	175 ng	175 ng
Secondary Antibody	2 µg	10 µg	75 ng

These values are based on a membrane trace that is 7-cm in length.

We further tested the method on different proteins. A comparison of microchip Western blots for detection of GAPDH from A431 cell lysate using the traditional (20 h) immunoassay, the microscale, non-cross-linked (2 h) immunoassay, and the cross-linked, flow (1 h) immunoassay are shown in **Figure 4-10**. As shown, comparable S/N is achieved for all methods; but the cross-linked flow method reduces assay time by 20-fold and reagent usage by ~30-fold. We also

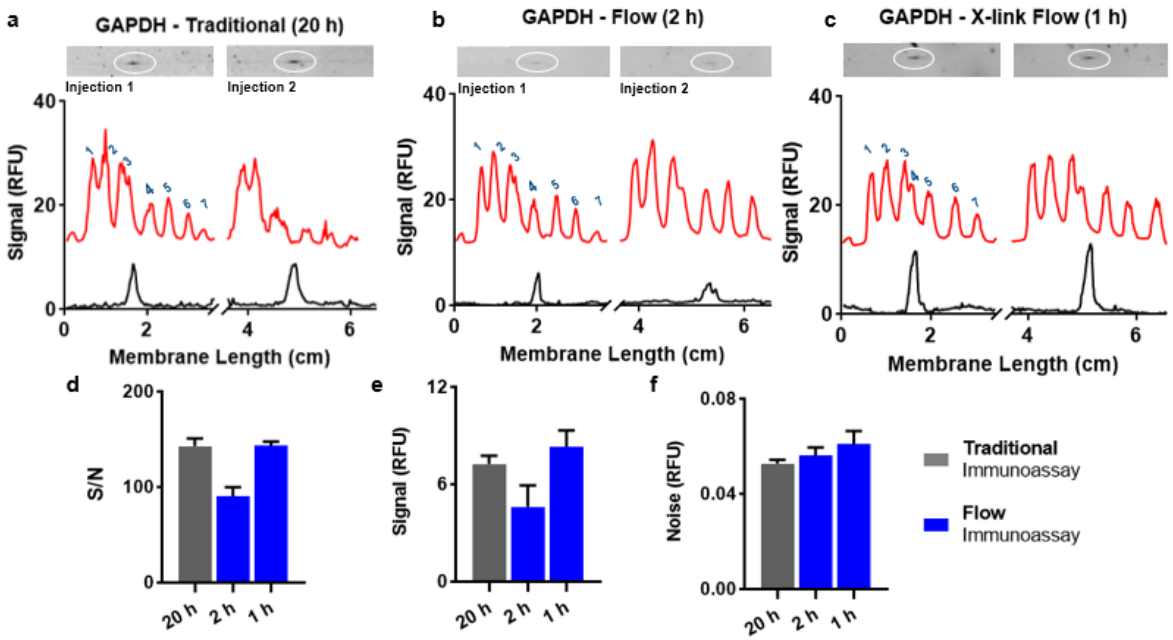

Figure 4-10. Microchip Western blotting of 100 µg/mL total protein A431 cell lysate was done for the detection of GAPDH. A comparison between a traditional immunoassay (a), a modified flow immunoassay (b) and the cross-linked (X-link) flow immunoassay (c) for detection of GAPDH are displayed. Membrane images and line scans from ImageJ are shown (black trace), where the line scan of the FITC-protein ladder (red trace) are overlaid. The arbitrary units of the signal intensities of the FITC-protein ladder were divided by 2500 to scale the ladder for the plot above. The error bars represent the standard deviation of the protein detected by the various immunoassay methods for repeated injections, separations, and depositions of the protein sample from the microchip. The FITC-protein ladder molecule weight labels 1-7 stand for: 11, 21, 32, 40, 63, 96, and 155 kDa. The S/N (d), signal (e), and noise (f) values calculated and plotted with n=3 injected and detected protein peaks are displayed showing comparable detection between the two immunoassay methods. Unpaired two-tailed Student's t-test statistics were performed with $p < 0.01$ to compare the S/N (d) of the traditional and flow immunoassay results in which the 20 h and 1 h data sets are not significantly different.

compared results to a 20 h immunoassay method for the detection of β-Tubulin in A431 cell lysate

(**Figure 4-11)**. As shown, comparable results were obtained for these proteins from lysate as well. These results suggest that the flow method can be reliably used for different proteins with minimal method development.

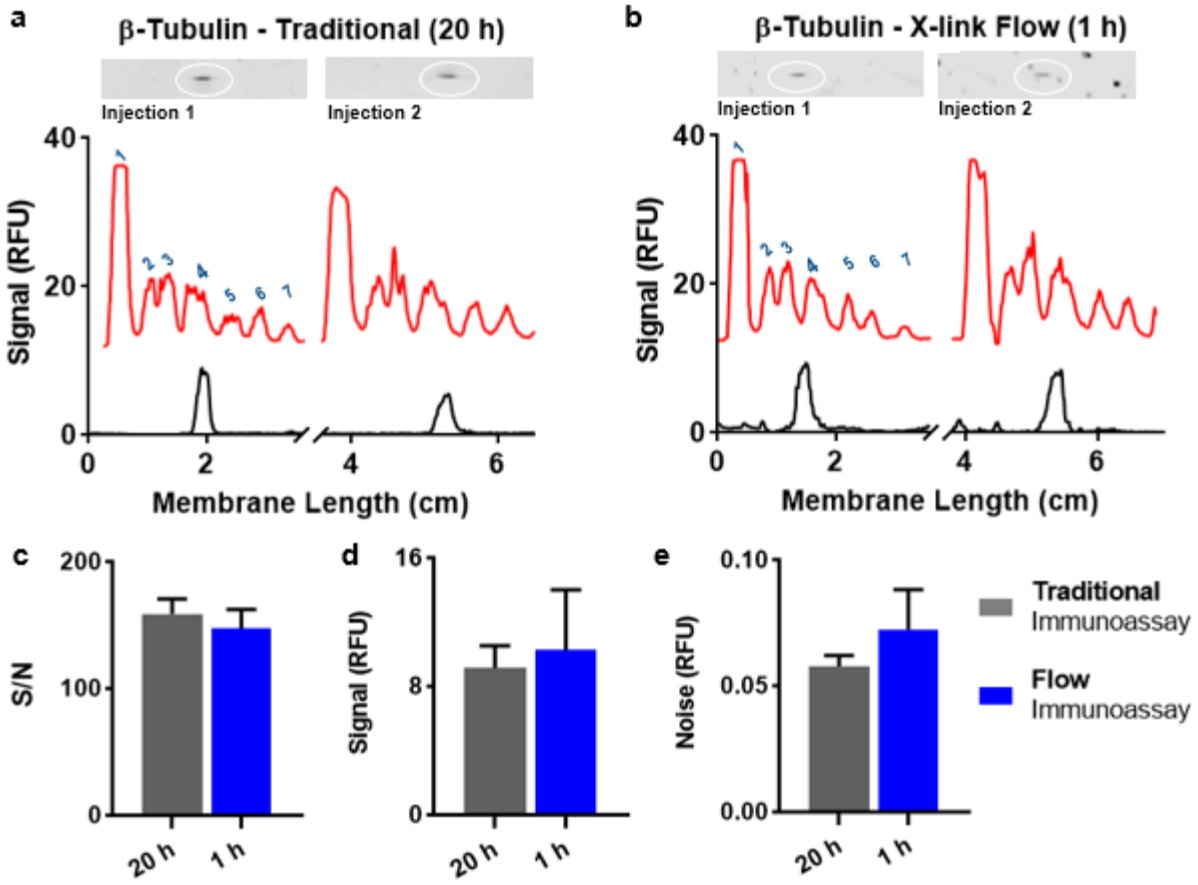

Figure 4-11. Microchip Western blotting of 100 µg/mL total protein A431 cell lysate was done for the detection of β Tubulin. A comparison between a traditional immunoassay (a), a modified flow immunoassay (b) and the cross-linked (X-link) flow immunoassay (c) for detection of β Tubulin are displayed. Membrane images and line scans from ImageJ are shown (black trace), where the line scan of the FITC-protein ladder (red trace) are overlaid. The arbitrary units of the signal intensities of the FITC-protein ladder were divided by 2500 to scale the ladder for the plot above. The error bars represent the standard deviation of the protein detected by the various immunoassay methods for repeated injections, separations, and depositions of the protein sample from the microchip. The FITC-protein ladder molecule weight labels 1-7 stand for: 11, 21, 32, 40, 63, 96, and 155 kDa. The S/N (c), signal (d), and noise (e) values calculated and plotted with n=3 injected and detected protein peaks are displayed showing comparable detection between the two immunoassay methods. Unpaired two-tailed Student's t-test statistics were performed with $p < 0.01$ to compare the S/N (c) of the traditional and flow immunoassay results in which the two data sets are not significantly different.

Conclusions

We have developed a microscale immunoassay method that achieves comparable S/N for the detection of proteins from microchip Western blotting. This development has resulted in a microfluidic Western blotting system that can detect a protein in under 1.5 h with 100-fold reduction in sample requirements and ~30-fold reduction in antibody reagents, while using conventional blotting materials and reagents. Further adaptations of this work could include parallelization of the fast, direct deposition immunoassay. This could easily be achieved in the current set-up to allow for four parallel immunoassays to be run simultaneously. Altogether, our microfluidic Western blotting methods will allow for improved analysis throughput and ease for multiplexed detection of proteins. The investigation and development of microfluidic techniques for Western blotting brings forth a next generation of techniques for protein detection to overcome the limitations of conventional Western blotting methods. With the use of glutaraldehyde cross-linking, it may be necessary to find antibody that can bind with cross-linked antigens. Thus far, this issue has not been reported. Further development of the method would involve application to other biological sources, targets, and a broader range of molecular weights.

Chapter 5 Conclusions and Future Directions

In this dissertation, developments of microfluidic Western blotting methods were presented. In order to reliably perform microchip electrophoretic separations, smooth etching with repeatable microfabrication of glass was needed. Rough etching in Borofloat glass was overcome by investigating fabrication methods of a different manufactured borosilicate glass, D263. D263 is manufactured with a down-drawn process versus floated. Etching of this substrate resulted in reliable and smoothly etched microchannels. This new etching method allowed for the microfabrication of a new microchip gel electrophoresis injection mode that improves the sample loadability of microchip Western blotting. This approach combined a fixed length, constant volume sample plug with on-line electrokinetic surcharging preconcentration. When applied to microchip Western blotting a 30-fold improvement on detection sensitivity was observed. Finally, to address the time-consuming immunoassay procedures used for antigen detection, a fast immunoassay was developed using microscale deposition of antibodies. In 1 h the same detection sensitivity in comparison to an overnight procedure is achieved; antibody consumption was reduced 30-fold.

Future Directions of Microchip Western Blotting

About forty years after its introduction, Western blotting is still a widely relied upon technique for protein detection. In comparison to other protein detection methods including mass spectrometry (MS), enzyme-linked immunosorbent assay (ELISA), immunohistochemistry (IHC), and

microscopy, Western blotting is applied at least two times more often than other techniques over the last ten years (**Figure 5-1**).[140] Although microfluidics has made great advances and

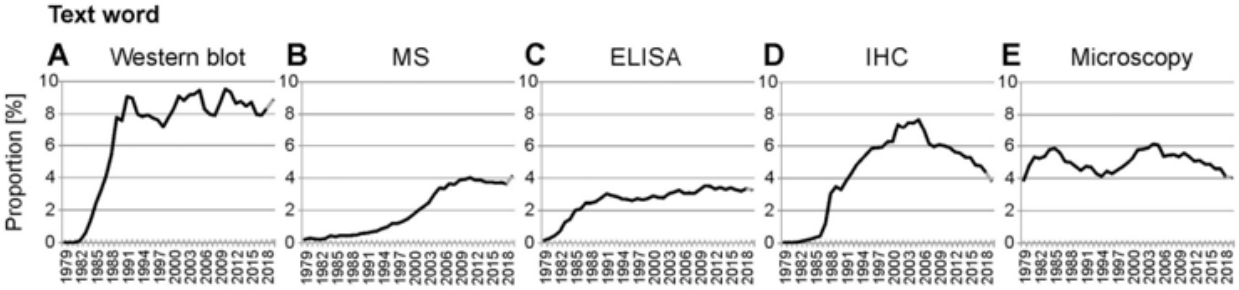

Figure 5-1. Proportions of application of five different techniques in relation to all protein-related publications estimated by the number of PubMed mentions in the Text words. The relative frequency of usage of Western blots, mass spectrometry (MS), enzyme-linked immunosorbent assay (ELISA), immunohistochemistry (IHC), and microscopy was estimated by counting the mentions of the techniques in the Text words (Text words comprise title, abstract, MeSH headings and subheadings, other terms field including keywords, chemical names of substances, secondary source identifier, personal name as subject [22]) (A–E). In order to avoid counting non-protein-related articles mentioning mass spectrometry, such as mass spectrometry of small molecules, I searched for protein-related articles only ((protein*[Text Word] OR proteins*[Text Word] OR proteom*[Text Word]) AND followed by the technique search terms). The following search terms for the five techniques were used: A, Western blot: (Western blot*[Text Word] OR Immunoblot*[Text Word]); B, MS: (mass spectrometry[Text Word] OR mass spectrometric*[Text Word]); C, ELISA: (ELISA[Text Word] OR enzyme-linked immunosorbent assay[Text Word]); D, IHC: (IHC[Text Word] OR Immunohistochemistry[Text Word]); E, microscopy: (microscopy[Text Word]). All numbers were set in relation to the total number of protein-related publications of the same year (A-E: percent, %). Grey part of the graph: preliminary PubMed entries for 2019. Adapted with permission.[140] Copyright 2019 Elsevier B.V.

improvements on Western blotting techniques, the commercialization of these methods are still in progress. A limitation of working with microchips are the formation of world-to-chip connections. Glass reservoirs and IDEX ports for syringe-driven sheath flow were attached with epoxy. In the MGE work presented here, conditioning of glass microchips was achieved by applying a vacuum to pull conditioning solutions and the sieving gel through the microchannels. This approach was also used to clear and regenerate the microchip after use. In the development of the CVI scheme, this conditioning process became significantly more complicated. It required several hours or more of preparation time due to the multiple injection channels. However, developing transparent

pressure connections to glass microchips could be investigated in the future to overcome such limitations. The development of pressure driven conditionings steps for glass microchips would improve the ease of working with microfluidic devices as well as the required conditioning time. Such developments would be needed for future commercialization for the wide use of microchip Western blotting.

Modifications to the grounding mechanism of the microchip were implemented to ground the end of the separation on-chip. Previously, grounding was achieved through electrical connection to the grounded translational stage requiring liquid contact between the polyvinylidene fluoride (PVDF) membrane and the stage. With grounding on-chip, deposition onto dry nitrocellulose membranes were achieved. This approach also simplified the deposition method onto the binding membrane in comparison. However, the deposition was still dependent upon positioning of the microchip; any uneven surfaces of the stage or membrane can alter the protein trail deposition. To further improve the robustness of depositing proteins on nitrocellulose membranes, we have begun investigation of interfacing CE with an inkjetting dispenser (**Figure 5-2**). Using a drop-on demand approach, a dispensing head with a piezoelectric inkjet element is interfaced with the end of the capillary. This allows for the deposition of proteins in 100

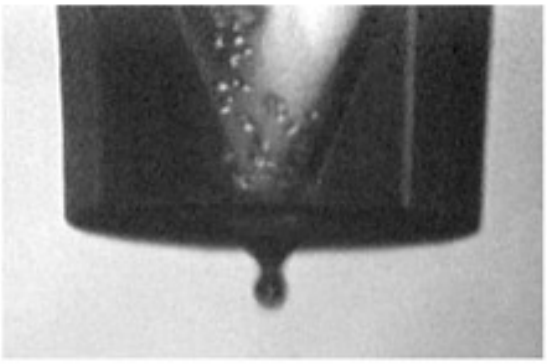

Figure 5-2. Human embryonic kidney cells (HEK293e) being dispensed at 240Hz using an ink-jet device with a 55mm orifice. The immediate cell viability was unchanged after being microdispensed. Reprinted.[141]

pL droplets with a moving membrane that produces a protein trace. The outlet of the capillary is placed in an inkjetting dispense; therefore, the deposition of separated proteins is no longer dependent on exact z-axis positioning of a capillary or microchip. Other methods for achieving drop-on demand inkjetting for biomaterials include electrostatic, thermal and acoustic approaches.[141,142] Integrating inkjetting technology with the microchip outlet is significantly more challenging to implement. If this capability is developed, along with ease of pressure applications to microchip conditioning, then the repeatability of microchip Western blotting deposition would greatly improve.

Parallelization of the Fast Immunoassay

The fast immunoassay developed in this work was originally designed for a single lane from microchip Western blotting, however, there is great potential for the parallelization of this method. Even with the current approach, which used a syringe pump to deliver immunoassay solutions, four lanes could be run simultaneously. Parallelized immunoassays could be approached in one of two ways. First, protein tracks deposited within mm of one another could be assayed for the same target proteins at one time. Secondly, protein tracks could be spaced apart or on individual membranes for parallelized deposition for different target proteins. The initial concept and design for the solution deposition were 3D printed parts that are simple and easy to use. 3D printing of more complicated structures and vacuum stages would be achievable. **Figure 5-3** displays a

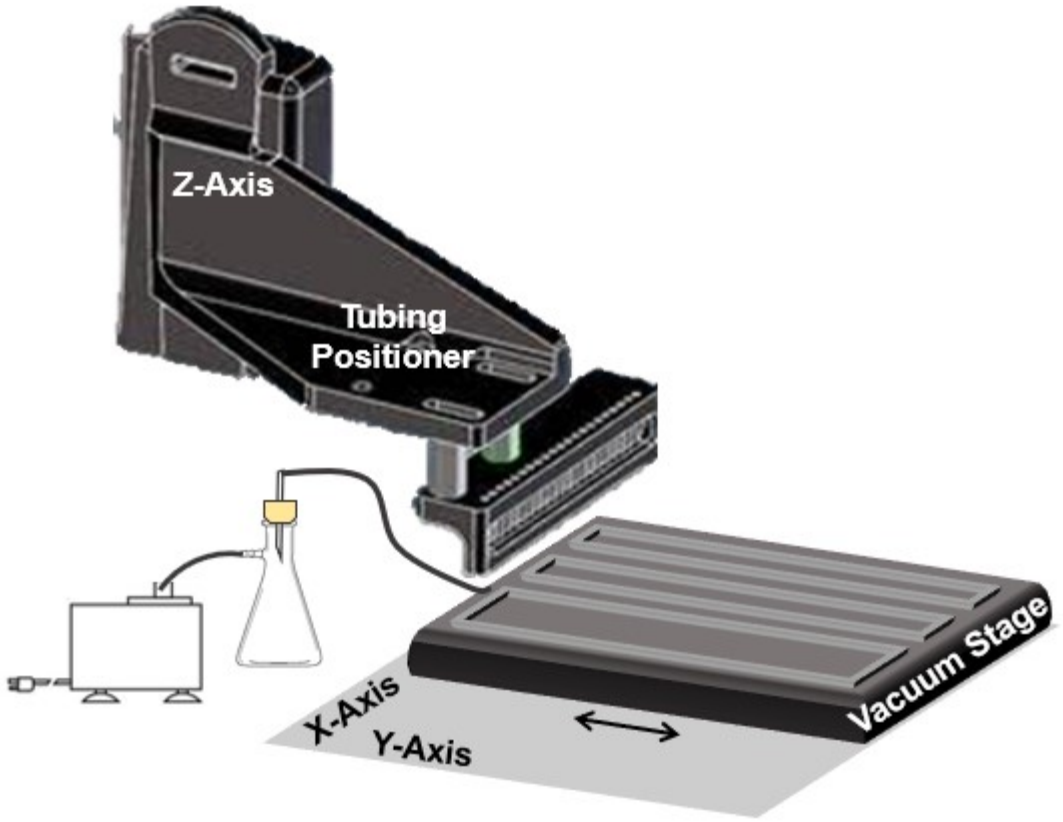

Figure 5-3. A representation of parallelized flow immunoassay deposition methods.

conceptual representation of these strategies. Further automation development in combination with these approaches would increase the utility of fast immunoassay methods.

Western Blotting in Therapeutic Strategies for Diabetes

In the pancreas, β-cells from Islets of Langerhans are responsible for insulin secretion. Replication of pre-existing β-cells and/or activation of endogenous β-cells progenitors is an important therapeutic research strategy for early prevention, postponement of development, and potential reversal of diabetes.[144] Research on therapeutic strategies to treat and/or reverse diabetes still heavily relies upon Western blotting for detecting proteins in signaling pathways that are involved in β-cell production. For example, the loss of mTORC1 signaling directly impairs insulin processing and β-cell homeostasis (**Figure 5-4)**.[145] A challenge in this research progress is the

sample volume/mass requirements needed for conventional Western blotting. For example, 40 µg of Islet proteins from transgenic mice were used for one SDS-PAGE Western lane. Being able to use 1 µg or less would greatly impact the amount of results that could be obtained from one mouse.

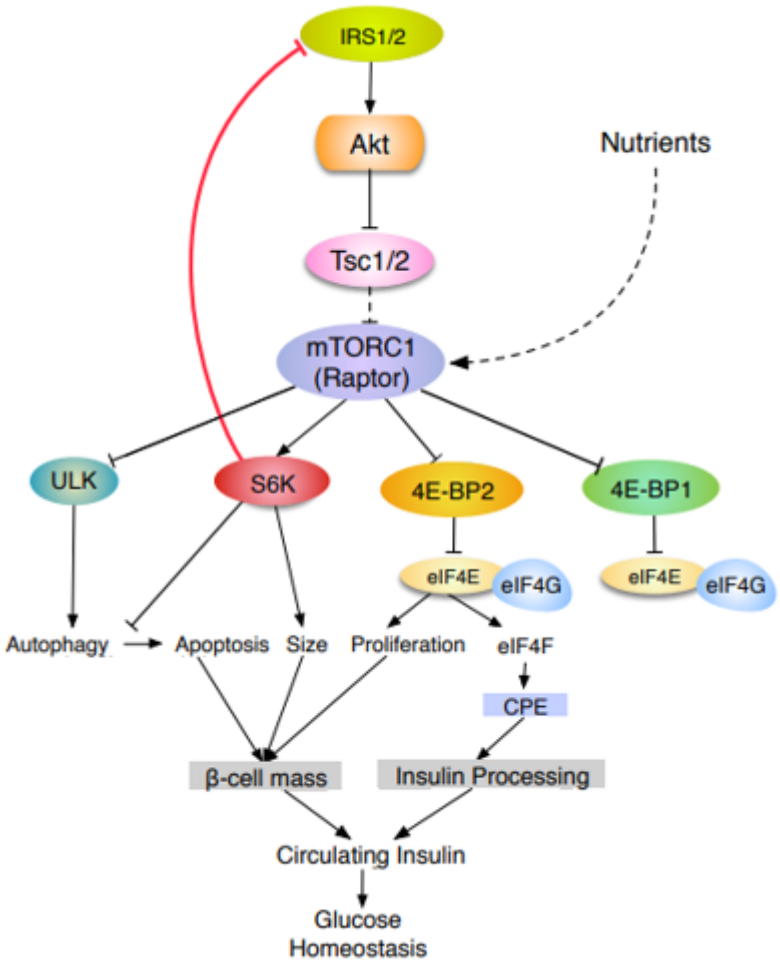

Figure 5-4. The schematic summarizes the results of the current experiments by showing how mTORC1 acting in downstream targets regulates β-cell mass and insulin processing. Activation of insulin and growth factor receptors recruit insulin receptor substrates (IRS) and induce phosphorylation of AKT. TSC2 phosphorylation and inactivation by Akt releases the inhibition of Rheb, leading to activation of mTORC1. mTORC1 regulates many biological processes by phosphorylation of many downstream. The current studies propose the following model in β-cells: 1. Phosphorylation of ULK regulates autophagy and β-cell survival, 2. Activation of mTORC1/S6K axis inhibits insulin signaling by a negative feedback loop mediated by phosphorylation and degradation of IRS1/2. In addition, mTORC1/S6K regulates cell size, inhibits autophagy and promotes survival. 3. mTORC1 phosphorylates 4E-BP1 and 2 leading to dissociation of eIF4E and initiates cap-dependent translation of mRNAs with complex 5'UTR structures. The current work suggests that 4E-BP2/eIF4E (and not 4E-BP1) regulates CPE levels and controls insulin processing. Reprinted with permission.[145] Copyright 2017 Springer Nature.

The speed of which those results are obtained could be increased through either microchip Western blotting or CE inkjetting Western blotting methods.

In preliminary work, we investigated sample preparation methods for Islets facing challenges in protein extraction on a small number of Islets at a time. The ability to break apart the connective tissue of small number of Islets with direct cell lysis on a microfluidic chip could overcome limitations and sample volume requirements of conventional cell lysis and protein extraction methods.[146] The development of a microfluidic device to perform small scale Islet sample processing would integrate well with microscale Western blotting methods.

References

(1) Andrade, J. D.; Hlady, V. Protein Adsorption and Materials Biocompatibility: A Tutorial Review and Suggested Hypotheses. In *Biopolymers/Non-Exclusion HPLC*; Advances in Polymer Science; Springer Berlin Heidelberg, 1986; pp 1–63.

(2) Srinivas, P. R. Introduction to Protein Electrophoresis. In *Protein Electrophoresis: Methods and Protocols*; Kurien, B. T., Scofield, R. H., Eds.; Methods in Molecular Biology; Humana Press: Totowa, NJ, 2012; pp 23–28.

(3) Tiselius, A. Electrophoresis of Serum Globulin. I. *Biochem. J.* **1937**, *31* (2), 313–317.

(4) Tiselius, A. Electrophoresis of Serum Globulin. *Biochem. J.* **1937**, *31* (9), 1464–1477.

(5) Ornstein, L. Disc Electrophoresis-I Background and Theory*. *Ann. N. Y. Acad. Sci.* **1964**, *121* (2), 321–349. https://doi.org/10.1111/j.1749-6632.1964.tb14207.x.

(6) Davis, B. J. Disc Electrophoresis – Ii Method and Application to Human Serum Proteins*. *Ann. N. Y. Acad. Sci.* **1964**, *121* (2), 404–427. https://doi.org/10.1111/j.1749-6632.1964.tb14213.x.

(7) Summers, D. F.; Maizel, J. V.; Darnell, J. E. Evidence for Virus-Specific Noncapsid Proteins in Poliovirus-Infected HeLa Cells. *Proc. Natl. Acad. Sci.* **1965**, *54* (2), 505–513. https://doi.org/10.1073/pnas.54.2.505.

(8) Laemmli, U. K. Cleavage of Structural Proteins during the Assembly of the Head of Bacteriophage T4. *Nature* **1970**, *227* (5259), 680–685. https://doi.org/10.1038/227680a0.

(9) Bier, M. *Electrophoresis: Theory, Methods, and Applications.*; Academic Press: New York, 1959.

(10) Vesterberg, O. A Short History of Electrophoretic Methods. *Electrophoresis* **1993**, *14* (12), 1243–1249. https://doi.org/10.1002/elps.11501401188.

(11) Reynolds, J. A.; Tanford, C. The Gross Conformation of Protein-Sodium Dodecyl Sulfate Complexes. *J. Biol. Chem.* **1970**, *245* (19), 5161–5165.

(12) Reynolds, J. A.; Tanford, C. Binding of Dodecyl Sulfate to Proteins at High Binding Ratios. Possible Implications for the State of Proteins in Biological Membranes. *Proc. Natl. Acad. Sci.* **1970**, *66* (3), 1002–1007. https://doi.org/10.1073/pnas.66.3.1002.

(13) Berg, J. M.; Tymoczko, J. L.; Stryer, L.; Berg, J. M.; Tymoczko, J. L.; Stryer, L. *Biochemistry*, 5th ed.; W H Freeman, 2002.

(14) Waehneldt, T. V. Sodium Dodecyl Sulfate in Protein Chemistry. *Biosystems* **1975**, *6* (3), 176–187. https://doi.org/10.1016/0303-2647(75)90025-8.

(15) Otzen, D. Protein–surfactant Interactions: A Tale of Many States. *Biochim. Biophys. Acta BBA - Proteins Proteomics* **2011**, *1814* (5), 562–591. https://doi.org/10.1016/j.bbapap.2011.03.003.

(16) Lakna. How Does SDS Denature Proteins https://pediaa.com/how-does-sds-denature-proteins/ (accessed Jan 27, 2020).

(17) Pitt-Rivers, R.; Impiombato, F. S. A. The Binding of Sodium Dodecyl Sulphate to Various Proteins. *Biochem. J.* **1968**, *109* (5), 825–830.

(18) Duchesne, L. G. M.; Lam, J. S.; MacDonald, L. A.; Whitfield, C.; Kropinski, A. M. Effect of pH and Acrylamide Concentration on the Separation of Lipopolysaccharides in Polyacrylamide Gels. *Curr. Microbiol.* **1988**, *16* (4), 191–194. https://doi.org/10.1007/BF01568528.

(19) Jones, M. N. Surfactant Interactions with Biomembranes and Proteins. *Chem. Soc. Rev.* **1992**, *21* (2), 127–136. https://doi.org/10.1039/CS9922100127.

(20) Pederson, T. Turning a PAGE: The Overnight Sensation of SDS-Polyacrylamide Gel Electrophoresis. *FASEB J.* **2008**, *22* (4), 949–953. https://doi.org/10.1096/fj.08-0402ufm.

(21) Nygaard, A. P.; Hall, B. D. A Method for the Detection of RNA-DNA Complexes. *Biochem. Biophys. Res. Commun.* **1963**, *12* (2), 98–104. https://doi.org/10.1016/0006-291X(63)90242-0.

(22) Kuno, H.; Kihara, H. K. Simple Microassay of Protein with Membrane Filter. *Nature* **1967**, *215* (5104), 974–975. https://doi.org/10.1038/215974a0.

(23) Towbin, H.; Staehelin, T.; Gordon, J. Electrophoretic Transfer of Proteins from Polyacrylamide Gels to Nitrocellulose Sheets: Procedure and Some Applications. *Proc. Natl. Acad. Sci.* **1979**, *76* (9), 4350–4354.

(24) Stott, D. I. Immunoblotting and Dot Blotting. *J. Immunol. Methods* **1989**, *119* (2), 153–187. https://doi.org/10.1016/0022-1759(89)90394-3.

(25) Gershoni, J. M.; Palade, G. E. Protein Blotting: Principles and Applications. *Anal. Biochem.* **1983**, *131* (1), 1–15. https://doi.org/10.1016/0003-2697(83)90128-8.

(26) Towbin, H.; Gordon, J. Immunoblotting and Dot Immunobinding — Current Status and Outlook. *J. Immunol. Methods* **1984**, *72* (2), 313–340. https://doi.org/10.1016/0022-1759(84)90001-2.

(27) Van Oss, C. J.; Good, R. J.; Chaudhury, M. K. Mechanism of DNA (southern) and Protein (western) Blotting on Cellulose Nitrate and Other Membranes. *J. Chromatogr. A* **1987**, *391*, 53–65. https://doi.org/10.1016/S0021-9673(01)94304-3.

(28) Hoffman, W. L.; Jump, A. A.; Kelly, P. J.; Ruggles, A. O. Binding of Antibodies and Other Proteins to Nitrocellulose in Acidic, Basic, and Chaotropic Buffers. *Anal. Biochem.* **1991**, *198* (1), 112–118. https://doi.org/10.1016/0003-2697(91)90514-T.

(29) Burnette, W. N. "Western Blotting": Electrophoretic Transfer of Proteins from Sodium Dodecyl Sulfate-Polyacrylamide Gels to Unmodified Nitrocellulose and Radiographic Detection with Antibody and Radioiodinated Protein A. *Anal. Biochem.* **1981**, *112* (2), 195–203. https://doi.org/10.1016/0003-2697(81)90281-5.

(30) Schlickeiser, S.; Pleyer, U. Western, Northern, and Southern Blotting. In *Basic Science Techniques in Clinical Practice*; Patel, H. R. H., Arya, M., Shergill, I. S., Eds.; Springer London: London, 2007; pp 48–57.

(31) Anderson, G. J.; M. Cipolla, C.; Kennedy, R. T. Western Blotting Using Capillary Electrophoresis. *Anal. Chem.* **2011**, *83* (4), 1350–1355. https://doi.org/10.1021/ac102671n.

(32) Jorgenson, J. W.; Lukacs, K. D. Zone Electrophoresis in Open-Tubular Glass Capillaries. *Anal. Chem.* **1981**, *53* (8), 1298–1302. https://doi.org/10.1021/ac00231a037.

(33) Thormann, W. Chapter 2 - Theoretical Principles of Capillary Electromigration Methods. In *Capillary Electromigration Separation Methods*; Poole, C. F., Ed.; Handbooks in Separation Science; Elsevier, 2018; pp 21–44.

(34) Landers, J. P. *Handbook of Capillary and Microchip Electrophoresis and Associated Microtechniques*; CRC Press, 2007.

(35) Foret, F.; Szoko, E.; Karger, B. L. On-Column Transient and Coupled Column Isotachophoretic Preconcentration of Protein Samples in Capillary Zone Electrophoresis. *J. Chromatogr. A* **1992**, *608* (1), 3–12. https://doi.org/10.1016/0021-9673(92)87100-M.

(36) Guttman, A.; Nolan, J. A.; Cooke, N. Capillary Sodium Dodecyl Sulfate Gel Electrophoresis of Proteins. *J. Chromatogr. A* **1993**, *632* (1), 171–175. https://doi.org/10.1016/0021-9673(93)80041-6.

(37) Guttman, A.; Nolan, J. Comparison of the Separation of Proteins by Sodium Dodecyl Sulfate-Slab Gel Electrophoresis and Capillary Sodium Dodecyl Sulfate-Gel Electrophoresis. *Anal. Biochem.* **1994**, *221* (2), 285–289. https://doi.org/10.1006/abio.1994.1413.

(38) Guttman, A. On the Separation Mechanism of Capillary Sodium Dodecyl Sulfate-Gel Electrophoresis of Proteins. *Electrophoresis* **1995**, *16* (1), 611–616. https://doi.org/10.1002/elps.1150160198.

(39) Dawod, M.; Chung, D. S. High-Sensitivity Capillary and Microchip Electrophoresis Using Electrokinetic Supercharging. *J. Sep. Sci.* **2011**, *34* (20), 2790–2799. https://doi.org/10.1002/jssc.201100384.

(40) Grossman, P. D.; Soane, D. S. Capillary Electrophoresis of DNA in Entangled Polymer Solutions. *J. Chromatogr. A* **1991**, *559* (1), 257–266. https://doi.org/10.1016/0021-9673(91)80076-S.

(41) De Gennes, P. G. Dynamics of Entangled Polymer Solutions. I. The Rouse Model. *Macromolecules* **1976**, *9* (4), 587–593. https://doi.org/10.1021/ma60052a011.

(42) De Gennes, P. G. Dynamics of Entangled Polymer Solutions. II. Inclusion of Hydrodynamic Interactions. *Macromolecules* **1976**, *9* (4), 594–598. https://doi.org/10.1021/ma60052a012.

(43) Wu, D.; Regnier, F. E. Sodium Dodecyl Sulfate-Capillary Gel Electrophoresis of Proteins Using Non-Cross-Linked Polyacrylamide. *J. Chromatogr. A* **1992**, *608* (1), 349–356. https://doi.org/10.1016/0021-9673(92)87142-U.

(44) Zhu, Z.; Lu, J. J.; Liu, S. Protein Separation by Capillary Gel Electrophoresis: A Review. *Anal. Chim. Acta* **2012**, *709*, 21–31. https://doi.org/10.1016/j.aca.2011.10.022.

(45) Zhang, C.-X.; Meagher, M. M. Sample Stacking Provides Three Orders of Magnitude Sensitivity Enhancement in SDS Capillary Gel Electrophoresis of Adeno-Associated Virus Capsid Proteins. *Anal. Chem.* **2017**, *89* (6), 3285–3292. https://doi.org/10.1021/acs.analchem.6b02933.

(46) Kahle, J.; Maul, K. J.; Wätzig, H. The next Generation of Capillary Electrophoresis Instruments: Performance of CE-SDS Protein Analysis. *Electrophoresis* **2018**, *39* (2), 311–325. https://doi.org/10.1002/elps.201700278.

(47) 2100 Bioanalyzer Instruments http://www.genomics.agilent.com/en/product.jsp?cid=AG-PT-106&_requestid=1285828.

(48) Nguyen, U.; Squaglia, N.; Boge, A.; Fung, P. A. The Simple Western^{TM}: A Gel-Free, Blot-Free, Hands-Free Western Blotting Reinvention. *Nat. Methods* **2011**, *8* (11). https://doi.org/10.1038/nmeth.f.353.

(49) Wenz, C.; Rüfer, A. Microchip CGE Linked to Immunoprecipitation as an Alternative to Western Blotting. *Electrophoresis* **2009**, *30* (24), 4264–4269. https://doi.org/10.1002/elps.200900347.

(50) Hamm, M.; Ha, S.; Rustandi, R. R. Automated Capillary Western Dot Blot Method for the Identity of a 15-Valent Pneumococcal Conjugate Vaccine. *Anal. Biochem.* **2015**, *478*, 33–39. https://doi.org/10.1016/j.ab.2015.03.021.

(51) Loughney, J. W.; Ha, S.; Rustandi, R. R. Quantitation of CRM197 Using Imaged Capillary Isoelectric Focusing with Fluorescence Detection and Capillary Western. *Anal. Biochem.* **2017**, *534*, 19–23. https://doi.org/10.1016/j.ab.2017.06.013.

(52) Pinto, D. M.; Arriaga, E. A.; Craig, D.; Angelova, J.; Sharma, N.; Ahmadzadeh, H.; Dovichi, N. J.; Boulet, C. A. Picomolar Assay of Native Proteins by Capillary Electrophoresis Precolumn Labeling, Submicellar Separation, and Laser-Induced Fluorescence Detection. *Anal. Chem.* **1997**, *69* (15), 3015–3021. https://doi.org/10.1021/ac9611677.

(53) Zhu, Z.; Lu, J. J.; Liu, S. Protein Separation by Capillary Gel Electrophoresis: A Review. *Anal. Chim. Acta* **2012**, *709*, 21–31. https://doi.org/10.1016/j.aca.2011.10.022.

(54) Sastre Toraño, J.; Ramautar, R.; de Jong, G. Advances in Capillary Electrophoresis for the Life Sciences. *J. Chromatogr. B* **2019**, *1118-1119*, 116–136. https://doi.org/10.1016/j.jchromb.2019.04.020.

(55) Jacobson, S. C.; Hergenroder, R.; Koutny, L. B.; Ramsey, J. M. High-Speed Separations on a Microchip. *Anal. Chem.* **1994**, *66* (7), 1114–1118. https://doi.org/10.1021/ac00079a029.

(56) Breadmore, M. C. Capillary and Microchip Electrophoresis: Challenging the Common Conceptions. *J. Chromatogr. A* **2012**, *1221*, 42–55. https://doi.org/10.1016/j.chroma.2011.09.062.

(57) Wu, D.; Qin, J.; Lin, B. Electrophoretic Separations on Microfluidic Chips. *J. Chromatogr. A* **2008**, *1184* (1–2), 542–559. https://doi.org/10.1016/j.chroma.2007.11.119.

(58) Creamer, J. S.; Oborny, N. J.; Lunte, S. M. Recent Advances in the Analysis of Therapeutic Proteins by Capillary and Microchip Electrophoresis. *Anal. Methods* **2014**, *6* (15), 5427–5449. https://doi.org/10.1039/C4AY00447G.

(59) Castro, E. R.; Manz, A. Present State of Microchip Electrophoresis: State of the Art and Routine Applications. *J. Chromatogr. A* **2015**, *1382*, 66–85. https://doi.org/10.1016/j.chroma.2014.11.034.

(60) Microfluidic Chips|PerkinElmer https://www.perkinelmer.com/category/microfluidic-chips (accessed Jan 27, 2020).

(61) Jin, S.; Anderson, G. J.; Kennedy, R. T. Western Blotting Using Microchip Electrophoresis Interfaced to a Protein Capture Membrane. *Anal. Chem.* **2013**, *85* (12), 6073–6079. https://doi.org/10.1021/ac400940x.

(62) Jin, S.; Furtaw, M. D.; Chen, H.; Lamb, D. T.; Ferguson, S. A.; Arvin, N. E.; Dawod, M.; Kennedy, R. T. Multiplexed Western Blotting Using Microchip Electrophoresis. *Anal. Chem.* **2016**, *88* (13), 6703–6710. https://doi.org/10.1021/acs.analchem.6b00705.

(63) Manz, A.; Harrison, D. J.; Verpoorte, E. M. J.; Fettinger, J. C.; Paulus, A.; Lüdi, H.; Widmer, H. M. Planar Chips Technology for Miniaturization and Integration of Separation Techniques into Monitoring Systems: Capillary Electrophoresis on a Chip. *J. Chromatogr. A* **1992**, *593* (1), 253–258. https://doi.org/10.1016/0021-9673(92)80293-4.

(64) Harrison, D. J.; Manz, A.; Fan, Z.; Luedi, H.; Widmer, H. M. Capillary Electrophoresis and Sample Injection Systems Integrated on a Planar Glass Chip. *Anal. Chem.* **1992**, *64* (17), 1926–1932. https://doi.org/10.1021/ac00041a030.

(65) Harrison, D. J.; Fluri, K.; Seiler, K.; Fan, Z.; Effenhauser, C. S.; Manz, A. Micromachining a Miniaturized Capillary Electrophoresis-Based Chemical Analysis System on a Chip. *Science* **1993**, *261* (5123), 895–897. https://doi.org/10.1126/science.261.5123.895.

(66) Fan, Z. H.; Harrison, D. J. Micromachining of Capillary Electrophoresis Injectors and Separators on Glass Chips and Evaluation of Flow at Capillary Intersections. *Anal. Chem.* **1994**, *66* (1), 177–184. https://doi.org/10.1021/ac00073a029.

(67) Stjernström, M. arten; Roeraade, J. Method for Fabrication of Microfluidic Systems in Glass. *J. Micromechanics Microengineering* **1998**, *8* (1), 33–38. https://doi.org/10.1088/0960-1317/8/1/006.

(68) Spierings, G. A. C. M. Wet Chemical Etching of Silicate Glasses in Hydrofluoric Acid Based Solutions. *J. Mater. Sci.* **1993**, *28* (23), 6261–6273. https://doi.org/10.1007/BF01352182.

(69) Iliescu, C.; Tay, F. E. H.; Miao, J. Strategies in Deep Wet Etching of Pyrex Glass. *Sens. Actuators Phys.* **2007**, *133* (2), 395–400. https://doi.org/10.1016/j.sna.2006.06.044.

(70) Iliescu, C.; Tay, F. E. H. Wet Etching of Glass. In *CAS 2005 Proceedings. 2005 International Semiconductor Conference, 2005.*; 2005; Vol. 1, pp 35–44 vol. 1. https://doi.org/10.1109/SMICND.2005.1558704.

(71) Simpson, P. C.; Woolley, A. T.; Mathies, R. A. Microfabrication Technology for the Production of Capillary Array Electrophoresis Chips. *Biomed. Microdevices* **1998**, *1* (1), 7–26. https://doi.org/10.1023/A:1009922004301.

(72) Jacobson, S. C.; Hergenroder, R.; Moore, A. W. J.; Ramsey, J. M. Precolumn Reactions with Electrophoretic Analysis Integrated on a Microchip. *Anal. Chem.* **1994**, *66* (23), 4127–4132. https://doi.org/10.1021/ac00095a003.

(73) Gong, M.; Wehmeyer, K. R.; Stalcup, A. M.; Limbach, P. A.; Heineman, W. R. Study of Injection Bias in a Simple Hydrodynamic Injection in Microchip CE. *ELECTROPHORESIS* **2007**, *28* (10), 1564–1571. https://doi.org/10.1002/elps.200600616.

(74) Kaniansky, D.; Marák, J. On-Line Coupling of Capillary Isotachophoresis with Capillary Zone Electrophoresis. *J. Chromatogr. A* **1990**, *498*, 191–204. https://doi.org/10.1016/S0021-9673(01)84247-3.

(75) Burgi, D. S.; Chien, R. L. Optimization in Sample Stacking for High-Performance Capillary Electrophoresis. *Anal. Chem.* **1991**, *63* (18), 2042–2047. https://doi.org/10.1021/ac00018a028.

(76) Chien, R. L.; Burgi, D. S. Sample Stacking of an Extremely Large Injection Volume in High-Performance Capillary Electrophoresis. *Anal. Chem.* **1992**, *64* (9), 1046–1050. https://doi.org/10.1021/ac00033a015.

(77) Jacobson, S. C.; Ramsey, J. M. Microchip Electrophoresis with Sample Stacking. *Electrophoresis* **1995**, *16* (1), 481–486. https://doi.org/10.1002/elps.1150160179.

(78) Breadmore, M. C.; Grochocki, W.; Kalsoom, U.; Alves, M. N.; Phung, S. C.; Rokh, M. T.; Cabot, J. M.; Ghiasvand, A.; Li, F.; Shallan, A. I.; et al. Recent Advances in Enhancing the Sensitivity of Electrophoresis and Electrochromatography in Capillaries and Microchips (2016–2018). *ELECTROPHORESIS* **2019**, *40* (1), 17–39. https://doi.org/10.1002/elps.201800384.

(79) Berson, S. A.; Yalow, R. S.; Bauman, A.; Rothschild, M. A.; Newerly, K. INSULIN-I131 METABOLISM IN HUMAN SUBJECTS: DEMONSTRATION OF INSULIN BINDING GLOBULIN IN THE CIRCULATION OF INSULIN TREATED SUBJECTS 1. *J. Clin. Invest.* **1956**, *35* (2), 170–190.

(80) Yalow, R. S.; Berson, S. A. Assay of Plasma Insulin in Human Subjects by Immunological Methods. *Nature* **1959**, *184* (4699), 1648–1649. https://doi.org/10.1038/1841648b0.

(81) Köhler, G.; Milstein, C. Continuous Cultures of Fused Cells Secreting Antibody of Predefined Specificity. *Nature* **1975**, *256* (5517), 495–497. https://doi.org/10.1038/256495a0.

(82) Rubenstein, K. E.; Schneider, R. S.; Ullman, E. F. "Homogeneous" Enzyme Immunoassay. A New Immunochemical Technique. *Biochem. Biophys. Res. Commun.* **1972**, *47* (4), 846–851. https://doi.org/10.1016/0006-291X(72)90570-0.

(83) Hage, D. S. Immunoassays. *Anal. Chem.* **1999**, *71* (12), 294–304. https://doi.org/10.1021/a1999901+.

(84) Cox, K. L.; Devanarayan, V.; Kriauciunas, A.; Manetta, J.; Montrose, C.; Sittampalam, S. Immunoassay Methods. In *Assay Guidance Manual*; Sittampalam, G. S., Coussens, N. P., Nelson, H., Arkin, M., Auld, D., Austin, C., Bejcek, B., Glicksman, M., Inglese, J., Lemmon, V., et al., Eds.; Eli Lilly & Company and the National Center for Advancing Translational Sciences: Bethesda (MD), 2004.

(85) Kurien, B. T.; Scofield, R. H. Western Blotting. *Methods San Diego Calif* **2006**, *38* (4), 283–293. https://doi.org/10.1016/j.ymeth.2005.11.007.

(86) iBind™ Western Systems https://www.thermofisher.com/us/en/home/life-science/protein-biology/protein-assays-analysis/western-blotting/detect-proteins-western-blot/ibind-western-system.html.

(87) SNAP i.d.® 2.0 Protein Detection System http://www.emdmillipore.com/US/en/product/SNAP-i.d.-2.0-Protein-Detection-System,MM_NF-C73105.

(88) Mazet, F.; Dunster, J. L.; Jones, C. I.; Vaiyapuri, S.; Tindall, M. J.; Fry, M. J.; Gibbins, J. M. A High-Density Immunoblotting Methodology for Quantification of Total Protein Levels and Phosphorylation Modifications. *Sci. Rep.* **2015**, *5*, 16995. https://doi.org/10.1038/srep16995.

(89) BlotCycler™ Touch - Precision Biosystems-Automated, Reproducible Western Blot Processing and DNA, RNA Analysis. *Precision Biosystems-Automated, Reproducible Western Blot Processing and DNA, RNA analysis*.

(90) GOBlot - The First Affordable Western Blot Processor https://www.cytoskeleton.com/western-blot-processor-goblot (accessed Mar 1, 2018).

(91) Ahmad, A. L.; Low, S. C.; Shukor, S. R. A.; Fernando, W. J. N.; Ismail, A. Hindered Diffusion in Lateral Flow Nitrocellulose Membrane: Experimental and Modeling Studies. *J. Membr. Sci.* **2010**, *357* (1), 178–184. https://doi.org/10.1016/j.memsci.2010.04.018.

(92) Kapur, V.; Charkoudian, J.; Anderson, J. L. Transport of Proteins through Gel-Filled Porous Membranes. *J. Membr. Sci.* **1997**, *131* (1), 143–153. https://doi.org/10.1016/S0376-7388(97)00037-9.

(93) Charcosset, C.; Yousefian, F.; Thovert, J.-F.; Adler, P. M. Calculation of Flow and Solute Deposition through Three-Dimensional Reconstructed Model of Microporous Membranes. *Desalination* **2002**, *145* (1), 133–138. https://doi.org/10.1016/S0011-9164(02)00398-3.

(94) Thomas, N.; Jones, C. N.; Thomas, P. L. Low Volume Processing of Protein Blots in Rolling Drums. *Anal. Biochem.* **1988**, *170* (2), 393–396. https://doi.org/10.1016/0003-2697(88)90650-1.

(95) Giri, B.; Pandey, B.; Neupane, B.; Ligler, F. S. Signal Amplification Strategies for Microfluidic Immunoassays. *TrAC Trends Anal. Chem.* **2016**, *79*, 326–334. https://doi.org/10.1016/j.trac.2015.10.021.

(96) Liu, Y.; Yu, J.; Du, M.; Wang, W.; Zhang, W.; Wang, Z.; Jiang, X. Accelerating Microfluidic Immunoassays on Filter Membranes by Applying Vacuum. *Biomed. Microdevices* **2012**, *14* (1), 17–23. https://doi.org/10.1007/s10544-011-9581-z.

(97) Effenhauser, C. S.; Manz, A.; Widmer, H. M. Glass Chips for High-Speed Capillary Electrophoresis Separations with Submicrometer Plate Heights. *Anal. Chem.* **1993**, *65* (19), 2637–2642. https://doi.org/10.1021/ac00067a015.

(98) Roper, M. G.; Shackman, J. G.; Dahlgren, G. M.; Kennedy, R. T. Microfluidic Chip for Continuous Monitoring of Hormone Secretion from Live Cells Using an Electrophoresis-Based Immunoassay. *Anal. Chem.* **2003**, *75* (18), 4711–4717. https://doi.org/10.1021/ac0346813.

(99) Lagally, E. T.; Simpson, P. C.; Mathies, R. A. Monolithic Integrated Microfluidic DNA Amplification and Capillary Electrophoresis Analysis System. *Sens. Actuators B Chem.* **2000**, *63* (3), 138–146. https://doi.org/10.1016/S0925-4005(00)00350-6.

(100) Schott D 263 Thin Borosilicate Glass http://www.matweb.com/search/datasheet.aspx?matguid=8df9f3e0106d43818ebe1862e76a1107&ckck=1 (accessed Nov 15, 2019).

(101) Smejkal, P.; Bottenus, D.; Breadmore, M. C.; Guijt, R. M.; Ivory, C. F.; Foret, F.; Macka, M. Microfluidic Isotachophoresis: A Review. *ELECTROPHORESIS* **2013**, *34* (11), 1493–1509. https://doi.org/10.1002/elps.201300021.

(102) Lu, Y.; Hou, X.; Wang, D.; Zhong, H. Advances of a Capillary Electrophoretic on-Line Concentration Technique: Electrokinetic Supercharging. *J. Liq. Chromatogr. Relat. Technol.* **2017**, *40* (10), 528–535. https://doi.org/10.1080/10826076.2017.1330756.

(103) Huang, H.; Xu, F.; Dai, Z.; Lin, B. On-Line Isotachophoretic Preconcentration and Gel Electrophoretic Separation of Sodium Dodecyl Sulfate-Proteins on a Microchip. *Electrophoresis* **2005**, *26* (11), 2254–2260. https://doi.org/10.1002/elps.200410393.

(104) Xu, Z.; Ando, T.; Nishine, T.; Arai, A.; Hirokawa, T. Electrokinetic Supercharging Preconcentration and Microchip Gel Electrophoretic Separation of Sodium Dodecyl Sulfate-Protein Complexes. *ELECTROPHORESIS* **2003**, *24* (21), 3821–3827. https://doi.org/10.1002/elps.200305625.

(105) Fu, L.-M.; Yang, R.-J.; Lee, G.-B.; Liu, H.-H. Electrokinetic Injection Techniques in Microfluidic Chips. *Anal. Chem.* **2002**, *74* (19), 5084–5091. https://doi.org/10.1021/ac025821w.

(106) Jacobson, S. C.; Hergenroder, R.; Koutny, L. B.; Warmack, R. J.; Ramsey, J. M. Effects of Injection Schemes and Column Geometry on the Performance of Microchip Electrophoresis Devices. *Anal. Chem.* **1994**, *66* (7), 1107–1113. https://doi.org/10.1021/ac00079a028.

(107) Shackman, J. G.; Watson, C. J.; Kennedy, R. T. High-Throughput Automated Post-Processing of Separation Data. *J. Chromatog. A* **2004**, *1040* (2), 273–282. https://doi.org/10.1016/j.chroma.2004.04.004.

(108) Sinton, D.; Ren, L.; Li, D. A Dynamic Loading Method for Controlling on-Chip Microfluidic Sample Injection. *J. Colloid Interface Sci.* **2003**, *266* (2), 448–456. https://doi.org/10.1016/S0021-9797(03)00630-1.

(109) Wells, S. S.; Dawod, M.; Kennedy, R. T. CE-MS with Electrokinetic Supercharging and Application to Determination of Neurotransmitters. *Electrophoresis* **2019**, *22*, 2946–2953. https://doi.org/10.1002/elps.201900203.

(110) Mishra, M.; Tiwari, S.; Gomes, A. V. Protein Purification and Analysis: Next Generation Western Blotting Techniques. *Expert Rev. Proteomics* **2017**, *14* (11), 1037–1053. https://doi.org/10.1080/14789450.2017.1388167.

(111) Sanders, B. J.; Kim, D. C.; Dunn, R. C. Recent Advances in Microscale Western Blotting. *Anal. Methods* **2016**, *8* (39), 7002–7013. https://doi.org/10.1039/C6AY01947A.

(112) Jin, S.; Kennedy, R. T. New Developments in Western Blot Technology. *Chin. Chem. Lett.* **2015**, *26* (4), 416–418. https://doi.org/10.1016/j.cclet.2015.01.021.

(113) Rodríguez-Ruiz, I.; Babenko, V.; Martínez-Rodríguez, S.; Gavira, J. A. Protein Separation under a Microfluidic Regime. *Analyst* **2017**. https://doi.org/10.1039/C7AN01568B.

(114) Štěpánová, S.; Kašička, V. Analysis of Proteins and Peptides by Electromigration Methods in Microchips. *J. Sep. Sci.* **2017**, *40* (1), 228–250. https://doi.org/10.1002/jssc.201600962.

(115) Dawod, M.; Arvin, N. E.; Kennedy, R. T. Recent Advances in Protein Analysis by Capillary and Microchip Electrophoresis. *Analyst* **2017**, *142* (11), 1847–1866. https://doi.org/10.1039/C7AN00198C.

(116) Gerver, R. E.; Herr, A. E. Microfluidic Western Blotting of Low-Molecular-Mass Proteins. *Anal. Chem.* **2014**, *86* (21), 10625–10632. https://doi.org/10.1021/ac5024588.

(117) Hughes, A. J.; Spelke, D. P.; Xu, Z.; Kang, C.-C.; Schaffer, D. V.; Herr, A. E. Single-Cell Western Blotting. *Nat. Methods* **2014**, *11* (7), 749–755. https://doi.org/10.1038/nmeth.2992.

(118) Pollard, T. D. A Guide to Simple and Informative Binding Assays. *Mol. Biol. Cell* **2010**, *21* (23), 4061–4067. https://doi.org/10.1091/mbc.E10-08-0683.

(119) Kusnezow, W.; Syagailo, Y. V.; Rüffer, S.; Baudenstiel, N.; Gauer, C.; Hoheisel, J. D.; Wild, D.; Goychuk, I. Optimal Design of Microarray Immunoassays to Compensate for Kinetic Limitations: Theory and Experiment. *Mol. Cell. Proteomics* **2006**, *5* (9), 1681–1696. https://doi.org/10.1074/mcp.T500035-MCP200.

(120) Liu, C.-Y.; Lu, D.-C.; Jiang, Y.-W.; Yen, Y.-K.; Chang, S.-C.; Wang, A.-B. Easy and Fast Western Blotting by Thin-Film Direct Coating with Suction. *Anal. Chem.* **2016**, *88* (12), 6349–6356. https://doi.org/10.1021/acs.analchem.6b00699.

(121) He, S.; Zhang, Y.; Wang, P.; Xu, X.; Zhu, K.; Pan, W.; Liu, W.; Cai, K.; Sun, J.; Zhang, W.; et al. Multiplexed Microfluidic Blotting of Proteins and Nucleic Acids by Parallel, Serpentine Microchannels. *Lab. Chip* **2014**, *15* (1), 105–112. https://doi.org/10.1039/C4LC00901K.

(122) Chang, H.-N.; Leroueil, P. R.; Selwa, K.; Gasper, C. J.; Tsuchida, R. E.; Wang, J. J.; McHugh, W. M.; Cornell, T. T.; Jr, J. R. B.; Goonewardena, S. N. Profiling Inflammatory Responses with Microfluidic Immunoblotting. *PLOS ONE* **2013**, *8* (11), e81889. https://doi.org/10.1371/journal.pone.0081889.

(123) Qi, L.-Y.; Yin, X.-F.; Liu, J.-H. Rapid and Efficient Isotachophoretic Preconcentration in Free Solution Coupled with Gel Electrophoresis Separation on a Microchip Using a Negative Pressure Sampling Technique. *J. Chromatogr. A* **2009**, *1216* (20), 4510–4516. https://doi.org/10.1016/j.chroma.2009.03.034.

(124) Heiger, D. N.; Cohen, A. S.; Karger, B. L. Separation of DNA Restriction Fragments by High Performance Capillary Electrophoresis with Low and Zero Crosslinked Polyacrylamide Using Continuous and Pulsed Electric Fields. *J. Chromatogr. A* **1990**, *516* (1), 33–48. https://doi.org/10.1016/S0021-9673(01)90202-X.

(125) Chinnasamy, T.; Segerink, L. I.; Nystrand, M.; Gantelius, J.; Svahn, H. A. Point-of-Care Vertical Flow Allergen Microarray Assay: Proof of Concept. *Clin. Chem.* **2014**, *60* (9), 1209–1216. https://doi.org/10.1373/clinchem.2014.223230.

(126) Lin, R.; Skandarajah, A.; Gerver, R. E.; Neira, H. D.; Fletcher, D. A.; Herr, A. E. A Lateral Electrophoretic Flow Diagnostic Assay. *Lab Chip* **2015**, *15* (6), 1488–1496. https://doi.org/10.1039/C4LC01370K.

(127) Karey, K. P.; Sirbasku, D. A. Glutaraldehyde Fixation Increases Retention of Low Molecular Weight Proteins (growth Factors) Transferred to Nylon Membranes for Western Blot Analysis. *Anal. Biochem.* **1989**, *178* (2), 255–259. https://doi.org/10.1016/0003-2697(89)90634-9.

(128) Mizzen, C. A.; Cartel, N. J.; Yu, W. H.; Fraser, P. E.; McLachlan, D. R. Sensitive Detection of Metallothioneins-1, -2 and -3 in Tissue Homogenates by Immunoblotting: A Method for Enhanced Membrane Transfer and Retention. *J. Biochem. Biophys. Methods* **1996**, *32* (2), 77–83.

(129) Jeon, J.-H.; Cho, S.-Y.; Kim, C.-W.; Shin, D.-M.; Kwon, J.-C.; Choi, K.-H.; Kim, I.-G. Improved Immunodetection of Human Papillomavirus E7. *Exp. Mol. Med.* **2002**, *34* (6), 496. https://doi.org/10.1038/emm.2002.69.

(130) Suzuki, Y.; Takeda, Y.; Ikuta, T. Immunoblotting Conditions for Human Hemoglobin Chains. *Anal. Biochem.* **2008**, *378* (2), 218–220. https://doi.org/10.1016/j.ab.2008.04.008.

(131) Van Eldik, L. J.; Wolchok, S. R. Conditions for Reproducible Detection of Calmodulin and S100 Beta in Immunoblots. *Biochem. Biophys. Res. Commun.* **1984**, *124* (3), 752–759.

(132) Nestal de Moraes, G.; Carvalho, É.; Maia, R. C.; Sternberg, C. Immunodetection of Caspase-3 by Western Blot Using Glutaraldehyde. *Anal. Biochem.* **2011**, *415* (2), 203–205. https://doi.org/10.1016/j.ab.2011.04.032.

(133) Lee, B. R.; Kamitani, T. Improved Immunodetection of Endogenous α-Synuclein. *PLOS ONE* **2011**, *6* (8), e23939. https://doi.org/10.1371/journal.pone.0023939.

(134) Newman, A. J.; Selkoe, D.; Dettmer, U. A New Method for Quantitative Immunoblotting of Endogenous α-Synuclein. *PLOS ONE* **2013**, *8* (11), e81314. https://doi.org/10.1371/journal.pone.0081314.

(135) Ermakov, S. V.; Jacobson, S. C.; Ramsey, J. M. Computer Simulations of Electrokinetic Transport in Microfabricated Channel Structures. *Anal. Chem.* **1998**, *70* (21), 4494–4504. https://doi.org/10.1021/ac980551w.

(136) Chaiken, I.; Rosé, S.; Karlsson, R. Analysis of Macromolecular Interactions Using Immobilized Ligands. *Anal. Biochem.* **1992**, *201* (2), 197–210.

(137) Modeling Micropatterned Antigen–antibody Binding Kinetics in a Microfluidic Chip. *Biosens. Bioelectron.* **2007**, *22* (7), 1403–1409. https://doi.org/10.1016/j.bios.2006.06.017.

(138) Bird, R. B.; Lightfoot, E. N.; Stewart, W. E. *Notes on Transport Phenomena. [By R.B. Bird, Warren E. Stewart and Edwin N. Lightfoot.*; New York; Chapman & Hall: London: John Wiley & Sons, 1958.

(139) Ouimet, C. M.; Dawod, M.; Grinias, J.; Assimon, V. A.; Lodge, J.; Mapp, A. K.; Gestwicki, J. E.; Kennedy, R. T. Protein Cross-Linking Capillary Electrophoresis at Increased Throughput for a Range of Protein–protein Interactions. *Analyst* **2018**, *143* (8), 1805–1812. https://doi.org/10.1039/C7AN02098H.

(140) Moritz, C. P. 40 Years Western Blotting: A Scientific Birthday Toast. *J. Proteomics* **2020**, *212*, 103575. https://doi.org/10.1016/j.jprot.2019.103575.

(141) Microdispensing http://www.microfab.com/biomedical/microdispensing (accessed Nov 25, 2019)

(142) Machekposhti, S. A.; Mohaved, S.; Narayan, R. J. Inkjet Dispensing Technologies: Recent Advances for Novel Drug Discovery. *Expert Opin. Drug Discov.* **2019**, *14* (2), 101–113. https://doi.org/10.1080/17460441.2019.1567489.

(143) Gudapati, H.; Dey, M.; Ozbolat, I. A Comprehensive Review on Droplet-Based Bioprinting: Past, Present and Future. *Biomaterials* **2016**, *102*, 20–42. https://doi.org/10.1016/j.biomaterials.2016.06.012.

(144) Jiang, W.-J.; Peng, Y.-C.; Yang, K.-M. Cellular Signaling Pathways Regulating β-Cell Proliferation as a Promising Therapeutic Target in the Treatment of Diabetes. *Exp. Ther. Med.* **2018**, *16* (4), 3275–3285. https://doi.org/10.3892/etm.2018.6603.

(145) Blandino-Rosano, M.; Barbaresso, R.; Jimenez-Palomares, M.; Bozadjieva, N.; Werneck-de-Castro, J. P.; Hatanaka, M.; Mirmira, R. G.; Sonenberg, N.; Liu, M.; Rüegg, M. A.; et al. Loss of mTORC1 Signalling Impairs β-Cell Homeostasis and Insulin Processing. *Nat. Commun.* **2017**, *8* (1), 1–15. https://doi.org/10.1038/ncomms16014.

(146) Coluccio, M. L.; Perozziello, G.; Malara, N.; Parrotta, E.; Zhang, P.; Gentile, F.; Limongi, T.; Raj, P. M.; Cuda, G.; Candeloro, P.; et al. Microfluidic Platforms for Cell Cultures and Investigations. *Microelectron. Eng.* **2019**, *208*, 14–28. https://doi.org/10.1016/j.mee.2019.01.004.